

Dry Grinding with CBN Wheels, The Effect of Structuring

Von der Fakultät Konstruktions-, Produktions- und Fahrzeugtechnik
der Universität Stuttgart
zur Erlangung der Würde eines Doktor-Ingenieurs (Dr.-Ing.)
genehmigte Abhandlung

vorgelegt von
Mohammad Rabiey
M.Sc. Mech. Eng.
aus Teheran

Hauptberichter: Univ.-Prof. Dr.-Ing. Prof. E.h. Dr.-Ing. E.h. Dr. h.c. mult.
Engelbert Westkämper, Universität Stuttgart
Mitberichter: Prof. Dr.-Ing. Taghi Tawakoli, HFU
Mitberichter: Prof. Dr.-Ing. Konrad Wegener, ETH-Zürich

Tag der mündlichen Prüfung: 15.06.2010

Institut für Industrielle Fertigung und Fabrikbetrieb (IFF)
der Universität Stuttgart 2010

IPA-IAO Forschung und Praxis

Berichte aus dem
Fraunhofer-Institut für Produktionstechnik und
Automatisierung (IPA), Stuttgart,
Fraunhofer-Institut für Arbeitswirtschaft und
Organisation (IAO), Stuttgart,
Institut für Industrielle Fertigung und
Fabrikbetrieb (IFF), Universität Stuttgart
und Institut für Arbeitswissenschaft und
Technologiemanagement (IAT), Universität Stuttgart

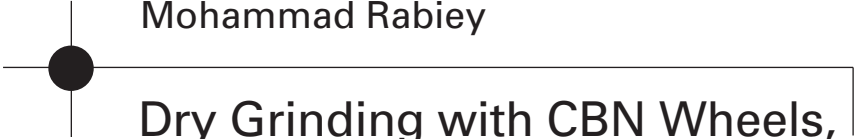
Herausgeber:

Univ.-Prof. Dr.-Ing. Prof. e.h. Dr.-Ing. e.h. Dr. h.c. mult. Engelbert Westkämper
und

Univ.-Prof. Dr.-Ing. habil. Prof. E.h. mult. Dr. h.c. mult. Hans-Jörg Bullinger
und

Univ.-Prof. Dr.-Ing. Dr.-Ing. E.h. Dieter Spath

Mohammad Rabiey



Dry Grinding with CBN Wheels, The Effect of Structuring

Nr. 503

Dr.-Ing. M.Sc. Mech. Eng. Mohammad Rabiey

Univ.-Prof. Dr.-Ing. Prof. e.h. Dr.-Ing. e.h. Dr. h.c. mult. Engelbert Westkämper
ord. Professor an der Universität Stuttgart
Fraunhofer-Institut für Produktionstechnik und Automatisierung (IPA), Stuttgart

Univ.-Prof. Dr.-Ing. habil. Prof. E.h. mult. Dr. h.c. mult. Hans-Jörg Bullinger
ord. Professor an der Universität Stuttgart
Präsident der Fraunhofer-Gesellschaft, München

Univ.-Prof. Dr.-Ing. Dr.-Ing. E.h. Dieter Spath
ord. Professor an der Universität Stuttgart
Fraunhofer-Institut für Arbeitswirtschaft und Organisation (IAO), Stuttgart

D 93

ISBN 978-3-939890-69-0

Jost Jetter Verlag, Heimsheim

Dieses Werk ist urheberrechtlich geschützt. Die dadurch begründeten Rechte, insbesondere die der Übersetzung, des Nachdrucks, des Vortrags, der Entnahme von Abbildungen und Tabellen, der Funksendung, der Mikroverfilmung oder der Vervielfältigung auf anderen Wegen und der Speicherung in Datenverarbeitungsanlagen, bleiben, auch bei nur auszugsweiser Verwertung, vorbehalten. Eine Vervielfältigung dieses Werkes oder von Teilen dieses Werkes ist auch im Einzelfall nur in den Grenzen der gesetzlichen Bestimmungen des Urheberrechtsgesetzes der Bundesrepublik Deutschland vom 9. September 1965 in der jeweils gültigen Fassung zulässig. Sie ist grundsätzlich vergütungspflichtig. Zuwiderhandlungen unterliegen den Strafbestimmungen des Urheberrechtsgesetzes.

© Jost-Jetter Verlag, Heimsheim 2011.

Printed in Germany.

Die Wiedergabe von Gebrauchsnamen, Handelsnamen, Warenbezeichnungen usw. in diesem Werk berechtigt auch ohne besondere Kennzeichnung nicht zu der Annahme, dass solche Namen im Sinne der Warenzeichen- und Markenschutz-Gesetzgebung als frei zu betrachten wären und daher von jedermann benutzt werden dürften.

Sollte in diesem Werk direkt oder indirekt auf Gesetze, Vorschriften oder Richtlinien (z. B. DIN, VDI, VDE) Bezug genommen oder aus ihnen zitiert worden sein, so kann der Verlag keine Gewähr für die Richtigkeit, Vollständigkeit oder Aktualität übernehmen. Es empfiehlt sich, gegebenenfalls für die eigenen Arbeiten die vollständigen Vorschriften oder Richtlinien in der jeweils gültigen Fassung hinzuzuziehen.

Druck: printsystem GmbH, Heimsheim

Geleitwort der Herausgeber

Über den Erfolg und das Bestehen von Unternehmen in einer marktwirtschaftlichen Ordnung entscheidet letztendlich der Absatzmarkt. Das bedeutet, möglichst frühzeitig absatzmarktorientierte Anforderungen sowie deren Veränderungen zu erkennen und darauf zu reagieren.

Neue Technologien und Werkstoffe ermöglichen neue Produkte und eröffnen neue Märkte. Die neuen Produktions- und Informationstechnologien verwandeln signifikant und nachhaltig unsere industrielle Arbeitswelt. Politische und gesellschaftliche Veränderungen signalisieren und begleiten dabei einen Wertewandel, der auch in unseren Industriebetrieben deutlichen Niederschlag findet.

Die Aufgaben des Produktionsmanagements sind vielfältiger und anspruchsvoller geworden. Die Integration des europäischen Marktes, die Globalisierung vieler Industrien, die zunehmende Innovationsgeschwindigkeit, die Entwicklung zur Freizeitgesellschaft und die übergreifenden ökologischen und sozialen Probleme, zu deren Lösung die Wirtschaft ihren Beitrag leisten muss, erfordern von den Führungskräften erweiterte Perspektiven und Antworten, die über den Fokus traditionellen Produktionsmanagements deutlich hinausgehen.

Neue Formen der Arbeitsorganisation im indirekten und direkten Bereich sind heute schon feste Bestandteile innovativer Unternehmen. Die Entkopplung der Arbeitszeit von der Betriebszeit, integrierte Planungsansätze sowie der Aufbau dezentraler Strukturen sind nur einige der Konzepte, welche die aktuellen Entwicklungsrichtungen kennzeichnen. Erfreulich ist der Trend, immer mehr den Menschen in den Mittelpunkt der Arbeitsgestaltung zu stellen - die traditionell eher technokratisch akzentuierten Ansätze weichen einer stärkeren Human- und Organisationsorientierung. Qualifizierungsprogramme, Training und andere Formen der Mitarbeiterentwicklung gewinnen als Differenzierungsmerkmal und als Zukunftsinvestition in *Human Resources* an strategischer Bedeutung.

Von wissenschaftlicher Seite muss dieses Bemühen durch die Entwicklung von Methoden und Vorgehensweisen zur systematischen Analyse und Verbesserung des Systems Produktionsbetrieb einschließlich der erforderlichen Dienstleistungsfunktionen unterstützt werden. Die Ingenieure sind hier gefordert, in enger Zusammenarbeit mit anderen Disziplinen, z. B. der Informatik, der Wirtschaftswissenschaften und der Arbeitswissenschaft, Lösungen zu erarbeiten, die den veränderten Randbedingungen Rechnung tragen.

Die von den Herausgebern langjährig geleiteten Institute, das

- Fraunhofer-Institut für Produktionstechnik und Automatisierung (IPA),
- Fraunhofer-Institut für Arbeitswirtschaft und Organisation (IAO),
- Institut für Industrielle Fertigung und Fabrikbetrieb (IFF), Universität Stuttgart,
- Institut für Arbeitswissenschaft und Technologiemanagement (IAT), Universität Stuttgart

arbeiten in grundlegender und angewandter Forschung intensiv an den oben aufgezeigten Entwicklungen mit. Die Ausstattung der Labors und die Qualifikation der Mitarbeiter haben bereits in der Vergangenheit zu Forschungsergebnissen geführt, die für die Praxis von großem Wert waren. Zur Umsetzung gewonnener Erkenntnisse wird die Schriftenreihe „IPA-IAO - Forschung und Praxis“ herausgegeben. Der vorliegende Band setzt diese Reihe fort. Eine Übersicht über bisher erschienene Titel wird am Schluss dieses Buches gegeben.

Dem Verfasser sei für die geleistete Arbeit gedankt, dem Jost Jetter Verlag für die Aufnahme dieser Schriftenreihe in seine Angebotspalette und der Druckerei für saubere und zügige Ausführung. Möge das Buch von der Fachwelt gut aufgenommen werden.

Engelbert Westkämper Hans-Jörg Bullinger Dieter Spath

Vorwort

Die Schleiftechnologie ist immer noch das wichtigste und meist verbreitete Verfahren für die Feinbearbeitung, auch wenn beim Hartdrehen und Hartfräsen ähnlich feine Oberflächen ohne Einsatz von Kühlschmierstoffen erreicht werden. Im Wettbewerb zwischen den Fertigungsprozessen konnte bisher das Schleifen auf den Einsatz von Kühlschmierstoff nicht verzichten. Die Entwicklung von Werkzeugmaschinen, die verschiedene Prozesse - wie Drehen, Schleifen, Bohren, Fräsen, Laserhärten und Schleifen - in einer Maschine kombinieren, zeigte den Bedarf des Trockenschleifens, da die anderen Prozesse ohne Einsatz von Kühlschmierstoffen funktionieren. Auch verstärkte Umweltauflagen und der Schutz der Maschinenbediener verdeutlichen, wie notwendig die Reduzierung bzw. der Verzicht auf Kühlschmierstoff beim Schleifen ist.

Im Kompetenzzentrum für Schleiftechnologie und Feinstbearbeitung (KSF) der Hochschule Furtwangen haben wir diesen Trend rechtzeitig erkannt und neuartige Prozesse für das Trockenschleifen entwickelt.

Herr Dr.-Ing. Mohammad Rabiey arbeitete über sechs Jahren in unserem Forschungsinstitut und hat - neben der aktiven Arbeit beim Aufbau des KSF, der Abwicklung von zahlreichen Forschungsprojekten und dem Verfassen vieler Veröffentlichungen - seine Doktorarbeit fertiggestellt. Die Promotionsarbeit von Herrn Dr.-Ing. Rabiey ist die erste wissenschaftliche Arbeit auf dem Gebiet des Trockenschleifens, die nicht nur die wissenschaftlichen Hintergründe und notwendigen Voraussetzungen und Analysen für das Funktionieren des Prozesses sehr genau darstellt. Diese Arbeit ist auch ein Wegweiser für die praktische Umsetzung des Trockenschleifens in der industriellen Produktion.

Ich bedanke mich bei Herrn Dr.-Ing. Rabiey für die hervorragende und vertrauensvolle Zusammenarbeit und die gut gelungene Doktorarbeit und wünsche ihm viel Erfolg.

Prof. Dr.-Ing. T. Tawakoli
August 2010

*To my lovely wife, Shahrzad without her support,
encouragement and love this work could not be
possible,*

&

*to my sweet daughter, Rana, who provided me the
inspiration to complete this work.*

Acknowledgments

It is not possible to mention all those who helped me in this research and dissertation. Below is an effort to acknowledge those who played the greatest roles.

I am grateful to my advisor Prof. Dr.-Ing. Prof. E.h. Dr.-Ing. E.h. Dr. h.c. mult. Westkämper, head of the “Institute of industrial manufacturing and management” at the University of Stuttgart and the director of “Fraunhofer Institute for production technology and Automation (IPA)” who provided me the possibility to do my PhD in the University of Stuttgart and for his sincere support during my study.

All the research works and experiments for this dissertation were carried out during my six years work as researcher and senior engineer in the “Competence Center of Grinding Technology & Precision Engineering (KSF)”. I am deeply indebted to my advisor and head of KSF, Prof. Dr. Tawakoli who has provided me with the guidance, tools and resources to make this undertaking possible. His fully technical review and his supportive discussions had been a great help to finalize this work as well.

I sincerely acknowledge my advisor, Prof. Dr. Wegener, head of the “Institute of manufacturing technology and machine tools” at ETH-Zurich and the director of “Inspire AG, institute of mechatronic production system and manufacturing technology“ for the reviewing of my work, corresponding technical discussion and useful hints.

I appreciate also the support of the Dr. Magg and Mr. Gerlitski from the company “Diamant Gesellschaft Tesch GmbH” for their technical help, SEM microscopy and providing the tools for the experiments. I appreciate the support of the University of Karlsruhe for the residual stress measurements and analysis too.

I am grateful to all students who did their B.Sc and M.Sc thesis regarding dry grinding under my supervision. The results of their work and co-operation are some of the important parts of this work. I would like to thank all my colleagues in KSF for their unconditional collaboration, in particular Mr. Rasifard, Mr. Lewis, Mr. Azarhoushang, Mr. Jandaghi, Mr. Struss and Mr. Rinderknecht. Many friends, faculties, and staffs have provided much support either directly or indirectly during the time I worked in KSF. I would like to take this opportunity to appreciate all their helps. Specially, I would like to thanks my colleagues, Ms. Kohmann, Ms. Matthans and Dr. Philipp, for their administration help during my work in KSF. I sincerely appreciate the support of the library team of Furtwangen University, specially Ms. Gunzenhauser and Ms. Vetter-Hauser.

I am grateful to my parents and family members. My daughter, Rana, I love her with all my heart. And finally, I am deeply indebted and eternally grateful to my wife, Shahrzad, for all her supports.

Zurich, June 2010

Mohammad Rabiey

CONTENTS

SYMBOLS & ABBREVIATIONS	15
1 INTRODUCTION	19
2 STATE OF THE ART	21
2.1 COOLANT REDUCTION METHODS	21
2.2 MECHANICAL & THERMAL INTERACTIONS IN GRINDING PROCESS	25
2.3 THERMAL DAMAGES BY DRY GRINDING OF METALS.....	33
2.4 CBN GRINDING WHEELS	35
2.5 NEW STRUCTURED GRINDING WHEELS	40
3 TASKS AND OBJECTIVES.....	43
4 EXPERIMENTAL EQUIPMENT AND MEASUREMENT PROCEDURES	47
4.1 GRINDING AND DRESSING FACILITIES	47
4.2 INFRARED TEMPERATURE MEASUREMENT SYSTEM	50
4.3 MEASUREMENT OF GRINDING WHEEL CHARACTERISTICS.....	52
4.4 SURFACE INTEGRTY MEASUREMENTS	54
5 DESCRIPTION OF CONCEPTS.....	57
5.1 INTRODUCTION TO MACRO-TOPOGRAPHY	57
5.2 MACRO-STRUCTURING USING SPECIAL CONDITIONING	59
5.3 MACRO-STRUCTURING USING SPECIAL ELECTROPLATING	62
5.4 MACRO-STRUCTURING USING LASER BEAM CONDITIONING ...	63
6 THEORETICAL ASPECTS AND MODELLING	65
6.1 INTRODUCTION	65
6.2 KINEMATIC ASPECTS AND CORRESPONDING MODELLING	66
6.2.1 Implication on wheel macro-topography.....	66
6.2.2 Implication on mean uncut chip thickness and area	71
6.2.3 Implication on dynamic cutting edges based on the stochastic nature of wheel topography	79
6.3 DYNAMIC ASPECTS AND CORRESPONDING MODELLING	86
6.3.1 Introduction	86
6.3.2 Implication on sliding forces and energy	88
6.3.3 Implication on ploughing forces and energy	91

6.3.4	Implication on cutting forces and energy	94
6.3.5	Validation of the force and energy models.....	96
6.4	THERMAL ASPECTS AND CORRESPONDING MODELLING	100
6.4.1	Implication on heat generation and heat partitioning	101
6.4.2	Implication on workpiece temperature	105
6.5	PREDICTION OF PROCESS USING ARTIFICIAL NEURAL NETWORK	108
7	EXPERIMENTAL ANALYSIS	115
7.1	STRUCTURING EFFECT ON GRINDING FORCES	115
7.2	STRUCTURING EFFECT ON SURFACE ROUGHNESS	121
7.3	STRUCTURING EFFECT ON GRINDING ENERGY	123
7.4	STRUCTURING EFFECT ON GRINDING TEMPERATURE	127
7.5	STRUCTURING EFFECT ON SURFACE INTEGRITY	131
7.5.1	Investigation of the microstructure.....	131
7.5.2	Investigation of residual stresses	137
7.6	STRUCTURING EFFECT ON CHIP SIZE.....	141
7.7	STRUCTURING EFFECT ON WHEEL WEAR	143
8	CONCLUSION AND SUMMARY.....	153
	ZUSAMMENFASSUNG	157
	REFERENCES.....	161

SYMBOLS & ABBREVIATIONS

Symbols:

a_d :	mm	Total dressing depth.
a_c :	mm	Depth of cut.
a_{ed} :	mm	Dressing depth, Dressing infeed.
b :	mm	Engaged wheel width.
b_d :	mm	Active width of dressing tool.
c_w :	J/kgK	Specific heat capacity of the workpiece.
d_e :	mm	Equivalent wheel diameter.
d_K :	mm	Grain diameter; mean grain diameter.
d_s :	mm	Diameter of grinding wheel.
d_w :	mm	Diameter of workpiece.
e :	J/mm ³	Specific cutting energy; energy per unit volume.
e_c :	J/mm ³	Total specific cutting energy; Total energy per unit volume.
e_{chip} :	J/mm ³	Specific energy of the chips.
f_{ab} :	--	Relative chip volume.
f_{ad} :	mm/rev	Dressing feed per wheel revolution
$f_{\tau k}$:	--	Ratio of workpiece shear strength to abrasive shear strength.
h_{cu} :	mm	Uncut chips thickness.
\bar{h}_{cu} :	mm	Mean uncut chips thickness.
h_{cu-max} :	mm	Maximum uncut chips thickness.
h_{cu-p} :	mm	Uncut chips thickness in point p.
h_{eq} :	mm	Equivalent chip thickness.
h_g :	W/m ² K	Convection coefficient for an abrasive grain.
h_{wg} :	W/m ² K	Convection coefficient for the workpiece at a grain contact.
k :	--	Constant.
k :	Pa	Shear flow stress of abrasive.
k :	N/mm	Loop stiffness of machine.
l_g :	mm	Geometric contact length.
l_p :	mm	Geometric contact length at point p.
n :	--	Number of grains in wheel.
n' :	--	Number of grains pass contact length in one second.
n_K :	--	Total number of grains in wheel.
q :	--	Speed ratio.
q :	W/mm ²	Heat flux.
q_{ch} :	W/mm ²	Heat flux to chips.
q_{chip} :	W/mm ²	Heat flux to chips.
q_f :	W/mm ²	Heat flux to coolant.
q_g :	W/mm ²	Heat flux to grain.
\bar{q}_g :	W/mm ²	Average heat flux to grains.
q_m :	--	Grain aspect ratio

Symbols & Abbreviations

q_s :	W/mm ²	Heat flux to grinding wheel, Heat flux to abrasive.
q_t :	W/mm ²	Total heat flux.
q_w :	W/mm ²	Heat flux to workpiece.
q_{wg} :	W/mm ²	Heat flux to workpiece at grain contact.
\bar{q}_{wg} :	W/mm ²	Average heat flux to workpiece at grains contacts.
r :	mm	Grain tip radius.
r_o :	mm	Effective radius of wear flat on tip grain.
t :	s	Time.
u :	--	Dimensionless parameter.
v_c :	m/s	Cutting speed, Grinding cutting speed.
v_{cd} :	m/s	Velocity of roll dresser, Dressing cutting speed.
v_{fad} :	mm/min	Dressing feed rate.
v_{ft} :	mm/min	Tangential feed rate.
v_w :	m/min	Speed of the workpiece.
w_m :	mm	Average grain mesh size.
x, y, z :	--	Axis of coordinate systems.
z :	mm	Grain indentation.
z_{crit} :	mm	Critical indentation.
A :	mm ²	Contact area.
A_1, A_2 :	mm ²	Piled up area.
A_{chip} :	mm ²	Uncut chip area.
A_{cu} :	mm ²	Total chip area.
\bar{A}_{cu} :	mm ²	Mean uncut chip area for active grains up to point p.
$A_{cu,i}$:	mm ²	Uncut chip area produced by grain i .
A_{cu-p} :	mm ²	Uncut chip area at point p.
A_R :	mm ²	Scratch area.
A_s :	mm ²	Total grain contact area in contact zone.
A_w :	mm ²	Contact area between wheel and workpiece.
A_{wg} :	mm ²	Projected area of a grain indentation.
\bar{A}_{wg} :	mm ²	Average projected area of grains indentation.
C :	mm ⁻²	Cutting edge density of unit area.
C :	--	Factor for temperature solution taking into account the Peclet.
C_K :	mm ⁻³	Cutting edge density of unit volume.
D_p :	--	Degree of penetration, Degree of indentation.
E :	Pa	Young's modulus
F :	N	Force.
\bar{F} :	N	Average Force, Mean force.
F_n :	N	Force normal to wheel surface.
F'_n :	N/mm	Specific normal force, Normal force per unit width.
F_t :	N	Force tangential to wheel surface.
F'_t :	N/mm	Specific tangential force, Tangential force per unit width.
G :	--	Grinding ratio.
H :	HRC; Pa	Workpiece Hardness.
H_{max} :	mm	Maximum height of the grain above the bond.
H_s :	Pa	Scratch Hardness.
K :	%	Volume percentage of abrasive grain in a wheel structure.

Symbols & Abbreviations

K :	--	Constant.
K_k :	--	Grinding wheel constant.
K_w :	--	Grinding wheel constant.
$K_0(u)$:		Bessel function of second kind order zero for an argument of value u .
L :	--	Dimensionless parameter.
L_K :	mm	Cutting edge spacing.
L_{K-stat} :	mm	Static cutting edge spacing.
N :	mm ⁻²	Cutting edge density.
\bar{N} :	mm ⁻²	Mean cutting edge density.
N_{ch} :	mm ⁻²	Cutting edge density per unit area that do real cutting.
N_{dyn} :	mm ⁻²	Dynamic cutting edge density per unit area.
N_{kin} :	mm ⁻²	Kinematic cutting edge density.
N_{L-stat} :	mm ⁻¹	Static cutting edge density per unit length.
N_{mom} :	--	Momentary number of active cutting grains.
\bar{N}_{mom} :	--	Average momentary number of active cutting grains.
N_{pl} :	mm ⁻²	Cutting edge density per unit area that do ploughing.
N_{sl} :	mm ⁻²	Cutting edge density per unit area that do sliding.
N_{stat} :	mm ⁻²	Static cutting edge density per unit area.
P :	W	Cutting or grinding power.
Pe :	--	Peclet number for moving band source.
$P(p)$:	--	Probability density function of cutting edges.
Q_{ch} :	W	Heat power transferred to chips.
Q_d :	--	Dressing ratio.
Q_f :	W	Heat power transferred to coolant.
Q_s :	W	Heat power transferred to grinding wheel.
Q_i :	W	Total heat power.
Q_w :	W	Heat power transferred to workpiece.
Q_w :	mm ³ /s	Material removal rate.
Q'_w :	mm ³ /mm · s	Material removal rate per unit width of contact.
R :	--	Ratio of the total heat flux into the wheel to the workpiece.
Ra :	μm	Measure of average surface roughness.
R_g :	N	Force on a grain normal to the workpiece.
R_{pv} :	μm	Peak to valley height.
R_{ws} :	--	Workpiece-abrasive subsystem partition ratio.
Rz :	μm	Measures of peak-to-valley roughness.
T :	^o C or K	Temperature.
T_{ch} :	^o C or K	Chip Temperature.
T_{max} :	^o C or K	Maximum value of workpiece surface temperature.
T_{wg} :	^o C or K	Temperature at a contact between grain and workpiece.
$T(z)$:	^o C or K	Workpiece background temperature in depth of z .
U_d :	--	Overlap ratio in dressing.
V_K :	mm ³	Mean volume of a abrasive grain.
V_{tot} :	mm ³	Total volume of a abrasive layer.
V_w :	mm ³	Total volume of workpiece material removed.
V'_w :	mm ³ /mm	Specific volume of workpiece material removed.

X :	--	Dimensionless parameter.
X_{exp} :		Value of experiment.
X_{mod} :		Value of model.
Y :	--	Dimensionless parameter.
Z :	--	Dimensionless parameter.
α :	grad/radian	Pyramid apex angle.
α_w :	m^2/s	Thermal diffusivity.
δ :	mm	Indentation due to elastic deformation.
χ :	--	Contact ratio.
λ_g :	W/mK	Heat conductivity of the abrasive.
λ_w :	W/mK	Heat conductivity of the workpiece.
θ :	grad/radian	Angle, Attack, angle, Tilt angle.
μ :	--	Friction coefficient; grinding force ratio.
ν :	--	Dimensionless correction coefficient.
ν :	--	Poisson's ratio
ρ :	kg/m^3	Density.
ρ_w :	kg/m^3	Density of workpiece.
σ_n :	Pa	Contact stress.
τ :	Pa	Shear stress of the workpiece.
ω :	--	Constant depends on pyramid apex angle.
ζ :	--	Structuring type coefficient.
ζ :	--	Structuring and wheel type coefficient.
Ψ :	grad/radian	Glancing angle.

Abbreviations:

CBN:	Cubic Boron Nitride.
HEDG:	High Efficiency Deep Grinding.
LM:	Levenberg-Marquardt.
RBF:	Radial Basis Function.
AE:	Acoustic Emissions.
HRC:	Rockwell Hardness.
<i>ch</i> :	Index for cutting.
<i>conv</i> :	Index for conventional wheel.
<i>g</i> :	Index defined for a grain.
<i>pl</i> :	Index for ploughing.
<i>stru</i> :	Index for structured wheel
<i>sl</i> :	Index for sliding

Chapter 1

1 INTRODUCTION

Technology is dominated by two types of people: those who understand what they do not manage, and those who manage what they do not understand.

A. Putt, from the book “Putt's Law”

Grinding is a very complex process due to the large number and wide variety of influencing parameters, stochastic nature of grain distribution, and undefined geometrical cutting edges as well as different modes of wheel wear and wheel loading problem. Figure 1.1 is a schematic of the important aspects and parameters of the grinding process.

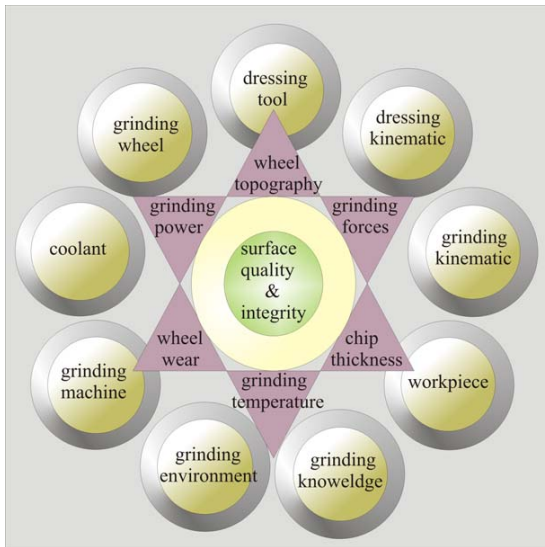


Figure 1.1: A systematic view of the important aspects of grinding process and related parameters

Higher material removal rate along with high surface quality are main goals in grinding processes but unfortunately these two factors are often in opposition, i.e. increasing one of them often means reducing the other. The reason for this is in the nature of grinding process. Increased material removal rate generally causes higher heat generation due to higher energy flux in the contact zone. Higher heat generation often causes higher wheel wear, and thermal damages or quality issues. That is why coolant is needed to reduce the effects of heat generation, heat transfer to the workpiece, wheel loading, and corrosion, and to help transport chips from contact zone.

But on the other hand, when considering the use of coolant in grinding processes the two important aspects are the economical and ecological aspects of wet grinding, which both are the matter of high interest to the industry. In Germany alone, there is consumption of over 850,000 tons emulsion or solution and 54,000 tons oil as coolant [Kloc95]. The cost of these coolant materials as well as filtering and waste disposal, cost of the coolant system itself, as well as maintenance and repair of such systems are so high that they encompass a share of about 16.9 % of overall production costs [Kloc96a]. This is even higher than tool cost. Explosive risks of the coolant, potential health problems for the machine operator, and also waste disposal of non-organic coolant materials are some important ecological problems in this regard. Reduction or elimination of coolant in machining processes is therefore of significant interest.

Dry grinding is thus a favourable process, if it does not cause any thermal damage to the workpiece. Although dry machining with defined cutting edge processes like turning and milling could be very successful to be industrialised, dry grinding has not been fully and successfully applied in industry yet. The main problem is high heat generation by grinding process. That is why a dry grinding process specially by high material removal rate is up to now an aim which is fully the state of the art as high valuable target.

One of the most efficient strategies for reaching this target is to reduce the heat generation. The reduction of heat generation is a rather critical objective for avoiding thermal damages. Most of the energy consumed in grinding is converted to heat. This is because of sliding and ploughing of abrasive grains in the process. Even for the grain cutting process, the frictional energy is very important because of the high wheel speed in grinding. Any aspect which reduces sliding and ploughing in the grinding process has a great effect on the reduction of heat generated on the contact length. The focus of this work as one of the methods for reduction of rubbing and ploughing process in ductile materials is increasing the chip thickness.

Based on this concept, structured grinding wheels can be developed to reduce the heat generation in grinding process which is a goal in dry grinding process. With structuring of the wheel either during production of the wheel or by special conditioning for vitrified and resin bond grinding wheels, it is possible to change the macro-topography of the wheel surface suitable for dry grinding. The present investigation introduces some novel concepts for the structured grinding wheels. The objective is to study the effects of wheel structuring on the reduction of grinding forces and specific energy, as an indicator of heat generation and temperature in dry grinding as well as investigation on the ground workpiece surface quality and integrity. A systematic experimental analysis by comparison of conventional and structured wheels, and description of the possible reasons for the results are the main approach in this work.

Chapter 2

2 STATE OF THE ART

In this chapter, a general overview on the state of the art in reduction of coolant in grinding process as well as a general review on the grinding process in terms of mechanical and thermal aspects are presented. The influence of grinding wheel specification like bonds and hubs, changing the topography due to the loading and wear as well as dressing condition will be reviewed. At the end of this chapter some of the recent structures of the wheels to improve the grinding process are presented.

2.1 COOLANT REDUCTION METHODS

Coolant has a great effect in machining processes, particularly in grinding. The role of the coolant in grinding processes can be categorized into cooling and lubrication in the contact zone, chip transportation, grinding wheel cleaning and corrosion reduction. Among these duties, the lubrication and cooling role are accomplished by reduction of heat generation through lubrication effect by providing a lubricating film and thus lowering the friction, as well as reducing the heat transferred to the workpiece and tool through cooling effect. Grinding wheel cleaning is done by flushing away chips from the grinding wheel surface which helps to reduce loading [Brin99, Hein99]. Coolants are divided into oil-based and water-based types according to DIN 51385. For both cases the coolant additives play an important role in increasing the effectiveness of the coolant.

Several papers have dealt with coolant effects in grinding. Comparison of oil-based and water-based coolants is still a matter of significant discussion. The grinding forces as an indicator of heat generation, wheel wear and workpiece surface roughness are mostly compared for both cases [Tawa05, Tawa07c, Webs02]. The residual stress is another factor which has been studied by researchers as well [Brin03, Brin05, Hein07]. The matter of boiling of the coolant in the contact zone which drastically decreases the coolant effectiveness has also been investigated [Shaf75, Howe87, Guo94, Kuri03].

It is also important to note that coolants have negative effects on the working environment in terms of the health of machinist, pollution and explosive risk (for oil-based coolants). Besides coolant cost, filtering and waste disposal of the coolant are even higher than the tool cost and a significant part of total cost [Kloc96a, Kloc97, Kloc00]. That is why, in many machining processes, decreasing or even eliminating the use of coolant is of special significance in the last decades. Among these machining processes, grinding is the most problematic in this regard, as the heat generation in the contact zone is generally much higher than for other machining process due to high friction between abrasive grits and workpiece [Brin99].

Many attempts have been made to reduce the coolant consumption in grinding processes by different researchers. Figure 2.1 shows a schematic of different strategies and methods employed to reduce the coolant consumption in grinding.

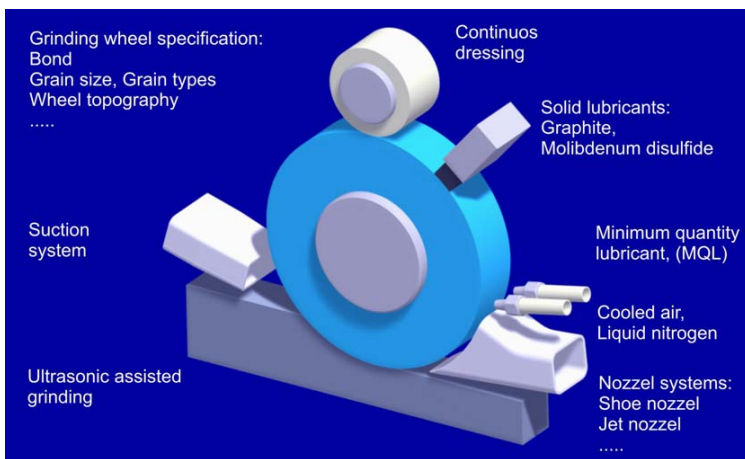


Figure 2.1: Methods for minimizing the use of grinding fluid [Hoff00]

Nozzle systems

Nozzle design is a very broad topic in grinding technology used to achieve the highest possible cooling and lubrication effect. Jet nozzles and shoe nozzles are two main developments in this regard. The coherent jet nozzle developed by Webster et al. helps to reduce the air barrier and to achieve a coolant velocity better matched with grinding speed [Webs02]. The concave form of the jet nozzle provides a longer coherent jet and better enrichment of the coolant in the contact zone [Webs95]. High velocity jet nozzles were investigated by Kovacevic and Mohan [Kova95], to give higher coolant pressure in front of the grinding contact arc. A flow velocity of 365 m/s and maximum pressure of 3800 bar with a flow rate of 3.64 l/min was achieved and compared with conventional nozzles

Shoe nozzles are low pressure systems which force the grinding fluid into the wheel structure by wrapping around the wheel and accelerating it with the grinding speed into the contact zone [Brin04]. The shoe nozzles are in many applications more effective than conventional or jet nozzles as it reduces the coolant consumption flow rate as well as grinding forces [Kloc00, Rame01].

Minimum Quantity Lubricant (MQL)

MQL is the application of a mist of lubricant into a high pressure air stream. The air is generally not cooled and fluid flow rate is extremely low. This technology enables a reduction of the coolant flow rate to values smaller than 50 ml/h [Kloc00]. Tönsch et al. [Töns00] studied MQL method in internal grinding with 24 ml/h and compare it conventional method with 660 l/h and found the reduction of forces but higher radial wheel wear in case of MQL Da Silva et al. [Dasi07] used the MQL method in grinding process with the consumption 40 ml/h and compared it with conventional cooling with 80 l/h and found better surface quality, more compressive residual stress and no loading by MQL method. Sadeghi et al. [Sade08] used the MQL method for grinding of Titanium alloy using alumina as a grinding wheel and found that the consumption between 50-60 ml/h is the optimized coolant supply rate when the normal and tangential forces are minimized.

Cryogenic and cool air

Cooled air has been used as coolant by Choi et al. [Choi01]. In this work, the tensile residual stress at the surface of workpiece was found by increasing the depth of cut. Combination of cooled air and oil has also been investigated and the reduction of oil was reported [Nguy03, Inou04]. A Higher material removal rate without thermal damage was reported in such condition. Hoffmeister et al. [Hoff04, Hoff07] studied the usage of the liquid nitrogen called cryogenic coolant. They also combined this method by minimum quantity lubricant to reduce the coolant. Reduction of grinding forces without problem in surface quality or surface integrity was reported.

Solid lubricants

Graphite and molybdenum disulfide (MoS_2) are the main solid lubricants which have been studied by several researchers. Weinert et al. [Wein98] used graphite in surface grinding by pressurizing it to the grinding wheel surface. The same idea was used by Hoffmeister et al. [Hoff00] for deep surface grinding and pendulum surface grinding and compared with using coolant. The process was not successful in the case of deep surface grinding, but for pendulum surface grinding the grinding forces seen by using graphite were approximately the same as coolant. Salmon [Salm03] used a hard titanium aluminium nitride TiAlN coating on an electroplated CBN wheel followed by a layer of molybdenum disulphide (MoS_2) as hard lubricant. The results showed that the coatings gave reduced wheel wear, lower grinding power, and lower loading. Shaji [Shaj02] applied graphite as lubricant for the vitrified aluminum oxide wheel and compared the process with conventional grinding and with dry grinding. The study shows that the grinding forces, grinding specific energy and grinding

temperature are lower in the case of using graphite compared to the other cases. He also used slotted wheel with its periphery filled with a phenolic resin/alumina-graphite mixture. The results showed an improvement in surface finish and residual stress, lower spindle power, and higher wheel wear, as compared to conventional wet grinding without the solid lubricant [Shaj03].

Continuous dressings

Grinding with continuous dressing is generally carried out to hold the grinding wheels topography and profile constant over the grinding time [West93, Mink03]. The sharp cutting edge and lower loading cause a need for less coolant with increasing material removal rate. The heat generation is also lower compared to conventional grinding and lower alternation of surface integrity over the workpiece length is achieved [Niew95, Hoff02].

Ultrasonic assisted grinding

Almost all the experiments applied for grinding process with ultrasonic assistance, either by workpiece vibration or tool vibration show a considerable reduction on grinding forces and energy which demonstrate the lower heat generation in process [Daus04, Zapp98, Uhlm98]. Tawakoli et al. [Tawa08b, Tawa08c] reported the results of ultrasonic assisted dry grinding using CBN wheel of steels. They observed the reduction of normal forces as well as no thermal damages of workpiece compared to the conventional grinding process where the thermal damages occurred as burn points on the workpiece surface.

Dry grinding

Tönshoff and Jung [Töns00] performed internal cylindrical dry grinding with sol-gel Aluminum-oxide of 100Cr6 steel specimens and reported fast loading of the wheel on specific material removal of 170 mm³/mm. Voll [Voll01] investigated on cylindrical dry grinding of C45 specimens with Aluminum-oxide with specific material removal rate of 15 mm³/mm·s. Dry grinding was used for the heat treatment of metals specially using Aluminum-oxide wheel [Brin03]. Dry grinding using a CBN wheel was also investigated with high cutting speed and for external cylindrical grinding [Köni94, Kloc96a, Kloc96b]. In the investigation the cutting speed up to 300 m/s with electroplated wheel was used. It is found that with increasing the grinding speed it is possible to increase the material removal rate without thermal damages. A material removal rate of 50 mm³/mm·s with cutting speed of 300 m/s was achieved. The problem of loading was also reported which causes the thermal damages and decrease the tool life. The contact length by external cylindrical grinding is generally small, which is the reason for higher material removal rate achieved by this process especially with a higher grinding speed compared to surface or internal grinding [Tawa07d]. Besides, the heat generation in dry grinding depends also on the grinding wheel width. Generally with small wheel width it is possible to have higher removal rate by dry grinding. In the case of the surface grinding or internal grinding the problem of heat generation and thermal damage is more significant. A higher grinding speed (over 150 m/s) needs special machine tools [Mück99]. These problems

cause the process to have very low material removal rate in the case of the surface grinding with resin or vitrified bond wheels, especially if low surface roughness is needed [Tawa08a]. The dressing method plays also a significant role on the heat generation by grinding process [Kloc05a]. Grain size and concentration are the other parameters influenced on the heat generation [Kloc05a]. A higher grain size with lower concentration cause lower heat generation but higher roughness as well. The main problem perhaps in dry grinding will be higher material removal rate by fine grinding which is one of the focus points of this work.

2.2 MECHANICAL & THERMAL INTERACTIONS IN GRINDING PROCESS

Grinding is a material removal process utilising a grinding wheel which is made up of a large number of randomly positioned abrasive grains [Chen02]. Unlike the defined cutting edge tool, this random nature of grain distribution on the wheel surface makes it more difficult to derive an analytical force, energy and temperature model describing many dynamic and complex interactions in the grinding process [Tawa07a]. The specific energy which is the energy required to remove a unit volume of material is generally extremely high in machining processes with undefined cutting edges like grinding, compared to the processes with defined cutting edges like turning or milling [Kloc05a]. Almost all the mechanical energy which causes elastic and plastic deformations, friction and surface generation through the process is converted to heat in the contact area [Brin03]. As a matter of fact, all components which take part in the chip formation process are affected by the thermal loads. Heat is partitioned to the workpiece, grinding wheel, chips and coolant [Rowe98]. In dry grinding, as there is no coolant, the share of coolant action in heat partitioning is almost zero as heat transfer to the surrounding air is very low and negligible. Any thermal damage in the workpiece is because of high heat generation in the tool-workpiece contact zone and the conduction of heat into the workpiece. Traditionally, dimensional accuracy and surface finish are considered to be the main criteria of the quality of the grinding process. However it is found that below-surface or near-surface properties such as workpiece residual stress, microstructure and hardness also belongs to the overall workpiece quality [Snoe78, Torr78]. Study of the interaction between the grains and workpiece has been a key role for understanding the process. The experimental analysis and the interpretation of the results as well as models have mainly been performed to facilitate the process. However there are still many unsolved problems and controversies in modelling of interactions occurring in grinding [Mari04]. The mechanical and thermal interaction of grain and workpiece are the main interactions to be studied.

2.2.1 Rubbing, ploughing and cutting

The interaction between grains and workpiece for ductile materials can be generally categorised into 3 phases [Tawa08a]. In the first phase of grain interaction with the

workpiece, a grain induces elastic deformation on the workpiece surface. In this phase there exists only a rubbing action. Then, in the second phase, with increasing the grain penetration into the workpiece surface, plastic deformation starts to occur. Due to the large negative rake angle of the grain, this phase, called the ploughing phase, produces a side flow to form ridges as well as piled up material in front of the grain [Zumg87]. This second phase continues up to the point that the plastic deformation reaches to a critical value along with sufficient grain penetration into the workpiece (Z_{c-crit}) so that the chip is formed and the cutting process takes place [Hokk88a, Hokk88b]. This is the only phase in which material removal occurs, and thus the only efficient one. This last phase requires the lowest specific energy [Malk89]. The other mechanisms of rubbing and ploughing lead to extremely high heat generation in grinding [Mari07].

Malkin [Malk89] showed that a portion of energy, referred to as sliding or rubbing energy, is consumed by the sliding friction between the wear flat area on the grain and the workpiece surface. His study proves a strong correlation between the grinding forces and wear flat area of abrasive grains. Hokkirogawa [Hokk98] studied the effect of attack angle on the ploughing process. He developed a map with which a critical attack angle, depending on the material properties of the abrasive and workpiece, can be found after which the cutting process occurs. De Vathaire et al. [Deva81] used an upper bound method to study and model the ploughing process for a pyramid grain shape. Torrance et al. [Torr90, Torr05] developed his model for ploughing in three dimensional effects to model the ploughing process. Shaw [Shaw96] proposed an extrusion model to represent the interaction of abrasive and workpiece.

Rubbing or sliding, ploughing and cutting mechanisms occur continuously during grain interaction with the workpiece. Their share are very different depending on the grain shape and grain distribution or general topography of the wheel as well as grain and workpiece material properties, grinding parameters and coolant enrichment [Tawa06]. The uncut chip thickness has a direct influence on the share of the different mechanisms. Giwerzew [Giwe03] investigated the ploughing process at a low cutting speed by scratch testing of a single grain. He has shown that, for the metals, with increasing uncut chip thickness the ploughing effect is decreased. Zeppenfeld [Zepp05] did similar tests for γ -Titanium aluminides as a ceramic workpiece. He found, in contrast with the results of Giwerzew, that the ploughing is actually increased with increasing the chip thickness in the case of ceramic materials.

The most important goal in grinding processes is usually to increase the cutting share, since rubbing and ploughing are usually the main source of undesirable heat generation [Tawa05]. Heat is generated through the friction between chips and abrasive grains as well as between chips and workpiece [Mari07]. Increasing the chip pocket size or available empty space on the wheel surface causes a decrease in both types of friction [Tawa08a]. Besides, increasing the mean uncut chip thickness in metal causes a decrease the ploughing and rubbing processes resulting in a reduction of heat in grinding of metals [Tawa08a].

2.2.2 Thermal aspects of grinding

Reduction of grinding temperature and thermal damage requires an analytical knowledge of the thermal aspects of grinding and heat partitioning as well as a deep understanding of kinematic aspects and chip formation processes. During the grinding process, several interactions take place between: the grain and workpiece, the bond and the workpiece and the chip and the bond. The interaction of the grain and the workpiece is actually the only desirable process as it results in chip removal. The interaction of the chip and bond results in friction and bond erosion. Interaction between bond and workpiece also results in undesirable friction. Due to friction and plastic deformation the mechanical energy introduced into the grinding process is almost completely converted into heat. [Brin94]. Figure 2.2 shows the different type and location of heat sources due to grain-workpiece interaction.

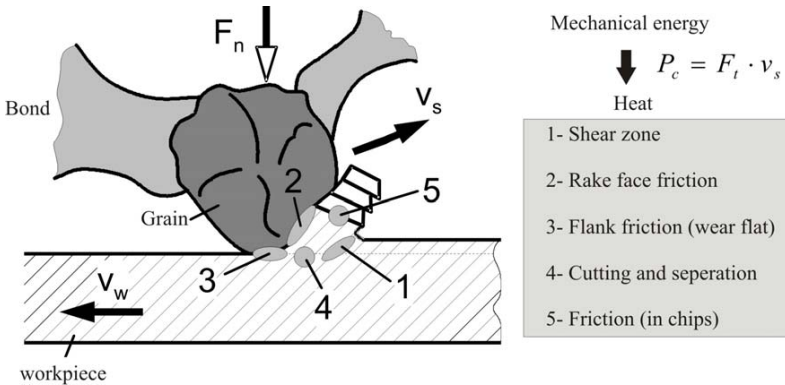


Figure 2.2: Heat generation in grain interaction with workpiece [Brin94]

In grinding, almost all the heat produced in the process is partitioned into the wheel, chips, workpiece and coolant. The exact determination of the amount of heat transferred to each part of the system is a very difficult task and has not yet been achieved. The most important part, however, is the share of heat flux into the workpiece. An amount between 5 to 85% of generated heat was found to flow into the workpiece [Brin94]. It can be seen that the complex influences of different parameters cause a wide variety of different partition ranges and much more difficulties to investigate the thermal aspects of grinding.

Previous research works in thermal aspects of grinding were started perhaps by the work of Outwater and Shaw [Outw52]. They investigated the surface temperatures generated in fine dry grinding based on heat generation on a shear plane, similar to cutting process. Their results show that about 65% of heat is partitioned into the chips. Hahn [Hahn62] proposed the friction hypothesis wherein rubbing forces on the wear flat of the abrasive grain and workpiece play a major role as compared to the forces due to cutting. By considering the heat

due to shear work as well as heat due to friction, Malkin and his colleagues [Malk89, Malk07] concluded that almost all of the ploughing and sliding energies at wear flat and 55% of the shear heat (in cutting process) are conducted to the workpiece. Choi [Choi86] asserts that 73% of the heat flows into the workpiece. It should be noted in this regard that the heat partitioning depends on the grinding parameters.

Des Ruisseaux and Zerkle [Desr70] conducted thermal analysis of the grinding process by considering the effects of coolant. They concluded that the effect of coolant in the contact zone is not considerable. Shafto et al. and Howes et al. [Shaf75, Howe87] mentioned that the effects of coolant depend on grinding temperature and the boiling point of the coolant. The influence of coolant would be drastically decreased if the coolant temperature were to reach the boiling point. Jin et al. and Lavin et al. [Jin01, Lavi90] showed that the effect of coolant is very considerable in the case of the creep feed grinding. Stephenson et al. and Rowe [Rowe01b, Step03] concluded that the heat flux into the chips is considerable in HEDG (High Efficiency Deep Grinding) comparing to the creep feed or conventional grinding.

There are different research works which concentrate on temperature modeling and the heat partitioning of the wheel and workpiece. Lavine developed a simple analytical model for heat partition between the wheel and the workpiece surfaces and the grinding fluid [Lavi88]. Demetriou and Lavine [Deme00, Lavi00] extended the convective heat transfer model to cover both up-grinding and down-grinding. Rowe et al. [Rowe96a, Rowe98, Rowe01a] developed analytical models to determine the grinding temperature by energy partition based on two strategies. The first strategies are based on the workpiece experiencing elevated background temperatures due to distributed action of all the grains operating in the grinding zone. This analysis is designated as the wheel contact analysis or global contact analysis. They considered the heat source at the workpiece surface as a band heat source moving across its surface at the given feed speed. The second analysis is based on the localized temperatures experienced at the abrasive grain tip – workpiece interface by spikes elevating above the background temperature. This analysis is designated as the grain contact analysis or local contact analysis. For this analysis, the grain is modeled as a stationary body subjected to a constant circular heat source in the grinding zone. Guo and Malkin [Guo94, Guo99, Guo00] investigated the variation of the energy partition along the length of contact in grinding. In their work, the models developed with consideration for grinding wheel pores filled with coolant. Hou and Komandori [Hou03a, Hou03b] presented an interesting thermal analysis of grinding processes by considering the stochastic nature of the wheel topography. Skuratov et al. [Skur07] developed a mathematical modeling for grinding temperature using two variable functions by solving the differential equations by Laplace and Fourier transformation and Green's function method.

It is notable that, at the moment, a fully theoretical calculation is only possible with very high inaccuracy. The temperature model can still be performed by calculation or measurement of specific energy and heat flux [Mari04]. That is why the measurement and modelling of the

grinding forces and specific energy are still the only way for accurate temperature calculation [Mari04]. In this work the model proposed by Rowe is used for thermal analysis by considering the stochastic model to calculate tangential force and specific energy.

2.2.3 Mechanical aspects of grinding

The single grit-workpiece interaction can be characterized by the uncut chip thickness and the amount of rubbing and ploughing produced in the process. From these, it is theoretically possible to model grinding force, specific energy and surface roughness. A complete review paper by Tönshoff et al. [Töns92] presents different models of wheel topography, chip thickness, grinding forces, grinding energy, temperature, surface integrity and surface roughness in terms of basic models. Furthermore, Brinksmeier et al. [Brin98] identified and summarized basic parameters that are fundamental to constructing process models for grinding processes. Most of these models were empirical relations between the input grinding parameters as depth of cut, grinding speed, speed ratio, equivalent diameter and the target parameters such as force, mean uncut chip thickness, etc. with some coefficient which must be identified experimentally. Brinksmeier et al. [Brin06] later published a review paper on modeling and simulation of the grinding process. In this paper they completely reviewed and cited the various new research studies.

Topography

Among all the parameters influencing the grinding process, the wheel topography plays a key role. Grain spacing and grain height over the bond greatly influences the grain penetration ability and chip size, and thus also affects the thermo-mechanical load on the grain and the workpiece. By increasing the grain spacing, the chip size will generally be increased [Fisc00]. A high concentration of abrasive on the wheel surface thus means smaller grain spacing and less wheel porosity [Tawa06]. By proper selection of porosity and grain spacing, it is possible to reduce the thermal damage [Brun98]. The amount of rubbing, ploughing and cutting processes highly depends on the wheel topography [Tawa08a]. The wheel topography as well as grinding parameters define the number of grains which come to contact with the workpiece. This number is one of the most important criteria in the grinding process. Actually, not all abrasive grains on the surface of a grinding wheel participate in the chip formation process. Some may cut, others may rub or plough, and a large number may not be participating in the grinding process at all but take a free ride. These can be referred as static and active cutting edges according to the review paper of Tönshoff et al. [Töns92]. The static cutting edges are the total number of cutting edges measured on the wheel at a specific depth relative to the overall engagement. It depends on the grain size and wheel micro and macro topography. Active cutting edges are the edges which come into contact with the work piece and depend on the static cutting edges and grinding parameters. With lower number of active cutting edges, the active grain distances will be increased and this causes an increase in chip

thickness [Tawa08a]. Figure 2.3 shows a schematic of active grains and active grain distances and the effect of larger grain separation on chip thickness.

Verkerk [Verk77] reported that adjacent cutting edges may be considered as a single cutting edge because they lack sufficient chip clearance space to act independently. He also reviewed different methods to measure static and active cutting edges. The random geometry and the probabilistic distribution of the cutting edges on the wheel surface makes the grinding process stochastic in nature. Using statistical algorithms, Lortz [Lort75] calculated the active cutting edge density and the chip thickness that follows a logarithmic standard distribution. Liao [Liao95] investigated on a fractal characterization of diamond grinding wheel topography. Hou and Komanduri [Hou03a] developed a model using stochastic approaches based on the normal distribution function of the grain size to approximate the grinding wheel topography.

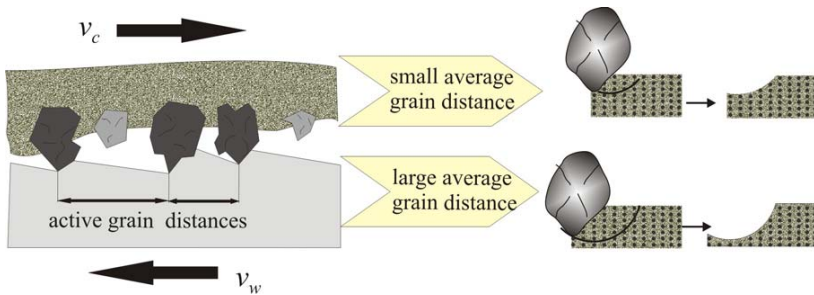


Figure 2.3: Schematic of active cutting edges and its effect on chip thickness

Chen and Rowe [Chen02] as well as Torrance and Badger [Torr00] developed a topography model based on a spherical grain shape distributed randomly in the bond and considered the effect of the dressing on changing wheel topography. Koshy et al. [Kosh93, Kosh99] developed a topography model for diamond grinding wheels which statistically estimates the average grain protrusion height and the normal distribution of the grain size. Hegeman [Hege00] developed a three dimensional model of wheel topography by a randomized arrangement of three dimensional ellipsoidal grains. Nguyen and Butler [Nguy05a, Nguy05b] developed a numerical model for the surface topography and then characterized a three dimensional workpiece surface.

Chip thickness

Based on the combination of wheel rotation as well as workpiece translation in surface grinding, the analysis of the grain path leads us to model the uncut chip thickness. A similar expression can be obtained based on the equality of total chip volume and total material removal rate. The different models were developed for the uncut chip thickness by various researchers [Kass 69, Wern71, Malk89, Warn98, Zepp05]. More recently, the grinding

process was simulated from the interaction of each grain, where the relative cutting edge positions are randomly generated [Chen96a, Chen96b, Chen96c, Zhou02] or deterministically given by previous measurement of the wheel topography [Steff83, Inas96]. Hecker et al. [Heck03a, Heck03b] modeled the chip thickness by Rayleigh probability density function and using this model calculated grinding force and power. Zeppenfeld [Zepp05] calculated more precisely the uncut chip thickness by considering the kinematic of surface grinding. Weber [Webe08] also calculated the uncut chip thickness by a parametric algorithm in surface grinding. Warnecke and Zitt [Warn98, Zitt99] developed a model as well as a software for chip formation and grinding forces. In their work, the grain shape and topography of the wheel are modeled in 3D form and the kinematic of the engagement are defined by mathematical models. Braun [Brau08] tried to continue the work of Zitt [Zitt99] in terms of kinematic simulation by defined-grain structured electroplated bond wheels. Pinto et al. [Pint08a, Pint08b] performed similar work by the defined grain structure of brazed grinding wheels.

Force and energy

Grinding force and specific energy are the essential parameters for evaluating the efficiency of the process. The prediction of the thermal characteristics of the process is not possible without proper prediction of the grinding forces and energy. The grinding forces generally are increased with increasing material removal rate [Malk89]. Relationships between grinding speed ratio, grinding power and material removal rate were investigated by Lindsay [Lind71]. Increasing the depth of cut at the constant feed rate in surface grinding will increase the grinding forces. But in contrast with forces, the specific energy increases generally with decreasing of the material removal rate, which called “size effect” [Rowe97]. Increasing the chip size usually decreases the specific energy [Mari04]. This is a key point for evaluating the grinding forces and grinding specific energy and also for heat generation [Tawa08a]. By variation of the grinding parameters the chip size or mean uncut chip thickness can vary so the forces and specific energy are varied. The other parameter is the topography of the wheel [Wern71]. Fine dressing increases the number of kinematic cutting edges which causes a reduction in mean uncut chip thickness and increasing the specific energy. Coarse dressing on the other hand reduces the specific energy. Blunt grains increase rubbing and ploughing in the process and increase the specific energy [Rowe97].

Hecker et al. [Heck03a, Heck03b] investigated the effect of the number of active cutting edges and developed a force and surface model. Comparison of various models for grinding forces and specific energy shows that the input parameters of depth of cut, grinding speed, workpiece speed, equivalent diameter, wheel and workpiece specification are the most important parameters in prediction of the process forces and energy [Töns92]. Tönshoff et al. [Töns92] presented several models and finally a basic model for the prediction of force and specific energy in grinding. But all these models require many experiments to find the accurate empirical coefficients in their equations.

2.2.4 Artificial neural network as an empirical analysis

The neural network method can be used as a numerical modelling approach to simulate and predict the behaviour of the grinding process [Kloc03]. It is a powerful computational tool which models the basic behavior of logical thought patterns by numerical representation, using many artificial neurons which are individual computational elements linked to each other. The typical network has a single layer of input neurons connected to at least one layer of hidden neurons, and then to a layer of output neurons. Each neuron is normally connected to all neurons in the following layer by a set of numerical weights and each is modeled by its own activation function; this is known as the Multilayer Perceptron (MLP) network. Overall the method can be a very useful feature if empirical or theoretical modeling proves to be very complex since it avoids the use of most theoretical modeling tools, and its ability to generalize a function provides an advantage over normal regression or empirical modeling [Brin06, Özel05]. Figure 2.4 presents a schematic of an artificial neural network.

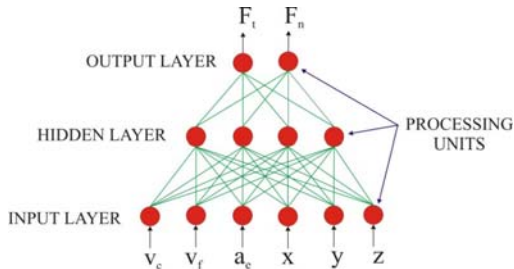


Figure 2.4: Schematic of artificial neural nets; input, hidden and output layer

Neural networks have already proven successfully for a variety of machining operations in studies conducted by many authors. Liao and Chen [Liao94] used experimental data to model a creep feed grinding process using back propagation for training the networks. Liu et al. [Liu97] used the scale conjugate gradient algorithm to predict grinding burn. A study published by Kwak and Song [Kwak01] used acoustic emission RMS (Root Mean Squared) average and Fast Fourier Transform as neural network inputs to successfully detect grinding burn and chatter vibration on-line. De Aguiar et al. [Deag05] highlighted the effectiveness of the neural network method as compared to statistical detection tools in the grinding of ductile-brittle transition materials, which are more difficult to diagnose on-line because of their special mechanical properties. Kumar and Choudhury [Kuma07] used Levenberg-Marquardt (LM) method to predict the wear and surface roughness by electro-discharge grinding.

Another application of the neural network was presented in a publication by Brinksmeier et al. [Brin98], in which measured grinding forces, workpiece surface roughness, and workpiece residual stresses were provided as inputs to a neural network used to optimize cylindrical grinding processes off-line. This work included comparison with fuzzy prediction and

multiple regression methods, highlighting the advantages and disadvantages of each. Furthermore, Brinksmeier et al. [Brin06] presented the application of artificial neural networks in grinding with more detail in his review paper and referenced many related research studies.

In neural network methods, there are a large variety of algorithms which can be applied but the most common example of such is the Levenberg-Marquardt algorithm which has already been very successfully applied to the neural network prediction of turning operations and some grinding operations. A very good example of this is the study by T. Özel and Y. Karpat [Özel05], in which the LM algorithm is used successfully to train various back-propagation networks for predicting tool flank wear and workpiece surface roughness in hard turning.

Although LM method is generally faster than other algorithm types, it is normally better suited to roughly linear prediction problems. The LM method also typically begins to lose its advantage if the network becomes very large and complex, losing computational efficiency [Demu01]. Another disadvantage of this type of network is its tendency to over-train or to become too well adapted to patterns that cannot be generalized well to the extent that is needed for suitable prediction [Wang01]. An alternative to this is the radial basis network, or RBF (Radial Basis Function) network type. Although it is similar to the MLP type network in that it uses a similar arrangement of neuron layers and weights and biases and with its own unique radial basis activation functions in the hidden layer, the RBF network offers a unique advantage. It begins with a single neuron in the hidden layer, and in the training process adds neurons to this layer until the output error is minimized [Demu01]. It thus eliminates the trial and error which is typically seen in hidden layer design of a typical MLP network. Wang et al. successfully applied the RBF network to classify ‘no contact’/‘normal grinding’/‘burn’ states on-line using acoustic emissions and power signals for different grinding operations [Wang01]. The result was an accurate on-line detection tool which highlighted the effectiveness of the fast-training radial basis function architecture as compared to other network and numerical analysis methods [Wang01].

2.3 THERMAL DAMAGES BY DRY GRINDING OF METALS

The heat generated by different mechanisms often leads to a high temperature increase in the grinding zone. High temperature in the contact zone may cause various types of thermal damage. Surface discoloration, structuring changes, tensile residual stress and cracking are some of the examples studied by many researchers [Mari04, Kloc05b, Malk07].

Two primary types of thermal damage in steel are widely referred to as re-hardening in the form of white layers which increases the hardness of the metal workpiece surface, and tempering or softening which decreases the hardness of the metal workpiece surface. In the first case, i.e. increasing the hardness by re-hardening, a rather hard surface layer can be

observed in some regions of the workpiece surface. Most of the time, this hard layer is seen as a white-coloured markings under the microscope after etching, so it is called white layer. Controlling such re-hardening as a potential heat treatment process has been investigated by Brinksmeier [Broc99, Brin03, Brin05]. Typically the white layer is accompanied by a soft layer located between the white layer and bulk material, which is also darker than the bulk material. The re-hardening surface layer is most likely one of the un-tempered martensites and the softer layer is referred to as one of the over-tempered or tempered martensites [Shaw96]. The presence of such a re-hardening surface layer depends on the chemical composition of the steel workpiece, grinding heat generation, and the coolant effect. The time-temperature-transition diagram (TTT Diagram) can be used to predict the transformation and/or decomposition of austenite [Avne74]. The temperature rise rate as well as cooling rate has a great influence on the hardening of steel. Under slow or moderate cooling rates, the carbon atoms are able to diffuse from the austenite structure. Then phase transformation to bcc (body-centred-cubic) takes place. This gamma-to-alpha transformation takes place by the process of nucleation and growth and is time dependent. A short cooling time inhibits the diffusion of carbon atoms out of solution, and carbon becomes trapped in the solution. The resultant structure is a supersaturated solid solution of carbon trapped in a body-centred tetragonal structure, which is called martensite.

The characterisation of the white layer is high brittleness and susceptibility to cracking and therefore may be considered as damage to the workpiece [Kloc05b]. However the fine grain microstructure martensite shows high hardness, but lower tendency for crack propagation and improved corrosion resistance. The fine grain microstructure of martensite is observed by a white color in many research studies [Zaru02, Denk03 Kloc05b]. In the case of the grinding of heat treated metals with high hardness, it is possible that the structuring change causes the reduction of hardness by precipitation of carbon from martensite in carbide forms [Mari04]. Rowe et al. [Rowe 95, Rowe96a, Rowe96b] showed that the grinding temperature for steels which causes the discoloration begins from 400-500 °C. Malkin [Malk06, Malk07] was able to calculate the grinding power induced in workpiece needed to change the structure which causes thermal damage. The severe type of thermal damage is known as burn which may also occur even without visible discoloration [Rowe01b]. Thermal damage to metal workpieces often results in tensile residual stresses in the workpiece. If the material is sensitive enough, the workpiece can crack due to residual stress or to the localized thermal expansion from the grinding process. This can occur either immediately after grinding or during in-service loading, thereby significantly reducing component life. The thermal stress was found to be the most significant contributor for the tensile residual stress and there is an onset temperature below which a tensile residual stress cannot be generated [Chen98]. The heated surface layer cannot expand because the bulk material remains cool causing a plastic deformation of the surface. By decreasing the temperature of the surface, thermal contraction leads to a tensile residual stress [Brin82a]. Moreover, this type of residual stress depends not only on the temperature magnitude but also on the temperature gradient [Kato00].

Residual stresses can also be compressive in grinding processes. The mechanical load on the workpiece by grinding wheel during the contact time generates a stress field which exceeds the yield strength of the material due to the plastic deformation [Brin82b]. Phase transformation of metals can also generate residual stresses. If the transformation is accompanied by a variation in the specific volume (for example austenite to martensite transformation), the interaction between transformed material and bulk material, where no phase transformation occurs, causes the residual stresses [Brin82a]. Several authors investigated the residual stresses in grinding [Cape02, Hein07]. The results demonstrate that the generation of residual stress in grinding is an extremely complex phenomenon as there are many parameters involved in the final results. That is why up to now there is no fully validated analytical model for the residual stress in grinding processes and almost all the models are rather empirical.

2.4 CBN GRINDING WHEELS

CBN as a superabrasive is characterized by very attractive range of properties as: high wear resistance, high hardness, acceptable thermal stability, good thermal conductivity and toughness and sharp cutting edges [Kloc05a]. CBN is one of the hardest materials and the hardest abrasive beyond 750 °C. In addition to good wear resistance, the chemical stability under high temperatures and good thermal conductivity make CBN the proper choice for dry grinding of metals and also for higher material removal rates [Köni94, Kloc95, Kloc97].

As with diamond crystal growth, CBN grain shape is governed by the relative growth rates on the octahedral (111) and cubic planes. However, the (111) planes dominate and, because of the presence of both B and N in the lattice, some (111) planes are positive terminated by B atoms and some are negative terminated by N atoms. In general, B (111) plane growth dominates and the morphology is a truncated tetrahedron. Twinned plates and octahedra are also common. The morphology can be driven toward the octahedral or cubo-octahedral morphologies by further doping and/or careful control of the pressure-temperature conditions [Mari07]. CBN is thermally stable in nitrogen or vacuum to at least 1,500°C. In air or oxygen, CBN forms a passive layer of B₂O₃ on the surface, which prevents further oxidation up to 1,300°C. CBN does not show any significant reactivity by transition metals such as iron, nickel, cobalt or molybdenum until temperature reach in excess of 1300 °C. This is reflected a low wear when grinding these materials with CBN abrasive in comparison with wear of diamond abrasives [Mari07]. By comparison, the wear rate using the alternative of SiC abrasive is 40 times greater than CBN. This is a further example of the need to consider the combined effects of the mechanical, chemical, and thermal wear processes as much as abrasive cost. The thermal conductivity of CBN is almost as high as that of diamond. At room temperature, thermal conductivity is 200 to 1,300 W/mK. The thermal expansion of CBN is about 20% higher than diamond.

2.4.1 Wheel bonds and wheel hub

The type of wheel bond has also great effects on the heat generation and chip formation in grinding. Table 2.1 demonstrates the properties of the different bonding [Koch00].

Table 2.1: Properties of different bonds [Koch00]

Bond	Metal	Resin	Vitrified	Electroplated
Heat conductivity	++	O \ +	-	++
Wear resistance	++	O \ +	+	++
Profile stability	++	O	+	++
Dressability	O	+	++	-
Self sharpening	O \ +	++	++	-
Mechanical strength	+	O	O \ +	++

++ very good \ + good \ O satisfactory \ - not suitable

Vitrified bond grinding wheels with superabrasives are suitable for dry grinding because of their good heat transfer properties. The resin bond wheel can quickly reach a self-sharpening effect, so they are also suited for dry grinding [Tawa07a]. Electroplated bond wheels have superior heat conduction properties, but they cannot usually be dressed [Tawa07a]. Wheel hub type also influences the heat transfer from the contact zone. The steel and aluminum have generally more advantages in comparison to resin and aluminium-resin due to their mechanical strength and heat conductivity. Table 2.2 compares different wheel hubs.

Table 2.2: Properties of different wheel hubs [Koch00]

Wheel hub	Steel	Aluminium	Aluminium-Resin	Resin
Heat conductivity	++	+	O \ +	-
Vibration absorption	-	-	O \ +	++
Mechanical strength	++	+	O	O
Capability for high grinding speed	+	++	O \ -	O \ -

++ very good \ + good \ O satisfactory \ - not suitable

2.4.2 Wheel loading and wheel wear

Wheel wear as well as wheel loading are two time-related factors that drastically affect the heat generation, surface quality and wheel life. The grinding wheel condition continuously

changes due to grain wear and chip accumulate in the spaces between grits. Figure 2.5 shows the different types of wear and loading in the grinding process.

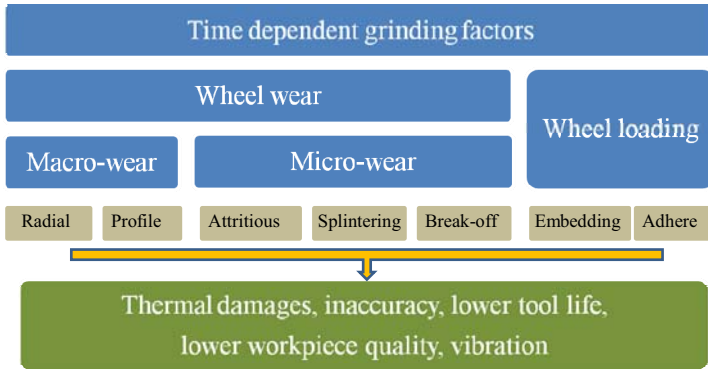


Figure 2.5: Time dependent factors in grinding process

Wheel loading

Grinding wheel loading can be classified to two categories: the chips either adhere to the bond/grain or embed themselves in spaces between grains and fill the porosities [Laue79]. König and Lauer [Laue80] mentioned also that welding between the initial chips and those built up by the loaded grits in the ensuing chip formation process could also accelerate loading. Loading results in excessive rubbing leading to an increase in heat generation. It causes some serious problems in grinding processes such as: excessive vibration, reduced part surface quality, rapid increasing of grinding forces and specific energy, higher temperature in the contact zone and reduction of wheel life. It is also possible that the chips deposit themselves back on the workpiece surface [Dorn84, Naga89].

Sharpening is the most common technique for controlling wheel loading and renews the cutting ability of the wheel. There are some different methods used to perform the sharpening process. Some of the methods include abrasive jet sharpening, chemical erosion, grinding mild, long chipping steel and electrical discharge sharpening method [Tawa93]. A very common method in sharpening of CBN wheels is grinding a vitrified aluminum oxide block against the wheel. From the newer methods of sharpening, vibration and laser assisted methods can be noted. Zhang and Miller [Zahn03] have explored the use of vibration to de-load grinding wheels. Chen [Chen04a, Chen04b] applied a laser cleaning technique to maintain a sharp wheel. Jackson et al. [Jack07] also investigated on wheel dressing and cleaning with laser. In addition, under an optimized grinding condition, self sharpening makes the process more efficient and can prevent the loading of a grinding wheel [Tawa93, Tawa06].

Wheel wear

Wheel wear may lead to profile deviation, roundness deviation and changes in grinding wheel sharpness and efficiency [Mari07]. The profile and roundness deviation are one of the macroscopic aspects of wear and the wheel sharpness can be categorized as a microscopic aspect of wear. Wear effects can be ascribed from a tribological point of view to the following main mechanisms: abrasion, adhesion, tribochemical reaction, surface disruption and diffusion [DIN 5032, Mari07]. The above mentioned wear mechanism leads to different types of wear which can be basically divided into attritious or flattening wear, splintering, partial grain break-off and total grain break off [Mari07]. Grain fracture is largely controlled by the friability of the abrasive, which is the ability of an abrasive to fracture. More friable grains are more susceptible to grain fracture prior to their final dislodgement from the wheel [Mari04]. Bond fracture is controlled by the wheel hardness. Harder wheels provide stronger bonds and reduce bond fracture [Malk89].

Attritious wear involves dulling of the abrasive grains due to the rubbing action between the grains and workpiece. Wear flats which form on the abrasive grains are mainly due to attritious wear [Uhl94, Shi06]. Grain splintering wear is caused by micro-cracks resulting from mechanical and thermal tensions. These micro-cracks lead to a micro-fracture or even to partial grain break-off [Enge02, Mari07]. In the case of total grain break-off, whole abrasive grains are detached from the bond. Thus bond breakage is the main reason for this type of wear. The bond can be broken either by mechanical overstresses due to high grinding forces or by excessive process temperatures [Malk89, Webe08]. Initially small wear flats are formed during dressing and then increased by attritious wear. Wear flat generation depends on the wheel grade and the friability of the abrasive grains. In the early stages of a grinding process, the grinding wheel is worn mainly by grain fracture or bond fracture due to the previous dressing operation. After dressing operation, some grains become less tightly gripped by the bond material and they can be easily broken off [Tawa05]. As grinding wheel use continues, however, micro-fracture begins to subside and attritious wear becomes the dominant wear mechanism. Attritious wear is significant because of the large number of grains that rub the workpiece material without cutting action. This attritious dulling of abrasive grains is one of the main reasons why the specific energy and heat generation in grinding is much higher than that of other machining processes. As the wear flat area increases, the sliding energy also increases. With larger wear flats, the force required to penetrate into the workpiece also increases, and consequently the tangential normal force is increased [Malk89]. Although attritious wear is only a small portion of the total wheel lost, it is considered the most important wheel wear mechanism because it controls the size of wear flats, the amount of workpiece burn and the magnitude of grinding forces [Chen98]. The most important method for refreshing the wheel from flattened grains, especially for resin bond, vitrified bond and metal-bond wheels, is wheel dressing. Dressing also plays an important role in micro-topography of the wheel in terms of active cutting edges and the resulting workpiece surface roughness.

2.4.3 Wheel dressing

The topography of the wheel surface is fully dependent on the dressing parameters such as depth of dressing or infeed (a_{ed}), dressing speed (v_{cd}) and dressing speed ratio (q) in the case of using rotary dressing rollers, as well as dressing lead (f_{ad}), appearing as overlapping ratio (U_d). The shape of the diamond dressing tool and the characteristics of the grinding wheel are also matters which should be taken into consideration for dressing. The active width of the dresser (b_d) depends on the shape of the dresser and on the infeed [Schu96, Link06]. Figure 2.6 illustrates the dressing parameters and their relation for the case of a rotary dressing wheel [Schu96].

The overlapping ratio has a great influence on the static cutting edges and the topography of the grinding wheel. Generally the dressing operation can be categorized into fine and coarse dressing types depending on the overlapping and dressing ratios as well as infeed. The fine dressing operation refers to the combination of large overlapping ratio ($U_d > 6$) with small infeed. Conversely, the combination of small overlapping ratio ($U_d < 4$) and large dressing infeed is categorized as coarse dressing operation.

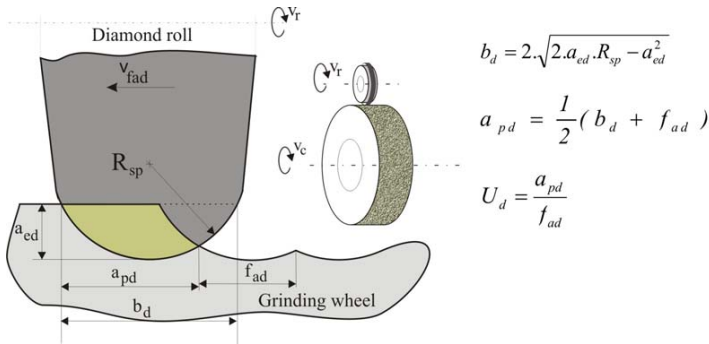


Figure 2.6: Dressing parameters using dressing roll and the geometrical relationships [Schu96]

If the dressing lead is bigger than the active width of the dresser i.e. $f_{ad} > b_d$, then the kinematic of the dressing operation causes a spiral form on the wheel surface with theoretical peak to valley height equal to dressing infeed. This kind of dressing can be used for special conditioning of the wheel which will be explained as one of the methods used to improve the dry grinding process seen in chapter 5.

2.5 NEW STRUCTURED GRINDING WHEELS

As it is concerned in previous sections, in order to reduce heat generation in grinding of metals, the number of total grains (static cutting edge density) and the number of grains which actually come to contact with workpiece (dynamic cutting edge density) should be reduced. Furthermore the chip spacing over the wheel surface should be increased. These targets can be realized by the newly designed wheels called structured wheels. T-Tool and T-Tool profile were originally developed to fulfill this requirement [Tawa94, Tawa01].

T-Tool is an innovative tool system with discontinuous or intermittent cutting process. This tool is plated with super abrasive grains in a single layer. As it is illustrated in figure 2.7, various slots and teeth are located on the outer surface of the tool.

In contrast to conventional tools the superabrasive coating is not situated on the outer surface of the tool but rather on the inner flanks. The innovative concept for this tool is its function as a multilayer superabrasive tool, although the tool has just one layer of superabrasive. The roughness of ground workpiece, the grinding forces and grinding power are thus relatively constant throughout the wheel life. T-Tool can guarantee a low grinding temperature, a long tool life, fine and consistent generated surface roughness and simple coolant conduction system. In contrast with conventional electroplated grinding wheels this tool can be dressed and needs no sharpening [Tawa94].

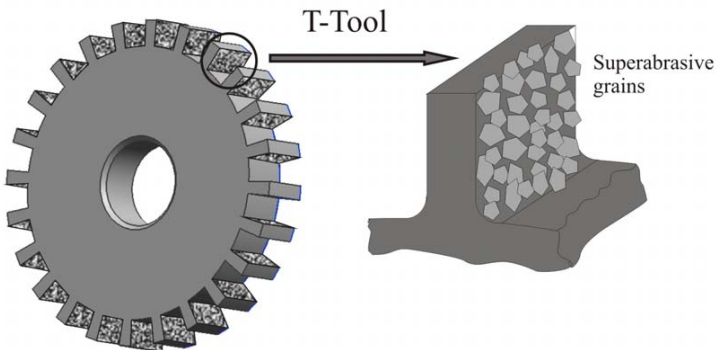


Figure 2.7: Schematic of T-Tool and the location of superabrasives on T-Tool

The next developed variation of T-Tool is the T-Tool Profile [Tawa01]. The principle of the T-Tool Profile is demonstrated in figure 2.8.

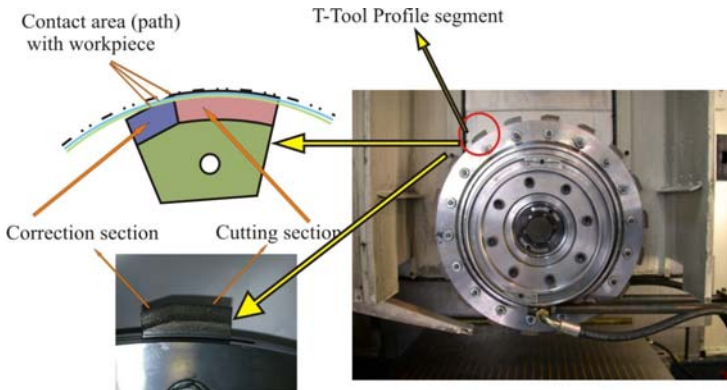


Figure 2.8: T-Tool Profile and an example of geometry of the segments in T-Tool-Profile

The grinding wheel consists of many segments with special geometrical aspects. Every segment is made up of a rounded cutting profile section with radius of the grinding wheel, and a straight correction profile section which is sloped away from the cutting path. Both of these sections have the same cross section profile and are joined at an interface. The rounded profile section or cutting section comes into contact with the workpiece and is subjected to wear, hence losing its geometry. The straight profile section or correction section is in contact with the workpiece only at the interface with the rounded profile. It does not come into contact with the workpiece at any other point. Since the interface of both the profile sections has the correct profile geometry, it is not worn and therefore produces a correct profile on the workpiece. With further wear, the interface of both sections moves forward so that the new and therefore, exact profiles are always ready to come into contact with workpiece, until the straight profile is used up and the end of its life is reached. The first experiments by grinding of the ductile and brittle materials have shown that the T-Tool profile, in comparison to conventional CBN grinding tools, can sometimes reduce grinding forces by up to 50% [Tawa01].

Conditioning tools can also be used for structuring of vitrified or resin bonded grinding wheels. The conditioning tool can be a form roller or a stationary diamond tip. Different patterns can be produced on the wheel. Verkerk et al. [Verk77] studied the effect of a simple groove by dressing on the surface roughness of the workpiece. Stepien [Step07] used such a structured grinding wheel and modeled the grinding forces. Oliveira et al. [Oliv10] used a similar idea and developed a system to produce different patterns by actuating a dressing tool with high frequency which is related to the rotational speed of the grinding wheel.

The next developments are based on the concept of micro-structuring of the grinding wheel surface. The defined position of the grains on the wheel surface either by brazing or

electroplating provide a good possibility for increasing the uncut chip thickness as well as chip pocket size. Figure 2.9 illustrates these two types of grinding wheels. Burkhard [Burk01, Burk02] investigated such tools, called Engineering Grinding Tools (EGT), for honing and grinding applications using brazing of a single layer diamond and CBN on the tool surface. By using these wheels, a decrease in grinding forces and an increase in material removal rate were achieved. Furthermore, Pinto et al. [Pint08b] used the same method and created different patterns to optimize the external grinding process.

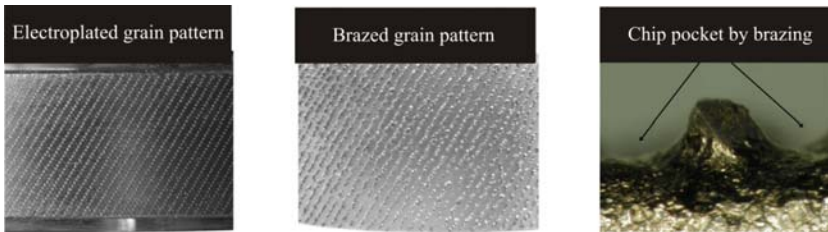


Figure 2.9: Wheel macro topography by Engineering Grinding Tools [Pint08a]

The same concept was developed and investigated by Aurich et al. [Auri03, Brau08] using electroplating instead of brazing techniques.. Their results show also reduction of forces and temperature in the surface grinding process.

Chapter 3

3 TASKS AND OBJECTIVES

Dry grinding is one of the most favourable and simultaneously difficult machining processes. The most important limitation for the researcher in dry grinding processes has been the material removal rate, due to the risk of thermal damage on the workpiece surface or subsurface. Higher material removal rate is coupled with higher heat generation. As in fully dry grinding there is no coolant to transfer the heat from the contact zone, a major part is transferred into the workpiece and causes thermal damages. Therefore material removal rate is limited by dry grinding. This constraint can cause an increase in processing time as well as production cost. The technical target of this dissertation is to increase the material removal rate without thermal damage or negative effects on the surface integrity of the workpiece. In order to reach this target chip formation should be so optimised that minimum possible friction and corresponding heat energy are generated.

The structuring of the wheel is one of the ways to reduce the friction and heat generation. The effect of structuring has not been investigated by dry grinding yet. So far, it has not been used in the industrial application. Hereby the objective of this research is to investigate and explain the effect of structuring of a grinding wheel on the process. It is assumed that structuring gives more opportunity for each cutting edge to do real cutting instead of rubbing or ploughing. In this research study, special structuring will be provided by dressing and conditioning processes of the resin and vitrified bonds, laser structuring of vitrified wheels, and special design and production of electroplated wheels. All of the mentioned methods for structuring of the wheel are new and have not been applied even in research works yet. A systematic approach towards the task is applied by variation of the grinding parameters and grinding wheels, and evaluation of the grinding outputs in terms of surface quality, surface integrity, grinding force and energy and wheel wear. Fig 3.1 shows the global aspects of the dry grinding process which should be taken into consideration. Although such parameters as workpiece material and grinding kinematic are also very important in grinding, to concentrate more on the input parameters of grinding wheels and grinding parameters, the grinding kinematic is limited to the surface grinding and workpiece material restricted to the 100Cr6

test specimens. In order to reach the above mentioned targets and a systematic approach to the objectives, the following partial work packages are considered:

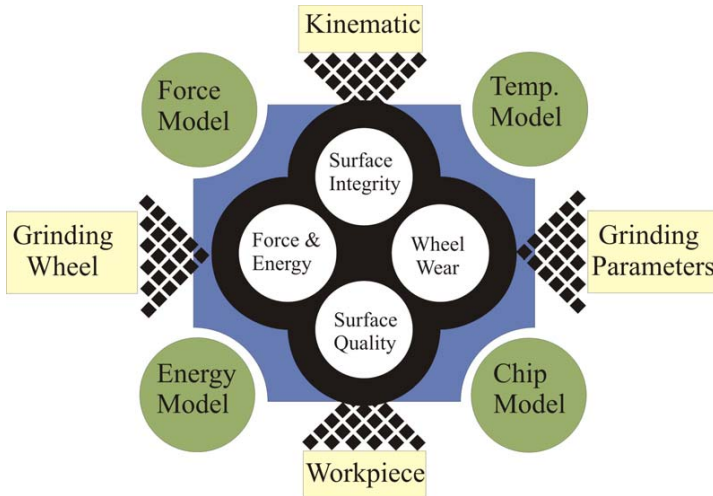


Figure 3.1: Schematic of the important aspects in dry grinding and objectives of the dissertation

Input parameter variation

- Process parameters

With the variation of different process parameters such as cutting speed, depth of cut and feed rate by different grinding wheels, the applicable parameters should be defined and also the implicated modelling should be verified.

- Grinding wheel types

Vitrified, resin and electroplated bond wheels are used to evaluate the corresponding parameters and modelling.

- Percentage of the contact layer after structuring either by conditioning, laser or electroplating

Process modelling

- Kinematics and chip formation model

The new concepts have a great influence on chip formation and kinematics of the process. The effect of the variation of input parameters on the chip thickness will be modelled.

Tasks and Objectives

- Stochastic analysis of the process

The stochastic nature of grain distribution on the wheel surface has a great influence on the process results. Any modelling which is expected to be near to reality should consider this stochastic nature. In this work, this matter has to be taken into consideration.

- Force and energy model

A force model for dry grinding must be developed. A series of experiments is conducted to calibrate the model. The effects of structuring to increase the mean uncut chip thickness and decrease the grinding forces are going to be modelled.

- Thermal model and assessment of grinding temperature

The effects of structuring on heat distribution and thermal analysis of the dry grinding process based on the existing temperature models, as well as verifying these models should be studied.

- Neural network simulation of workpiece burn, grinding forces, and roughness

The assessment of grinding burn and forces as well as prediction of roughness of the ground surface using neural network simulation will be studied.

Assessment of grinding forces, specific grinding energy and surface roughness

- Grinding forces

The grinding forces which vary according to variation of inputs such as depth of cut, feed rate and cutting speed, as well as structuring, will be characterised.

- Surface roughness of the workpiece

The roughness of the ground surface will be studied and the influences of wheel structuring and input parameters will be characterised.

- Specific grinding energy

The specific grinding energy will be investigated under the variation of the equivalent uncut chip thickness as one of the most important parameters in the grinding process.

Assessment of surface integrity of the workpiece and of grinding wheel wear

- Surface integrity of the workpiece

Grinding burn is a form of thermal damage that reveals itself as visible discoloration on the ground surface in steels. The burn is accompanied by material microstructure changes as well as residual stresses on the workpiece. Both matters are also studied and the effect of structuring on surface integrity will be discussed.

- Wheel wear

The effects of special structuring on grinding wheel wear will be studied and the results will be illustrated. In addition, the effect of wheel loading will be investigated.

Chapter 4

4 EXPERIMENTAL EQUIPMENT AND MEASUREMENT PROCEDURES

In this chapter, the test facilities and instruments which were used for experimental analysis and measurements will be explained.

4.1 GRINDING AND DRESSING FACILITIES

The grinding machine, grinding wheels and dressing equipments are the main facilities which are necessary for tests and experiments in the grinding process. Hereby these three items will be briefly described.

Grinding machine

Surface grinding machine	Machine technical information
	Max. spindle power :85 KW
	Max. rotational speed of spindle :7500 (rpm)
	Max. grinding length :800 (mm) Max. grinding width :800 (mm) Max. grinding height :800 (mm)
	Max. feed rate :30 (m/min)

Figure 4.1: Micro-Cut AC8 surface grinding machine used in all experiments.

Experimental Equipment and Measurements

The grinding tests were done by a CNC surface grinding machine type Micro-Cut AC8 from the company ELB-Schliff Werkzeugmaschinen GmbH, as illustrated in figure 4.1. The machine is equipped with an NC controller of Sinumerik 8400 from the company Siemens AG. The position resolution of the machine is 1 μm .

Grinding force measurement

A four-piezoelectric component system of type 93366BB from the company Kistler AG was used as a dynamometer to measure grinding forces. Each of three orthogonal components of force were amplified with a separate amplifier. A low pass filter was used to eliminate high frequency noise. Using an A/D converter and a signal processing system, the data was transferred to a PC with corresponding software as well as correct calibration, the grinding forces were accurately measured.

Grinding wheel types

Three different wheel bonding types were used in the experiments: resin, vitrified and electroplated wheels. All of the tests were performed using CBN-abrasive wheels with a diameter of 400 mm, width of 15 mm and with grit size of B126 provided by the company Diamant Gesellschaft Tesch. The wheel specifications as well as type of structuring and the approximate contact layer resulting after structuring used in this work, are illustrated in table 4.1.

Table 4.1: Wheel specification, structuring type and corresponding contact layer

Grinding wheel specification 400 x 15 (mm x mm)	Structuring type	Contact layer (%)			
		100%	75%	50%	25%
Vitrified bond CBN grinding wheel, B126 C125	Diamond conditioning	100%	75%	50%	25%
Vitrified bond CBN grinding wheel, B126 C125	Laser conditioning	100%		80%	
Resin bond CBN grinding wheel, B126 C100	Diamond conditioning	100%	75%	50%	25%
Electroplated bond CBN grinding wheel, B126	Special electroplating	100%		22%	

The structured wheels had the same bond and grit size as a normal (conventional) wheel. For the resin and vitrified bonds, a structuring with approximately of 25%, 50% and 75% contact layer was performed to be compared with the conventional wheel. The structuring of vitrified bond wheel using laser with about 80% contact layer, as well as structuring of electroplated wheel with about 22% contact layer, were also applied to the CBN wheels. The concept of structuring of different wheels will be explained in more detail in chapter 5.

Experimental Equipment and Measurements

Dressing and conditioning tools

Dressing of the vitrified and resin bonded wheels was done using a rotary diamond roll from the company Dr. Kaiser. The diamond tip radius of the dresser was 0.2 mm. Conditioning of the grinding wheels was achieved by stationary as well as rotary dressers. For a CBN wheel the dresser diamond type can be CVD (Chemical Vaporized Deposition) or PCD (polycrystalline Diamond). In this study the CVD stationary diamond dresser was used for the resin bonded wheel, and a PCD diamond dressing roll which was rather flat at the tips used for the vitrified bond wheel to produce the special macro-topography of the grinding wheel surface. Figure 4.2 shows both dressing tools used for conditioning of the grinding wheels.



Figure 4.2: The two types of dressing tools used for wheel conditioning; a) CVD stationary tool, and b) PCD rotary diamond wheel

The vitrified bond grinding wheel was conditioned with a diamond roll dresser with a width of 0.5 mm and inclined angle of 60° . The same condition was applied for the resin bond wheel, this time using stationary single point CVD diamond dresser. Hereby, as the stationary single point dresser has more wear comparing with rotary diamond wheel dresser, the dresser tip was measured under the microscope to define each time the real form of the diamond tip. The initial radius of the diamond tip was 0.5 mm with an inclined angle of 60° . Dressing tool wear makes the tip so flat that the width of the tip of the dresser which will be in contact with the grinding wheel varies after some dry conditioning, up to 0.85 mm from the primary condition. The wear amount of the conditioning tools must be taken into consideration in calculation for the conditioning.

4.2 INFRARED TEMPERATURE MEASUREMENT SYSTEM

Temperature measurement was carried out by an infrared point Optris Thermometer CT from the company Optris. Sensor temperature range was -40 to 900 °C. The system accuracy is $\pm 1\%$ of measured data. The repeatability of the system is $\pm 0.5\%$ where the response time of the system is 150 ms. The emissivity and transmissivity of the sensors were adjustable between 0.1-1.1 using programming keys to calibrate the system. To have a more accurate emissivity the portion of the workpiece facing the sensors was painted with a black color. The optical resolution of 22:1 with a CF lens of 0.6 mm focused spot diameter at 10 mm distance was the best condition which could be used to measure the temperature in dry grinding setup by this system. The temperature which was measured by the system is the average of a spot circle with diameter of 0.6 mm. The system is calibrated using a precise thermometer by heating the same black colored workpiece (that which was also used in grinding) in an oven, and simultaneous temperature measurement with both systems. To have flexibility for re-positioning of the sensors after grinding with a definite depth of cut, a vertical positioning system was developed to adjust the system with workpiece surface level. Figure 4.3 illustrates the set-up of the temperature measurement system.

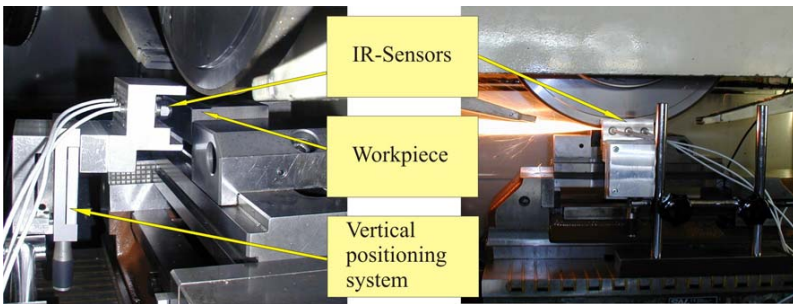


Figure 4.3: Infrared temperature measurement system set-up

Due to the high response time of the system, this instrument is generally not accurate enough for high precision temperature measurement to develop or verify a heat or temperature model. But the goal, in this work, was to compare the tendencies of the effects of structured wheels and conventional wheels on workpiece temperature during grinding. That is why, for the stated purpose, the measurement is accurate enough. Besides, in the experiments with temperature measurement, the feed rate is selected rather low to reduce the effect of low frequency response. The other problem of temperature measurement by point sensors is the precise focusing of the sensor on the defined exact measuring points. In reality this is rather difficult and it takes so much time for a good test reliability that it is almost impossible to achieve. To solve this problem, three sensors were used which were installed at a definite position on the developed fixture. The sensors were installed at different heights from a given

Experimental Equipment and Measurements

reference level (workpiece surface level). The height distance between sensors was 0.3 mm. The sensors were levelled parallel to the grinding wheel direction of movement (feed direction). The sensors were not used to measure temperature at an exact defined position on the workpiece, as it can be seen from figure 4.4. The measured temperatures were instead used to find the maximum temperature on the workpiece surface using extrapolation approach, as explained below.

Grinding wheel	: B126, C125, Vitrified	Grinding speed	: $v_c = 60$ m/s
Wheel width	: 15 mm	Feed rate	: $v_{ft} = 0.5$ m/min
Wheel diameter	: 400 mm	Depth of cut	: $a_c = 20$ μ m
Material	: 100Cr6, 60 HRC	Grinding type	: Dry grinding

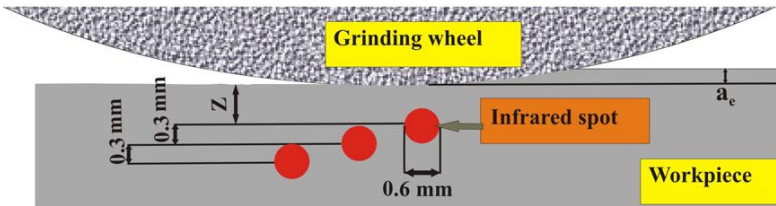
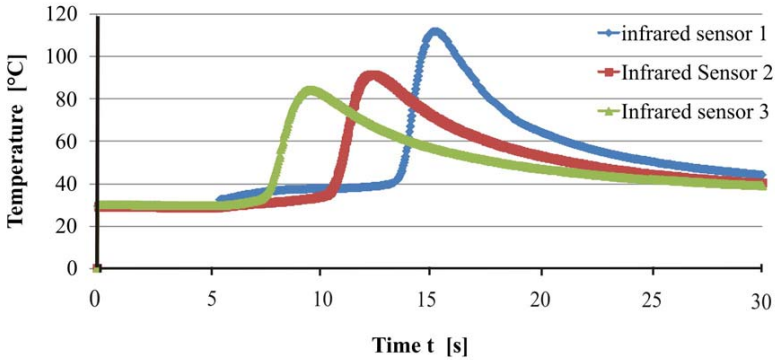


Figure 4.4: Temperature measurement by infrared system

It is well known and widely reported by different authors that the temperature change in the case of conduction heat transfer in steel has an exponential relation with distance [Taka66, Kato00]. Based on this theory, the following formulation can be written for the grinding process setup [Kato 00]:

$$T(Z) = T_{\max} \cdot e^{KZ} \quad (4.1)$$

Where $T(Z)$ is the temperature at point z under the heat source (contact point) in degrees Celsius. T_{\max} is the maximum temperature at the workpiece surface (where $z=0$). K is a constant which depends on the grinding parameters and material properties and Z is the distance under the workpiece surface in meters. Based on figure 4.4 for the three temperature measurement sensors, it can be written:

$$T(Z) = T_{\max} \cdot e^{KZ} \quad \text{Sensor1} \quad (4.2)$$

$$T(Z + 0.0003) = T_{\max} \cdot e^{K(Z+0.0003)} \quad \text{Sensor2} \quad (4.3)$$

$$T(Z + 0.0006) = T_{\max} \cdot e^{K(Z+0.0006)} \quad \text{Sensor3} \quad (4.4)$$

In these equations, $T(Z)$, $T(Z+0.0003)$ and $T(Z+0.0006)$ are measured and known. As it was mentioned, to have more accurate results, the tests were mostly applied with low feed rate to reduce any error due to low frequency response.

4.3 MEASUREMENT OF GRINDING WHEEL CHARACTERISTICS

The methods employed to monitor the topography of the grinding wheel can be categorized to stylus and optical techniques. The stylus method used for vitrified and resin bond wheel after special conditioning. The optical microscopy used to monitor the macro-topography of the electroplated as well as laser structured vitrified wheel.

Measurement of wheel macro-topography using replica

There are several problems with measurement using a stylus directly on the CBN wheel surface. The most significant is wear of the stylus tip during tracing of the wheel surface. As CBN is very hard and would be directly in contact with the expensive stylus, the wear causes inaccurate measurement and defects in the stylus. On the other hand, if the radius of the stylus is large enough to reduce the wear effect, the accuracy of measurement would be poor due to limited vertical movement of the stylus on the tips and valleys. That is why the measurement is normally made using a replica of a portion of the surface, and a suitable size stylus tip should be selected to accurately replicate the surface. In this study, the stylus method was used on replicas using appropriate replication material. Figure 4.5 illustrates the measurement results of the trace across a 12mmx8mm replica, creating a 3D topography model using a measuring machine of type MarSurf TS50 from the company Mahr GmbH (Germany) with appropriate software from the same supplier.

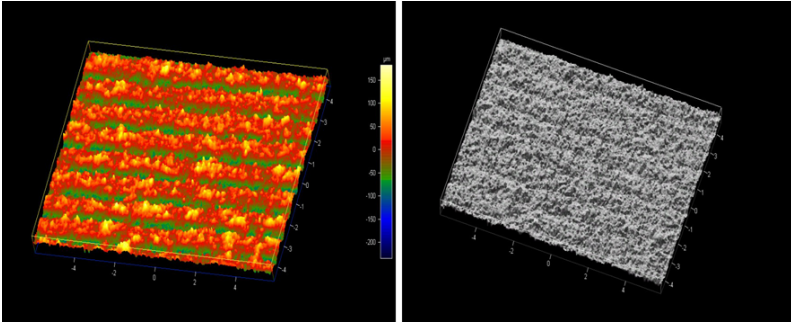


Figure 4.5: Macro-structure measurement of the special conditioned resin bond CBN wheel, using stylus measurement technique on a replica

The grinding wheel surface demonstrated in figure 4.5 was of the resin bonded wheel which was conditioned to produce a single spiral using a CVD single point dresser. The measurement presents a spiral producing a macro-topography of about 25% abrasive contact layer (figure 4.5 is a pair or negative pattern of the wheel surface). Another method incorporating the stylus is to measure the macro-structure of the wheel based on external cylindrical grinding of a metal workpiece so that the wheel and workpiece have the same number of revolutions per minute. In this setup, the negative pattern of the wheel will be replicated on the workpiece. Then, the workpiece can be traced by a roughness tracer and with calculation software the pattern on the workpiece can be recognized and measured. However, due to the ductility and plastic deformation of the workpiece, this method is not accurate enough.

Optical digital microscopy and SEM of wheel topography

For the structured electroplated wheel as well as structured vitrified wheel produced by laser beam conditioning, the optical microscopy measurement technique gives rather accurate results as the macro topography is rather good visible. The optical digital microscope type VHX 100, from the company Keyence was used for macro and micro topography measurements. With a 2.1 million CCD image sensor, the optical lenses provide up to 1000X magnification with which even the very smaller grains can be detected and measured. The system is provided using a 3D and depth composition function. With low magnification, a relatively large field of view can be achieved, including a number of abrasive grains. The bond and grains are not always easy distinguished, especially for vitrified wheels with rather high abrasive grain concentrations. By means of the digital microscopy and higher magnification with multiple pictures in different focusing depths, and using special software, it is possible to produce a 3D picture of the grains to view the micro-topography of the wheel. An example of micro-topography measurement is presented in figure 4.6.

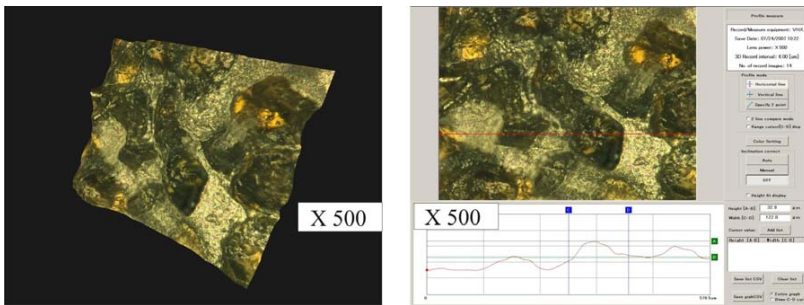


Figure 4.6: Micro-topography measurement using 3D digital optical microscopy

The CBN wheel surface shown has an electroplated bond with a grain size of B126. Scanning Electron Microscopy (SEM) observation was also done to track the wheel micro-topography changes, as well as investigation of grinding wheel loading.

Wheel wear measurement

In order to evaluate total wheel wear as well as surface quality of the workpiece, a roughness and form measuring system of type Hommel Tester T8000 from the company Hommel-Etamic GmbH was used. The wheel wear measurement was carried out by taking a shallow grinding pass on a thin steel specimen which was wider than the wheel, and then using the option of form tracing on the T8000 measuring instrument. The workpiece surface roughness was periodically measured vertical to the grinding feed direction in order to evaluate grinding wheel wear.

4.4 SURFACE INTEGRITY MEASUREMENTS

The workpiece surface integrity in terms of microstructure, hardness and residual stresses was measured to evaluate the quality of the ground surface. Hereby the measuring instruments which were used are briefly described.

Metallographic analysis

Metallographic analysis was one of the most important analyses for evaluating the microstructure of the workpiece. Workpiece specimens were prepared from the ground workpiece as well as bulk material. The specimen is provided by cutting, lapping, polishing and etching the workpiece. A 3% solution of alcohol - nitric acid was used for the etching. Then the specimen was investigated with an optical microscope. The optical microscope used for metallographic analysis was Variophot from the company Leitz with up to 1000X magnification.

Experimental Equipment and Measurements

Hardness measurement

The hardness as well as micro-hardness measurements were carried out with a hardness measuring instrument Miniload 2 from the company Leitz. For the Vickers micro-hardness test a proven load of 1.96 N (HV) and for hardness test a proven load of 9.81 N were applied. The hardness was measured in different regions of the specimen to investigate the effects of heat and temperature at different heights below the ground surface.

Residual stress measurement

Residual stress analysis of the ground workpieces was performed at the University of Karlsruhe based on X-ray diffraction using the $\sin^2\psi$ -method on the $\{211\}$ -lattice plane of the ferrite phase in the steel samples. A ψ -Diffractometer Karlsruher Design equipped with a scintillation counter and a V-filter on the diffracted beam path was used to collect photon intensity from a Cr $K\alpha$ -radiation source. The measurements were conducted over the range $148^\circ \leq 2\theta \leq 166^\circ$ at a step size of $\Delta 2\theta = 0.1^\circ$ per 10 second and 15 different tilt angles were used over the range $-70^\circ \leq \psi \leq 70^\circ$ at $\Delta\psi = 10^\circ$. The primary beam spot size was defined by a collimating tube of diameter 1.5 mm while the divergence of the diffracted beam was controlled by a symmetrising slit. The stress state was derived from the strain data assuming that the material is homogenous and elastically isotropic, using the following X-ray Elastic Constants: Young's Modulus $E_{\{211\}} = 220000$ MPa and Poisson's ratio $\nu^{\{211\}} = 0.28$.

Chapter 5

5 DESCRIPTION OF CONCEPTS

In this chapter, the new grinding wheel concepts developed for dry grinding are presented. The special macro-topography produced by structuring using conditioning of the resin and vitrified bonds will be explained. The special structured electroplated wheel to realize discontinuous grinding, as well as special structured vitrified bond wheel using the laser beam process will be described.

5.1 INTRODUCTION TO MACRO-TOPOGRAPHY

The topography of the grinding wheel surface plays an important role in the bi-lateral interaction of the wheel and workpiece in terms of chip formation, heat generation, workpiece surface quality and wheel wear. The cutting process in grinding is the sum of the singular microscopic cutting process whose temporal and local super position leads to macroscopic material removal [Mari07]. Hereby one of the most important parameters is the dynamic cutting edges [Kloc05a]. The number of dynamic cutting edges is the most relevant wheel surface parameter which can give us proper information about grinding performance. The number of dynamic cutting edges depends on the static distribution of cutting edges on the wheel as well as kinematic of the grinding process and the dynamic grinding effects. The static number of cutting edges, which is the total number of cutting edges on the wheel over the bonded surface at a definite level, is determined by the initial wheel structure and characteristics, which are the parameters such as grain size, wheel porosity and cutting edge density; as well as by the wheel dressing operation.

Based on consideration of the grain interactions, the relationship between grinding parameters (or inputs influencing the grinding process), and outputs of grinding process, can be summarised. The high efficiency of the grinding performance may be achieved by optimisation of the grinding wheel surface topography and chip formation, in contrast with the material properties as well as the grinding environment. The grinding environment includes mostly the cooling and lubrication processes used, and the machine tool.

The grinding system behaviour is thus considered primarily from the viewpoints of geometry, kinematics, dynamic, energy, and material properties. The performance of a grinding process, particularly of the grinding wheel, is usually assessed using force, power, temperature, and workpiece surface roughness, as well as workpiece surface integrity.

The overall topography of the wheel surface can be categorized into macro and micro topography. The macro-topography as well as micro-topography of the grinding wheel define the type and form of the cutting edges, as well as grain spacing and grain height over the wheel surface [Tawa08a]. Any topography change has a significant influence on the total grinding process in terms of heat generation and workpiece quality [Tawa06]. With structuring of the wheel either during production or in later stages by special conditioning in the case of vitrified and resin bonded wheels, it is possible to change its micro and macro-topography.

The micro-topography defines the micro-geometry, type and form of the cutting edges. Hereby the general grain density, grain shape and grain type are considered at the time of manufacturing. The process forces and energy are greatly influenced by micro-topography. The grains, which lose their sharpness and become flat, cause more micro rubbing and micro-ploughing and produce more heat during the process. That is why the sharp grain in dry grinding is a matter of importance. And because of the same reason proper dressing process has key role in dry grinding.

The macro-topography is defined through grain location and distribution on the wheel surface, amount of porosity and rate of concentration of porosity, as well as geometry and contour of the wheel. Hereby, the placement of a grain or a group of grains and space between the grains, where there is no contact between wheel and workpiece, is a matter of important consideration. The macro-topography has a great influence on the grinding process and also plays an important role by changing the number of dynamic cutting edges, and cutting condition.

In this research study, a defined macro-topography by structuring of different wheels was developed by applying three novel methods of:

- Defined macro-structure using special conditioning
- Defined macro-structure using laser conditioning
- Defined macro-structure using a special electroplating process

The next section presents each of the three above mentioned methods and the resulting macro-structure of the wheels, followed later by corresponding modelling of different grinding parameters based on the novel conditioning tools.

5.2 MACRO-STRUCTURING USING SPECIAL CONDITIONING

Explanation of the general concept

As it is mentioned in the previous section, in grinding processes, chip formation has a major role in all aspects of the process and it should be optimised so that minimum possible rubbing between grinding wheel and workpiece, and corresponding heat is generated. The grits which do not apply real cutting but instead cause ploughing and rubbing action should be out of contact as much as possible. In the other words, the opportunity for the dynamic cutting edges to perform only real cutting instead of rubbing or ploughing, should be increased.

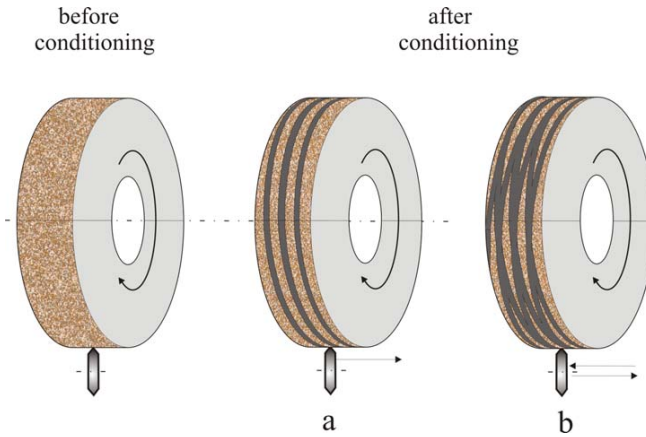


Figure 5.1: Macro-structure schematic of grinding wheel surface before and after conditioning; (a) single spiral and (b) double spiral in opposite direction

The first idea to be discussed in this section is to provide a spiral groove on the wheel surface using conditioning of the wheel with rather high feed rate of the dressing tool to produce the helical screw pattern with defined lead on the wheel surface as shown in figure 5.1. At least one such spiral groove must be produced on the whole periphery of the wheel so that we can label it a special defined surface structure on the wheel. The angle of this spiral depends on the conditioning parameter and shape of the dresser, particularly the form of the dresser tip. The depth of the groove must be so defined that the grain at the bottom of the grooves are never in contact with the workpiece during the whole process, even after wheel wear occurs. The suitable bonds for such conditioning are vitrified and resin bonds.

The reduction of static cutting edges by definite conditioning of the grinding wheel produces a specific macro-structure on the wheel surface, giving more chance to each cutting edge to perform real cutting. With this new structure, the maximum chip thickness will be increased

to a condition, depending on the material specification, grit size, structuring condition and grinding parameters. This maximum chip thickness has a key role in each grinding process and especially in dry grinding without lubrication. Figure 5.2 shows the cross section of the wheel in two different positions.

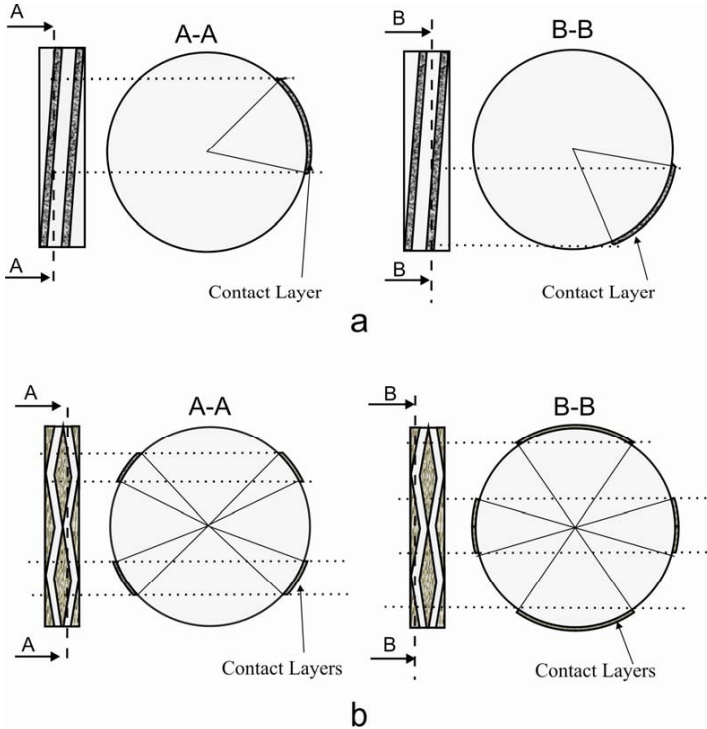


Figure 5.2: Schematic of the cross sections of the macro-structured wheel surface; a) single spiral , b) multi spiral

As it can be seen (and will be explained in more detail in the next sections), the discontinued contact in each cross section (not across the whole wheel width) between workpiece and grinding wheel makes a very short contact time, but an effective one. In this period heat energy has enough time to spread and disperse so that the workpiece surface temperature will be reduced. In addition, there is enough space for the chips to be located in the empty space between grains on the surface structure, effectively reducing rubbing between chips and workpiece surface as compared to a conventional process. As well, the heated chips which transfer a portion of heat from the contact zone have less chance to be transferred again to the workpiece surface. Since the total heat transferred to the workpiece will be considerably

Description of Concepts

lower, grinding temperature is reduced and the possibility of workpiece thermal damage is reduced.

As an advantage of this concept comparing with the discontinued grinding process by conventional segmented wheel, it can be mentioned that there is no fluctuation in terms of power or vibration due to complete separation of the wheel and workpiece in even a very short period of time. There is thus a separation of contact in each cross section of the wheel, but the contact points shift from one side of the grinding wheel to the other side so that there is never a time that the wheel is completely out of macroscopic contact with the workpiece. On the other hand, it should be mentioned that if the spiral grooves on the wheel surface are not symmetric, in addition to the normal force and tangential forces, there is also a slight axial force which is orthogonal to the other grinding forces. But by using a small spiral inclined angle (less than 5 degrees), this axial force is so low that it does not have any considerable effect on the grinding process and therefore it can be easily neglected.

Grinding wheel conditioning

As it was discussed in chapter 2, the topography of the wheel surface (for resin and vitrified bonds) is fully influenced by the dressing parameters. The dressing condition and corresponding equations explained in chapter 2 reveal the importance of the overlapping ratio and infeed on the topography of the grinding wheel.

If the dressing lead is less than the active width of the dresser, i.e. $f_{ad} < b_d$ the normal dressing condition is applied. Figure 5.3 (a) shows the schematic of the wheel structure after such dressing. If the dressing lead is bigger than the active width of the dresser i.e. $f_{ad} > b_d$, then the kinematic of the dressing operation causes a spiral form on the grinding wheel surface with theoretical peak to valley height equal to dressing infeed.

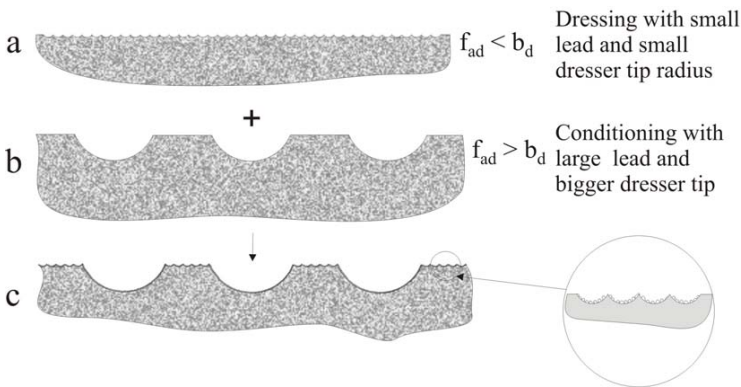


Figure 5.3: The total process of special conditioning of the wheel; a) dressing, b) conditioning, c) final topography as superposition of (a) and (b)

If this dressing infeed and the active width of the dresser are large enough, a great portion of the grains which are located in the groove will not be in contact with the workpiece during grinding. Figure 5.3 (b) demonstrates the effect of large f_{ad} on the wheel surface as in special conditioning.

By combination of the above mentioned cases a and b, i.e. first a dressing operation with small lead and small infeed, followed by second conditioning this time with larger lead and larger infeed, a new topography will be produced on the wheel, illustrated in figure 5.3 (c), which is a favourable topography for dry grinding resulting in a reduction in grinding forces and heat generation, as it will be seen from the grinding results in the next chapters.

The second conditioning can be in different forms such as one spiral, double spiral or multi spiral. Figure 5.3 (c) illustrates the combination of these two dressing processes and the schematic of the final topography of the wheel. The first dressing with small lead and small infeed varies the micro-topography of the wheel, and the second dressing with larger lead and larger infeed produces a new macro-topography on the overall wheel surface.

5.3 MACRO-STRUCTURING USING SPECIAL ELECTROPLATING

Electroplated grinding wheels contain just a single layer of abrasive grains, and cannot be dressed, unlike the other grinding wheel types. That is why the performance of such wheels varies due to wheel wear throughout the wheel life which causes some variation in the quality of the ground workpiece [Shi06]. But on the other hand, due to very good heat conduction properties of electroplated CBN wheels, these wheels can have some advantages for dry grinding. In the case of using an electroplated wheel, the most important variable is the grit size and distribution of grits which defines the topography of the grinding wheel, especially in dry grinding where no coolant is used.

In order to compare the influence of the different bonding types as well as macro-topography of the wheel on various dry grinding parameters, a special electroplated bond wheel was designed and developed for this study. The hub was machined to a high accuracy within 2 μm , and wheel run out within 5 μm . The grain size used was B126, the diameter of the wheel was 400 mm and the wheel width 15 mm. Another electroplated CBN wheel with the same specification (i.e. same diameter, width and grain size) was provided to compare the results of the structured wheel with those of the conventional one in terms of forces, roughness, temperature, and so on.

The special structure or special macro-topography of the new electroplated wheel makes a 22% contact layer between wheel and workpiece. The structure form on the wheel surface is totally different from that of the vitrified and resin bonded conditioned wheels. Figure 5.4 illustrates the special structured electroplated bond wheel.

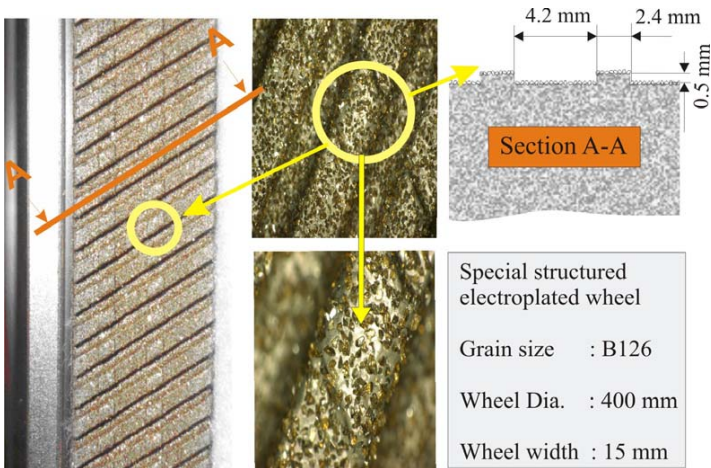


Figure 5.4: The structured electroplated bond CBN wheel; pattern and dimensions

The discontinued contact between workpiece and grinding wheel in each cross section of the wheel makes a very short and effective contact time. In this process heat energy has enough time to spread and disperse so that the workpiece surface temperature will be reduced.

If the geometry of the islands of grits is not properly designed so that there is no overlapping between the grinding path of the grits on the cross section of the wheel, it is possible that the one or more lines of unground material appears on the workpiece surface. The form and the contact layer area can be varied depending on the application. Increasing the contact layer causes grinding results to be closer to that of the conventional wheel.

5.4 MACRO-STRUCTURING USING LASER BEAM CONDITIONING

Combination of laser treatment with grinding is used in terms of the hardening of the workpiece, wheel conditioning and preheating for higher stock removal of the brittle material [West95]. Wheel structuring can also be done by laser. Different pattern can be produced on the wheel using laser. In this research, laser structuring was carried out on a CBN vitrified grinding wheel with diameter of 400 mm, width of 15 mm, grit size and concentration of B126 C125. A Nd:YAG laser machine was used to make blind holes on the wheel surface. Blind holes with a depth of 5 mm were drilled into the surface of a conventional wheel using laser, so that the macro-topography of the wheel was changed as illustrated in figure 5.5. The spot diameter of the laser beam was about 500 μm .

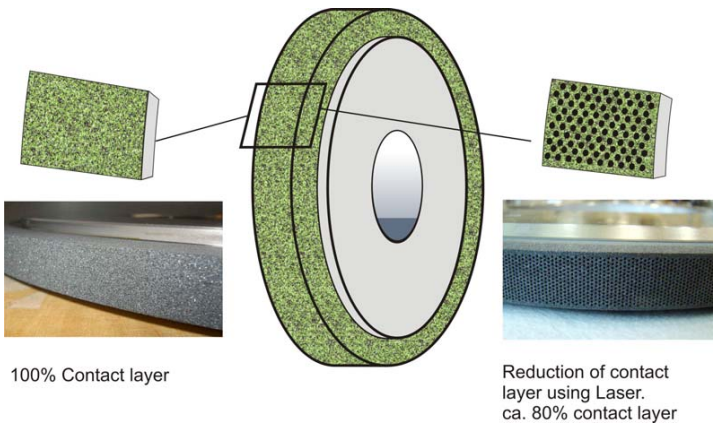


Figure 5.5: Comparison of the conventional and laser structured vitrified grinding wheel

Figure 5.6 demonstrates the pattern on the wheel surface. Measurement of the wheel surface was done using digital microscopy. Fifty blind holes were measured randomly to specify the average dimensions of the pattern on the wheel surface. Based on the measurement of the holes and the dimension of the wheel, about 20% contact layer was lost after structuring so the contact layer was about 80% comparing with the 100% layer of the conventional CBN wheel. The investigation on the grinding parameters and the resulting outputs will be presented in the next chapters.

Grain size	: CBN, B126	Concentration	: C125
Wheel width	: 15 mm	Bond	: Vitrified
Wheel diameter	: 400 mm	Wheel type	: Laser structured

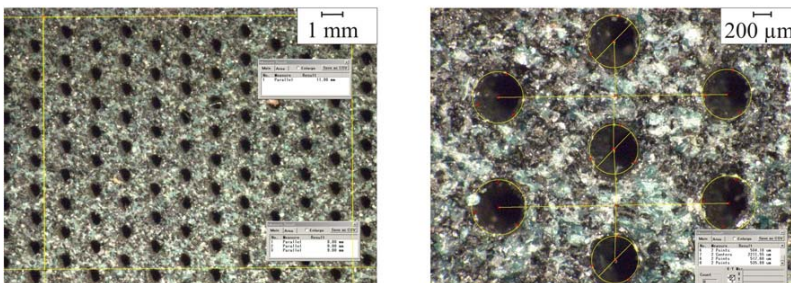


Figure 5.6: Laser structured vitrified CBN wheel surface, pattern and dimensions

Chapter 6

6 THEORETICAL ASPECTS AND MODELLING

In this chapter, the models used for the investigation in this study will be explained and will be applied to the new grinding wheel concept. The implications of the structuring of the grinding wheels on different grinding parameters are studied, particularly in comparison with conventional grinding wheels. These parameters and corresponding modelling are categorized based on the kinematic, dynamic and thermal aspects investigated. Some of the parameters needed in the models are experimentally measured and applied.

6.1 INTRODUCTION

In grinding processes, the superposition of singular microscopic cutting grains causes the material removal. Therefore the study of the interaction of a single grain with the workpiece, as well as the summation of all grain interactions with the workpiece, is the basis of the process behavior. In this regard, the most important parameter is the number of cutting edges engaged with the workpiece, so-called the number of dynamic or active cutting edges [Kass69, Wern71]. However, due to the stochastic nature of grain distribution on the wheel surface as well as geometrically undefined grain cutting edges, an exact determination of the geometrical engagement conditions of the singular cutting edges is not possible. However, the results of such stochastic interaction can be explained in terms of cutting parameters. The main cutting parameters of the removal process are the theoretical chip thickness, length, and engagement angle [Mari04]. Knowing the overall relations between input values, cutting values and chip size, as well as process output values, the behavior of the process can be cohesively described and used to improve the set-up of the machining process. This can be used to imply a wheel specification suitable for the grinding application and the choice of parameters leading to an economical grinding process [Mari07].

As it was described in the chapter 2, the topography of the wheel, uncut chip thickness, material removal rate, grinding forces, grinding energy and heat & temperature models are the subject of interest in most of the grinding models. This chapter focuses on these models as

well as verifying them based on the new concept of grinding wheel structuring in dry grinding applications.

6.2 KINEMATIC ASPECTS AND CORRESPONDING MODELLING

Material removal mechanism, chip formation, topography of the wheel and the interaction of grains into the workpiece are the subjects studied by kinematic analysis of the process. Hereby, uncut chip thickness will be discussed as one of the most important parameters, as well as a basis for further modelling. The effect of macro-topography, especially in the case of structured and conventional grinding wheels in terms of wheel parameters such as cutting edge density, grain spacing and geometric contact length, as well as kinematic and dynamic cutting edges, are the focus points of this section.

6.2.1 Implication on wheel macro-topography

As it was explained in chapter 5, the macro-topography of the wheels can be changed artificially by conditioning as well as by laser pattern and special electroplating. Each of these methods has a great influence on the topography parameters of the wheel, especially static as well as kinematic cutting edges in terms of grain distribution and grain spacing. These parameters have a direct correlation with uncut chip thickness.

Grain spacing can generally be considered in terms of average grain size d_k or average grain mesh size w_m and as cutting edge density per unit volume C_K , defined as the number of grains per unit volume of the wheel, using a grain volume concentration K , which is a percentage of total grain volume ($n_K \times V_K$) with respect to the total volume of the abrasive layer V_{tot} . Some grain spacing models were developed for the conventional grinding wheel by various researchers [Wern71, Yege86, Tawa93, Paul90, Link92, Spie94, Cina95]. All of these models considered a defined grain structure; cubic structure for example, and a defined grain shape such as pyramid or sphere form to instruct the model. For the purpose of this study, the model developed by Linke [Link92] and Paulmann [Paul90] is considered. Based on this model, the grains are distributed in cubic form. The structure and related parameters are presented in table 6.1.

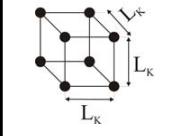
The cutting edge density C_K , according to this model, is defined as:

$$C_K = \frac{n_K}{V_{tot}} = \frac{K}{V_K} \quad (6.1)$$

where n_K is the number of grains in wheel or in total abrasive layers, which can be calculated from this equation with other parameters known and V_K is the mean volume of the abrasive grain.

Theoretical Aspects and Modelling

Table 6.1: Model of grain distribution for calculation of theoretical grain spacing

Theoretical grain distribution structure (cubic)	Number of grains per volume unit	grain spacing L_K
	$1 = 8 \cdot \frac{1}{8}$	$L_K = \left[\frac{1}{C_k} \right]^{\frac{1}{3}}$

Besides, the cutting edge density per unit area C can be calculated based on the cutting edge density per unit volume. Defining L_K as the cutting edge spacing, for the above mentioned model based on table 6.1, C is defined as:

$$C = C_K \cdot L_K = C_K^{\frac{2}{3}} \quad (6.2)$$

The static number of cutting edges per unit area N_{stat} , which will be discussed in next section, depends on the height of the grain above the bond and it is actually less than amount of C . In order to calculate the N_{stat} for the grains whose tips are just above the bond and therefore visible, some of the authors investigated and suggested a dimensionless correction coefficient ν [Schl82, Yege86] for the multilayer wheels as resin and vitrified bond wheels, with which the cutting edge density of visible grain or the N_{stat} for all the visible grains can be theoretically calculated:

$$N_{stat} = \nu \cdot C \quad (6.3)$$

So far, the N_{L-stat} defined as static grain density per unit length, and L_{K-stat} defined as static grain spacing, can be calculated as follows:

$$N_{L-stat} = \sqrt{N_{stat}} \quad (6.4)$$

$$L_{K-stat} = \frac{1}{N_{L-stat}} \quad (6.5)$$

Based on this analogy, L_{K-stat} is equal in lateral, longitudinal and radial directions. On the other hand, in order to calculate cutting edge density, it is necessary to consider a defined geometry for the grain. Comparing different grain shapes such as octahedron, ellipsoid and sphere [Schl82, Yege86, Linke92, Tawa93, Wern94, Ver194, Spie94], the best conformity between

above mentioned idealized and real grain geometry is seen with the ellipsoid model [Zitt99]. In this dissertation, the ellipsoid model is considered for the calculation of individual grain volume. Using this model the volume of an abrasive grain is:

$$V_K = \frac{\pi}{6} \cdot q_m \cdot w_m^3 \tag{6.6}$$

where w_m is the average grit mesh size and q_m is the grit aspect ratio. Triemel used the ellipsoid model for CBN wheels and found that $q_m = 1.41$ [Trie 75, Zitt99]. As an example, calculation for the resin-bonded wheel used in experiments will be presented. The grinding wheel B126 C125 has 4.4 carats/cm³ CBN abrasive while mass density of CBN is $\rho_{CBN} = 3.48$ g/cm³. Considering the amount of 0.5 for ν which matched relatively well with practical experiments reported in the literatures [Yege86] and the average grit mesh for B126 of 0.116 mm, knowing a carat is 0.2 g based on DIN 1301-1, using equations (6.1) to (6.6), C_k , K , C , L_k , V_k , N_{stat} and L_{K-stat} can be calculated. The results are shown in table 6.2:

Table 6.2: Basic topography parameters of resin bond CBN wheel B126 C100

K	V_K (mm ³)	C_K (mm ⁻³)	C (mm ⁻²)	N_{stat} (mm ⁻²)	L_{K-stat} (mm)
25%	0.00115	217	36	18	0.235

Figure 6.1 shows the surface of the above mentioned resin bond grinding wheel using a digital optical microscope and the real static number of grains per unit area N_{stat} .

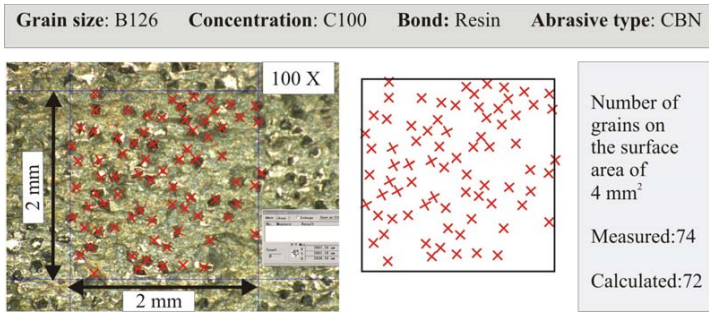


Figure 6.1: Static number of grains for resin-bond CBN grinding wheel

The grain distribution and concentration were measured by counting the number of grains per unit area as seen in figure 6.1. The measurement was performed randomly in 5 different regions of the wheel. The results of calculations and measurements are found to be very close to each other. The vitrified bond CBN wheel was similarly investigated and the calculation and experimental measurements also had similar results. The abrasive grains on an

Theoretical Aspects and Modelling

electroplated CBN wheel are generally more concentrated than on the two above mentioned wheels. Figure 6.2 presents the experimental measurement for number of grains in an electroplated CBN wheel with an identical grain size of B126.

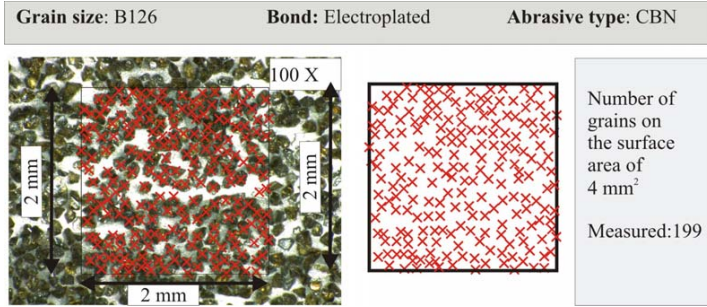


Figure 6.2: Static number of grains for an electroplated bond CBN wheel

Based on measurements on four different regions of the electroplated wheel surface, the cutting edge density per unit area will be:

$$C = \frac{\text{Number of grains}}{\text{Area}} = \frac{202}{4} = 50.5 \text{ (mm}^{-2}\text{)}$$

As it can be observed, the number of cutting edge per unit area is about 2.3 times higher, comparing to the resin bond wheel.

In the case of the structured wheel, as it was explained in chapter 5, the contact layer between the wheel and workpiece is reduced. This is due to an area decrease in the superabrasive layer on the wheel, similar to a decrease in the grain density of the wheel surface. Considering a parameter of contact ratio χ as the percentage of the contact layer for a structured wheel, with respect to that of the conventional wheel, the value of χ has a great influence on the grinding process, as it will be seen in the next chapters. The parameter of χ can be either calculated for special conditioning or measured if a special pattern on the wheel is used.

Figure 6.3 presents the schematic and calculation of the contact ratio for three of the wheels applied in the experiments. For example the diameter of the hole can be measured in the case of a laser-structured vitrified wheel, and by counting the number of the holes in a definite area, the ratio of total whole area to the total wheel surface can be found. As it was discussed in chapter 5, for the case of the laser-structured vitrified wheel, the parameter χ is about 0.8 or 80% . The same calculation can be applied for the electroplated wheel as well as conditioned wheels.

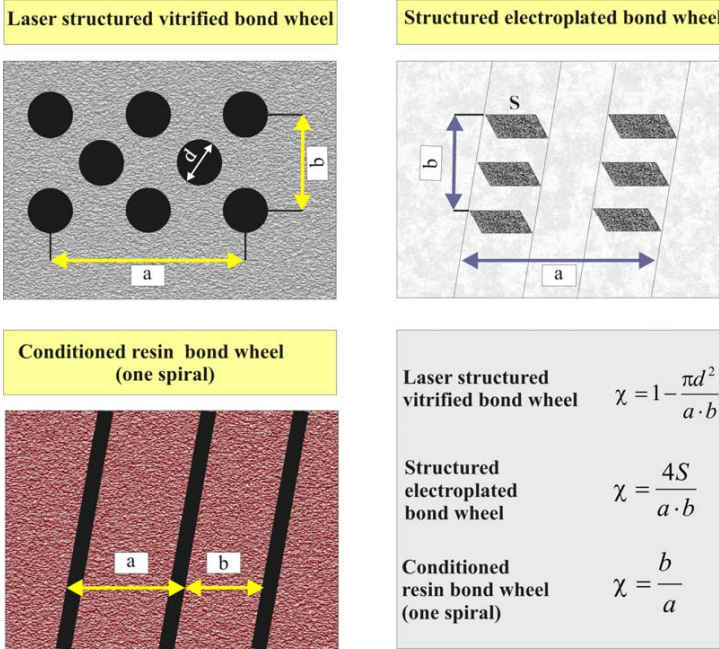


Figure 6.3: Schematic of the structured wheels and the related contact layer ratios (exaggerated)

Reduction of contact area causes an increase in grain spacing and a theoretical decrease in the static cutting edge density. This increase in grain spacing or reduction of static cutting edges is not entirely uniform on the wheel surface, but due to the stochastic nature of the grinding process, the variation in the grain density is nearly uniform. The analogy is based on the fact that the same material removal on the workpiece is performed by fewer cutting edges and this is similar to the case of a lower cutting edge density on the wheel surface. Therefore, it can be assumed with an acceptable approximation that the cutting edge density per unit area of structured wheel C_{stru} is proportional to the percentage of the abrasive layer and to the conventional static cutting edge density C_{conv} . In general, the following expression can be assumed:

$$C_{stru} = \chi^{\zeta} \cdot C_{conv} \quad (6.7)$$

where C_{stru} and C_{conv} are the cutting densities of the structured and conventional wheels, respectively, and ζ is a constant between 0 and 1, depending on the structuring form and

Theoretical Aspects and Modelling

should be experimentally found. When the structuring form is more uniform over the wheel surface, the value of ζ is near to 1. In this dissertation, the index “*stru*” is used for structured wheel and the index “*conv*” for the conventional wheel.

6.2.2 Implication on mean uncut chip thickness and area

The comparison of the mean uncut chip area of conditioned and conventional wheels leads us to the comparison of the mean uncut chip thickness. The total uncut chip area can be expressed by mean uncut chip area as:

$$\sum_{i=1}^{\bar{N}_{mom}} A_{cu,i} \approx \bar{A}_{cu} \cdot \bar{N}_{mom} \quad (6.8)$$

where \bar{N}_{mom} is the momentary number of active cutting grains, $A_{cu,i}$ is the uncut chip area of the active grain i , and \bar{A}_{cu} is the mean uncut chip area. \bar{N}_{mom} can be calculated as shown by [Zepp05]:

$$\bar{N}_{mom} = K_w \cdot N_{kin} \cdot l_g \cdot b \quad (6.9)$$

where K_w is a grinding wheel constant, l_g is the geometrical contact length (the elastic deformation on the wheel and workpiece which influence the contact length [Qi97] is not considered in this study) and b is the engaged wheel width and N_{kin} is kinematic cutting edge density on the wheel surface. The kinematik cutting edges density N_{kin} has a direct relation to the static cutting edges density N_{stat} as [Shaw96]:

$$N_{kin} = N_{stat} \cdot \left(\frac{v_w}{v_s} \right)^m \cdot (\theta')^m \quad (6.10)$$

Where v_w is the workpiece speed, v_s is the grinding speed, θ' is wheel rotation angle during contact length and m is constant for a particular wheel. Based on the equation (6.10), for a definite grinding parameter, i.e grinding speed, depth of cut, feed rate and grinding wheel diameter, the static cutting edge density and kinematic cutting edge have such relation:

$$N_{kin} = K_k \cdot N_{stat} \quad (6.11)$$

Where K_k will be a constant for a definite grinding parameter. While static number of cutting edges or grains (it is assumed that each grain has one cutting edge as investigated by Verkerk [Verk77]) is the sum of all the edges or grains on the surface of the grinding wheel, kinematic cutting edges (grains) are defined as only those grains which actually take part in chip formation [Töns92] in the material removal process. Kinematic cutting edges in the peripheral

direction of the wheel depend on the topography of the wheel (i.e. grain spacing or number of static cutting edges as well as height distribution of the cutting edges over the wheel surface), and on the kinematic interaction between grinding wheel and workpiece.

In order to calculate the number of kinematic cutting edges it is necessary to know the static cutting edge density. The static cutting edge density was supposed by Tönschof as [Töns03]:

$$N_{stat} = C_K \cdot z = (C)^{\frac{3}{2}} \cdot z \quad (6.12)$$

Here, it is assumed that the number of static cutting edges in each height of z is directly proportional to the value of z . Due to the normal distribution of the grains on the wheel surface, for a major part of the probability distribution curve, the above mentioned assumption is valid with an acceptable approximation.

As it was discussed in the previous section, wheel structuring causes a decrease in static cutting edge density in any z , but on the other hand, reduction of the cutting edge density with the same material removal rate increases the grain penetration which causes more cutting edges to come into contact, and therefore there is an increase in the number of kinematic cutting edges. So the rate of reduction of kinematic cutting density as well as increasing mean uncut chip thickness and mean uncut chip area of the structured wheel needs to be calculated.

The following formulations and models are basic investigations of these parameters.

The total material removal rate Q'_w can be written as:

$$Q_w = v_c \cdot \sum_{i=1}^{\bar{N}_{max}} A_{cu,i} \quad (6.13)$$

where v_c is the grinding speed.

The uncut chip thickness h_{cu} and uncut chip area A_{cu} for a spherical shaped grain tip, based on figure 6.4, can be expressed with a negligible error as follows [Lier98]:

$$A_{cu} = \frac{4}{3} \cdot h_{cu}^{3/2} \cdot r^{1/2} \quad (6.14)$$

The mean uncut chip area \bar{A}_{cu} can be calculated as:

$$\bar{A}_{cu} = \frac{1}{h_{cu-max}} \int_0^{h_{cu-max}} A_{cu} \cdot dh_{cu} \quad (6.15)$$

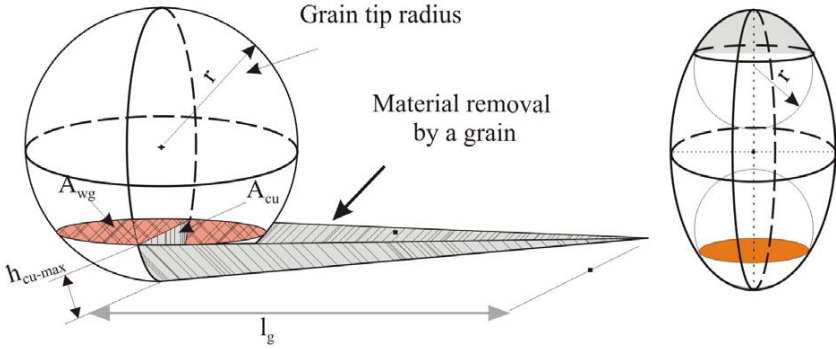


Figure 6.4: Schematic of the spherical grain showing theoretical uncut chip thickness h_{cu} and cross-section area A_{cu}

To find the mean uncut chip area based on mean uncut chip thickness, if r is considered constant and the variation of h_{cu} is assumed to vary linearly from 0 to h_{cu-max} , using equations (6.14), and the integral of (6.15) gives:

$$\bar{A}_{cu} = \frac{8}{15} \cdot h_{cu-max}^{3/2} \cdot r^{1/2} \quad (6.16)$$

The mean uncut chip thickness will also be calculated using above mentioned assumptions as:

$$\bar{h}_{cu} = \frac{l}{h_{cu-max}} \int_0^{h_{cu-max}} h_{cu} \cdot dh_{cu} = \frac{h_{cu-max}}{2} \quad (6.17)$$

using equations (6.16) and (6.17):

$$\bar{A}_{cu} = \frac{16\sqrt{2}}{15} \cdot \bar{h}_{cu}^{3/2} \cdot r^{1/2} \quad (6.18)$$

For the kinematic cutting edges, it is assumed that in each depth of penetration z , that uncut chip thickness and depth of penetration are the same. Figure 6.5 illustrates the kinematic of the grinding process. Considering this kinematic of surface grinding as illustrated in figures 6.4 and 6.5, for a point on the contact length, it is assumed that the contact length and uncut chip thickness has a linear correlation.

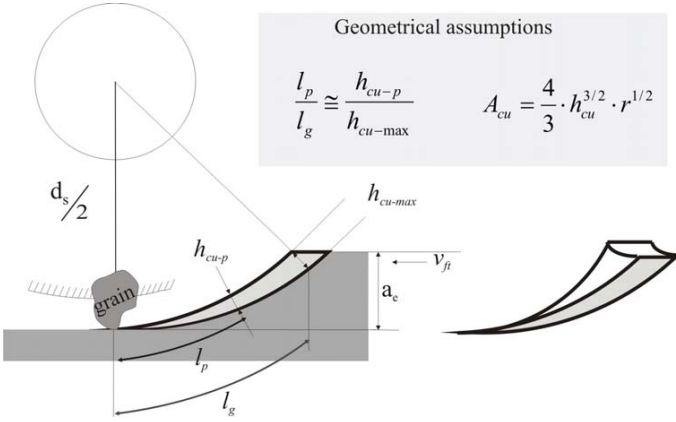


Figure 6.5: Grinding kinematic and chip formation

Based on this assumption, with an acceptable approximation:

$$\frac{l_p}{l_g} \cong \frac{h_{cu-p}}{h_{cu-max}} \quad (6.19)$$

To have a more accurate calculation, the total uncut chip area can be written as:

$$\sum_{i=1}^{\bar{N}_{mom}} A_{cu,i} = \int_0^{\bar{N}_{mom}} \bar{A}_{cu-p} \cdot dN_{mom} \quad (6.20)$$

where \bar{A}_{cu-p} is the mean uncut chip area for active grains up to point p on the contact length. The variation of N_{mom} on the contact length for a definite grinding parameter can be expressed as [Töns03]:

$$dN_{mom} = \bar{N}_{stat} \cdot b \cdot K'_w \cdot dl \quad (6.21)$$

where K'_w is a constant depends to grinding wheel and grinding parameters. At a definite point p on the contact length, with the uncut chip thickness of h_{cu-p} , the average static cutting edge density \bar{N}_{stat} using equation (6.12) will be:

$$\bar{N}_{stat} = \frac{1}{h_{cu-p}} \int_0^{h_{cu-p}} C_K \cdot h_{cu} \cdot dh_{cu} = \frac{1}{2} C_K \cdot h_{cu-p} \quad (6.22)$$

Theoretical Aspects and Modelling

and the mean uncut chip area \bar{A}_{cu-p} using equations (6.14) and (6.15) will be:

$$\bar{A}_{cu-p} = \left(\frac{4}{3}\right) \cdot \frac{l}{h_{cu-p}} \int_0^{h_{cu-p}} r^{\frac{1}{2}} \cdot h_{cu}^{\frac{3}{2}} \cdot dh_{cu} = \frac{8}{15} r^{\frac{1}{2}} \cdot h_{cu-p}^{\frac{3}{2}} \quad (6.23)$$

Using equations (6.20) to (6.23):

$$\sum_{i=1}^{\bar{N}_{max}} A_{cu,i} = \int_0^l \frac{8}{15} r^{\frac{1}{2}} \cdot h_{cu-p}^{\frac{3}{2}} \cdot \frac{l}{2} C_K \cdot h_{cu-p} \cdot b \cdot K_w \cdot dl \quad (6.24)$$

And changing the variable based on equation (6.19):

$$\sum_{i=1}^{\bar{N}_{max}} A_{cu,i} = \frac{8}{105} \cdot r^{\frac{1}{2}} \cdot C_K \cdot b \cdot l_g \cdot K_w \cdot h_{cu-max}^{\frac{5}{2}} \quad (6.25)$$

As the material removal rate for both structured and conventional wheels is the same ($Q_{w-conv} = Q_{w-stru}$) and at the same grinding cutting speed ($v_{c-conv} = v_{c-stru}$), from equation (6.13) it can be written:

$$\sum_{i=1}^{\bar{N}_{max}} A_{cu,i-stru} = \sum_{i=1}^{\bar{N}_{max}} A_{cu,i-conv} \quad (6.26)$$

Based on the explanation of the last section regarding the static cutting edge density of the conventional and structured wheel, it is inevitable that the structuring causes a reduction in kinematic and so far a reduction on the momentary number of active cutting grains. To quantify this reduction of the cutting edges the following assumptions are considered:

$$\frac{(K'_w C)_{stru}}{(K'_w C)_{conv}} = \chi^{\xi} \quad (6.27)$$

where ξ is a constant between 0 and 1, depending on the structuring form and grinding wheel specification and should be experimentally found.

If the other grinding parameters and dressing conditions for the structured and conventional wheel are equal, using equations (6.25) – (6.27), the theoretical ratio of the mean uncut chip thickness of structured ($\bar{h}_{cu-stru}$) and conventional ($\bar{h}_{cu-conv}$) wheels becomes:

$$\frac{\bar{h}_{cu-stru}}{\bar{h}_{cu-conv}} = \chi^{\frac{-3}{5}\xi} \quad (6.28)$$

The constraint which must be applied to equation (6.28) is that at least one grain must exist in each cross section of the wheel in order to cut the material. For this extreme situation the uncut chip thickness has the maximum possible amount which is defined as [Malk89]:

$$h_{cu,max-stru} \leq h_{cu,max} \approx 2 \cdot \pi \cdot d_s \cdot \frac{v_{ft}}{v_c} \cdot \sqrt{\frac{a_e}{d_s}} - \pi^2 \cdot d_s \cdot \left(\frac{v_{ft}}{v_c} \right)^2 \quad (6.29)$$

This means the value of χ , theoretically and practically, cannot be near to zero. Now, using equations (6.28) and (6.18), the theoretical ratio of the mean uncut chip area of the structured wheel ($\bar{A}_{cu-stru}$) to the conventional chip area ($\bar{A}_{cu-conv}$) will be:

$$\frac{\bar{A}_{cu-stru}}{\bar{A}_{cu-conv}} = \chi^{\frac{-9}{10} \xi} \quad (6.30)$$

Figure 6.6 presents the theoretical ratio of mean uncut chip thickness as well as mean uncut chip area of structured wheel to conventional wheel for different values of χ based on the above-mentioned assumptions.

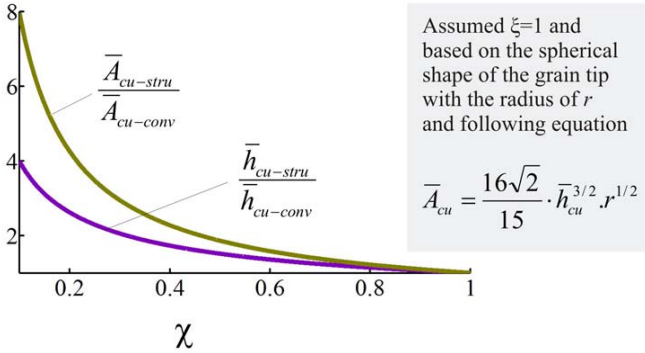


Figure 6.6: Theoretical ratio of mean uncut chip thickness \bar{h}_{cu} and mean uncut chip area \bar{A}_{cu} of the structured wheel and conventional wheel

Equations (6.28) and (6.30) are the basis of changes from kinematic aspects of the grinding process in the case of structured wheels compared to conventional wheels. The parameters of uncut chip thickness, uncut chip area are the important parameters in the interaction between grinding wheel and workpiece. It can be seen that with the structuring both of these parameters are increased. The lower the contact area the higher the chip thickness. It will be seen in the next sections that these parameters have major roles in the dynamic aspects of the

Theoretical Aspects and Modelling

process in terms of grinding forces and energy, as well as for heat generation in the contact zone and temperature on the workpiece surface.

The material removal rate, calculated using equations (6.8), (6.9) and (6.13) will be:

$$Q_w = v_c \cdot \bar{A}_{cu} \cdot K_w \cdot N_{kin} \cdot l_g \cdot b \quad (6.31)$$

The material removal rate and geometric contact length for surface grinding can also be expressed as:

$$Q_w = v_{ft} \cdot a_e \cdot b \quad (6.32)$$

Considering the geometrical contact length l_g as [Mari04]:

$$l_g = \sqrt{a_e \cdot d_s} \quad (6.33)$$

and using equations (6.31) – (6.33) the uncut chip area can be expressed as:

$$\bar{A}_{cu} = \frac{1}{K_w \cdot N_{kin}} \cdot \frac{1}{q} \cdot \sqrt{\frac{a_e}{d_s}} \quad (6.34)$$

where q is speed ratio defined as $\frac{v_c}{v_{ft}}$. Using equation (6.18) and (6.34), the mean uncut chip thickness will be:

$$\bar{h}_{cu} = 0.8I \cdot \left(\frac{I}{K_w \cdot N_{kin}} \right)^{0.5} \cdot (I - \cos \theta)^{0.25} \cdot \left(\frac{I}{q} \right)^{0.5} \cdot \left(\frac{a_e}{d_s} \right)^{0.25} \quad (6.35)$$

where $\theta = \arccos\left(\frac{r - \bar{h}_{cu}}{r}\right)$ (6.36)

The parameter of θ is defined as attack angle.

Figure 6.7 presents the relation between mean uncut chip thickness and attack angle at constant speed ratio and depth of cut, based on equation (6.35). An increase of the attack angle causes an increase in mean uncut chip thickness. In contrast, an increase in kinematic cutting edge numbers causes a reduction of mean uncut chip thickness.

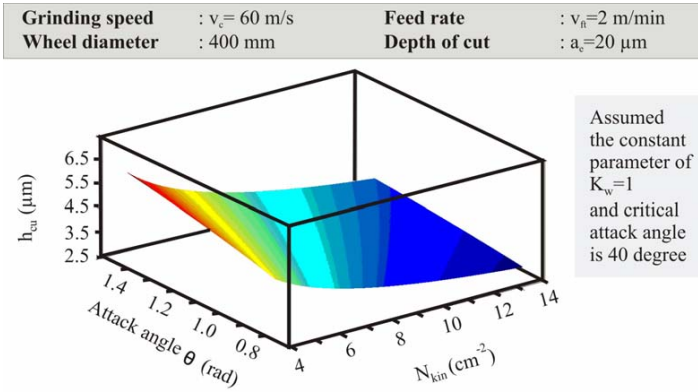


Figure 6.7: Mean uncut chip thickness versus kinematic cutting edge density and attack angle

It will be discussed in next section that the chip formation for metals occurs when the attack angle is more than a critical value (about 40 degree), otherwise the grains just rub and plough the material and there is no cutting action. For many grains which come to contact with the workpiece the attack angle is so small that no chip formation occurs. The ratio of kinematic grains to the total number of grains on the wheel is very low even less than 1% [Tawa06, Yege86]. At a definite set of grinding parameters, the rest of the grains are divided into two groups. The first group are the grains which have no contact with the workpiece during the process. The second group are the grains which have contact with workpiece in form of sliding (rubbing) and ploughing without chip formation. These grains are active as they are in contact with the workpiece and have a great role in the generation of heat, energy and also grinding forces. That is why the author named the summation of these grains and kinematic cutting edges as dynamic cutting edges, because both of them influence the dynamic of the process. Thus in all the upcoming chapters, dynamic cutting edges are considered to be the summation of both kinds of grains, while kinematic cutting edges are only those grains which have a role in actual cutting and chip formation, whereas:

$$N_{kin} = N_{cut} \quad (6.37)$$

$$N_{dyn} = N_{cut} + N_{plough} + N_{slide} \quad (6.38)$$

In next section, it will be observed that in the case of a structured wheel, due to higher penetration, the attack angle is greater and the number of grains which plough the material are fewer, therefore the grinding process is more efficient.

6.2.3 Implication on dynamic cutting edges based on the stochastic nature of wheel topography

The aim of this section is to estimate the dynamic cutting edges as well as the grains which plough or rub the workpiece material without chip formation, i.e. the grains which come into contact without resulting material removal. This will be done based on the stochastic nature of grain distribution. As it will be seen, these grains have a main influence on increasing grinding energy and corresponding heat generation. Comparing these grains for conventional and structured grinding wheels provides a kinematic clarification of the advantages of the structured wheel and its higher efficiency in terms of reducing grinding energy and heat generation.

The dynamic cutting edge is generally dependent on the stochastic distribution of grain size and grain height above the wheel surface as well as kinematic of the process. This distribution usually takes the form of a normal distribution [Zitt99, Hou03a] as illustrated in figure 6.8. Hou et al. [Hou03a] assumed that this normal distribution on the wheel surface is due to the different grain sizes (i.e. grain diameter) and presented interesting results for fine and cut-off grinding processes. In this work, it is assumed that all grains have the same grain size but are distributed at different heights over the wheel surface. The other assumption used to simplify the model is that the effect of dressing conditions and wheel wear (which play an important role in grain distribution) are not considered. As the goal of this section is to compare the structured and conventional wheels, with the same grinding and dressing conditions for each, these assumptions have no great influence on the results of the comparison.

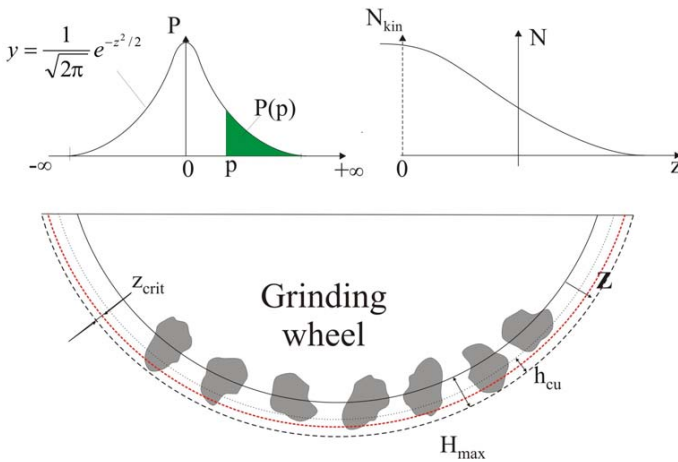


Figure 6.8: Normal distribution of the grain size [Hou03a]

The normal distribution is known generally as:

$$y = \frac{1}{\sqrt{2\pi}} e^{-z^2/2} \quad (6.39)$$

and the probability density function $P(p)$ will be expressed as [Hou03a]:

$$P(p) = \frac{1}{\sqrt{2\pi}} \int_p^{\infty} e^{-z^2/2} dz \quad (6.40)$$

$$p = \left(\frac{H_{\max}}{2} - z \right) \cdot \frac{4.4}{H_{\max}/2} \quad (6.41)$$

where H_{\max} is the maximum height of the grain above the bond surface and z is the indentation depth of the grain into the workpiece. The amount of 4.4 can be considered as a very safe upper limit of the normal distribution probability function, as this function converges rapidly after this amount and declines to zero [Hou03a].

The dynamic cutting edge density N_{dyn} is the density of cutting edges which come into contact with workpiece at each z . It can be expressed as [Hou03a]:

$$N_{dyn} = C \cdot P(p) \quad (6.42)$$

If the normal distribution of the grain height above the bond is considered the same for both structured and conventional wheels, it can be seen that the ratio of static cutting edges of the structured wheel to those of the conventional wheel in each z will be the maximum cutting edge density (where $z=0$) multiplied by the probability function at each z . Using equation (6.7) for the cutting edge density ratio of structured and conventional wheels, and equation (6.42) for the probability function, then:

$$N_{dyn-stru} = C_{stru} \cdot P(p) = \chi^{\zeta} \cdot C_{conv} \cdot P(p) \quad (6.43)$$

This number of static cutting edges is just those edges at a defined height over the wheel surface which are able to come into contact with the workpiece at a specific depth of cut, but whether they come to contact or not depends on the grinding parameters. That is the reason why the static cutting edge numbers are rather different than the kinematic cutting edge numbers.

In order to find the number of grains which slide and plough over the workpiece surface without performing material removal, it is necessary to find the threshold indentation depth of the grains under which the sliding, ploughing and cutting processes occur. The rubbing (or

Theoretical Aspects and Modelling

sliding) mode can be categorized into three phases: rubbing in elastic deformation, rubbing in plastic deformation, and rubbing in the cutting phase. Considering the indentation of δ due to elastic deformation alone, the grains which only perform rubbing without ploughing or cutting can be determined. δ depends on the loop stiffness of the machine as well as the workpiece material and grinding wheel Young's module [Ghos07]. The modes of ploughing and cutting, on the other hand, depend on the attack angle θ (or degree of penetration D_p) and the shear strength of the materials involved. To identify which mode is most likely to occur, Hokkirigawa [Hokk88a, Hokk88b] made a map of the wear mechanism as shown in figure 6.9.

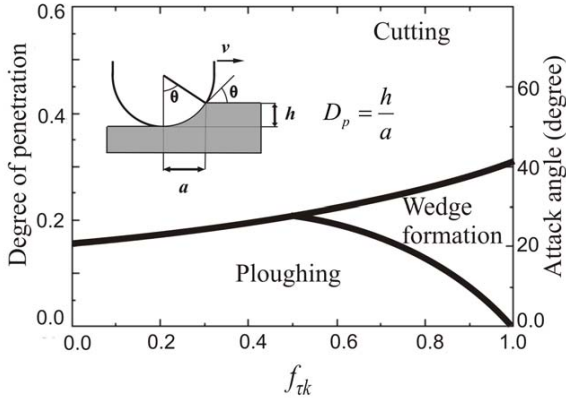


Figure 6.9: Mechanism of abrasive interaction with metal as a function of the degree of penetration or attack angle [Hokk88b]

In this figure, based on empirical assumptions, the attack angle θ or degree of penetration D_p is plotted versus the f_{tk} which is the shear strength at the contact interface. It should be mentioned that strain rates are not considered in this basic model. The higher strain rate as in the case of ultrasonic assisted grinding can considerably change the characterisation mentioned in figure 6.9 [Tawa08c].

The attack angle was previously expressed in equation (6.36). From the graph of Hokkirigawa, it can be concluded that for example, micro-cutting occurs at attack angles higher than 30° . Based on the attack angle amount it can be seen that minimum degree of penetration for cutting to occur is approximately 0.24 of the grain tip radius r . Below this amount, chip formation by cutting may not occur. In fact, below this critical depth, only rubbing and/or ploughing are considered to take place. For an ellipsoid grain model of D181, Verlemann [Ver194] reported that r can vary from $d_k/4$ (at the beginning of grinding process) up to d_k (with increasing wear). By using the assumption of Verlemann for the beginning of the process, i.e $r = d_k/4$, the critical or minimum indentation z_{crit} , based on the Hokkirigawa map, will be $0.06d_k$. Hou et.al. supposed that the amount of $0.025d_k$ was the critical or minimum

indentation z_{crit} [Hou03a]. Figure 6.10 shows a schematic of grain tip radius and grinding regimes.

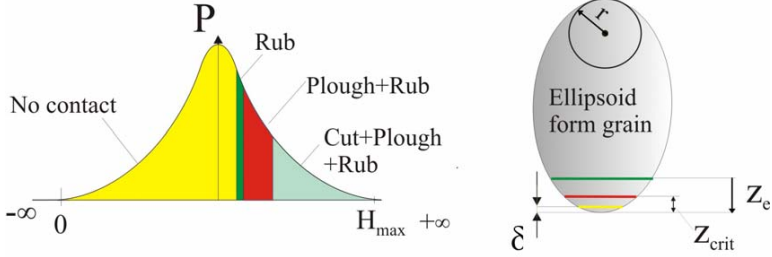


Figure 6.10: Distribution of kinematic grains by ploughing and cutting

It should be mentioned that, after ploughing, the plastically deformed material piles up at the sides of the grain, so the real depth of cut needed to remove built up material is greater than theoretical depth of cut. This matter is neglected in this work.

Based on equations (6.39) to (6.43), and figures 6.9 and 6.10, the probability of grains performing cutting or ploughing in each z can be calculated as follows:

$$N_{dyn} = C \cdot \frac{I}{\sqrt{2\pi}} \int_p^{+\infty} e^{-z^2/2} dz \quad (6.44)$$

where for sliding (rubbing), $N_{sl} = C \cdot P(p_1)$ where p_1 is:

$$p_1 = \left(\frac{H_{max}}{2} - z \right) \cdot \frac{4.4}{H_{max}/2} \quad (6.45)$$

for ploughing (when $z > \delta$), $N_{pl} = C \cdot P(p_2)$ where p_2 is::

$$p_2 = \left(\frac{H_{max}}{2} - (z - \delta) \right) \cdot \frac{4.4}{H_{max}/2} \quad (6.46)$$

and for cutting (when $z > z_{crit}$), $N_{ch} = C \cdot P(p_3)$ where p_3 is::

$$p_3 = \left(\frac{H_{max}}{2} - (z - z_{crit}) \right) \cdot \frac{4.4}{H_{max}/2} \quad (6.47)$$

Theoretical Aspects and Modelling

Using equations (6.44)-(6.47) and knowing the grinding parameters and grinding wheel specification in terms of surface topography, the grains which take part in cutting, ploughing and rubbing can be calculated using material removal rate constraints. Figure 6.10 illustrates a schematic of the probability of cutting, ploughing and rubbing. The grains with insufficient indentation, with z_{crit} as the critical indentation, simply plough or rub the workpiece. A greater indentation depth causes cutting to occur. The material removal rate can be calculated analytically using the above mentioned normal distribution of the grain heights. In order to calculate the material removal rate, the uncut chip area should be determined for each active grain based on its indentation depth. The integration of all these chip areas multiplied by grinding speed will be the material removal rate, as previously defined in equation (6.13). Based on the same approach and using equations (6.44) and (6.47), the material removal rate of a grain can be written as [Hou03b]:

$$Q'_w = v_c \cdot l_g \cdot b \cdot C \cdot \frac{1}{\sqrt{2\pi}} \int_{p_s}^{+\infty} A_{cu} \cdot e^{-z^2/2} dz \quad (6.48)$$

Substituting of A_{cu} from equation (6.14) in equation (6.48), and by a simple variable bypass, the integral of (6.48) can be calculated. The material removal rate based on equations (6.32) must be equal to the one using (6.48). Therefore using these two equations a definite z will be calculated with which cutting with the definite material removal rate occurs. By knowledge of Z_{crit} , δ and using equations (6.44) – (6.48), the cutting edge density of cutting N_{ch} , ploughing N_{pl} and sliding N_{sl} can be calculated.

In order to clarify the matter, an example will be studied for the CBN wheel B126 C100 mentioned in section 6.2.1. For such CBN grains, the minimum indentation z_{crit} , based on Verlemann's assumptions, is approximately 7.8 μm , and based on the Hou and Komanduri assumptions, is about 3.15 μm . It seems that for this CBN wheel the amount suggested by Verlemann, especially at the beginning of the process, is overestimated and the Hou & Komanduri's assumption is underestimated. Hereby for further calculations, the amount of $r = d_t/8$ is used which makes a critical or minimum indentation amount of 3.78 μm . This amount is also experimentally investigated. With a depth of cut less than 3 μm in dry grinding with a conventional CBN wheel of grain size B126, no considerable spark was found which normally demonstrates real cutting condition and chip formation in the grinding process. At a depth of cut of 5 μm , however, the grinding spark can clearly be observed. For the amount of δ , an elastic indentation of 1 μm is considered in this example. With a normal distribution for the grain height variation between 0 to 24 μm for the grinding wheel type B126 C100, which was experimentally measured, the depth of grain indentation into the workpiece can be iterated for a given set of grinding conditions using equations (6.44) – (6.48). In this calculation, a value for indentation depth z is assumed, and the analytical value of the material removal rate is calculated. If the analytical value is less than the experimental value, the indentation value is increased and vice versa. This process should be repeated until the two values of calculated material removal rate and real material removal rate are rather equal.

Considering the above mentioned parameters, for the wheel and grinding condition explained in section 6.2.1, the calculation results shows the value of 0.101 for N_{ch} , 2.964 for N_{pls} and 5.514 for N_{sl} . The ratio of the cutting edges which perform micro cutting (kinematic grains) to the total number of grains on the wheel surface is about 0.3%. So it can be seen that in fine grinding a very small ratio of the total grains participate in actual chip formation. The ratio of the edges which perform micro-rubbing to the grains which do micro-cutting, however, is about 5460%. This means the grains which generate heat by rubbing in the process are about 54 times more than the grains which perform chip formation. The ratio for the number of grains which perform micro-ploughing to the number of grains which do micro cutting is about 2934%. This is the reason why the grinding process has such a high specific energy and why heat generation is so considerable. The total number of grains on the wheel surface which do cutting (n_{ch}), ploughing (n_{pl}) and sliding (n_{sl}) (rubbing) can be calculated as:

$$n_{ch} = \pi d_s \cdot b \cdot N_{ch} \quad (6.49)$$

Similarly: $n_{pl} = \pi d_s \cdot b \cdot N_{pl}$; $n_{sl} = \pi d_s \cdot b \cdot N_{sl}$ (6.50)

The number of grains which do cutting as well as ploughing and sliding for a wheel with a width (b) of 15 mm and wheel diameter (d_s) of 400 mm will be 1904 , 55870 and 103936, respectively. So far the total number of grains which cut (n'_{ch}) as well as plough (n'_{pl}) and slide (n'_{sl}) in one second, with the grinding speed (v_s) will be:

$$n'_{ch} = v_s \cdot b \cdot N_{ch} \text{ (grain/sec.)} \quad (6.51)$$

Similarly the sliding and ploughing can be calculated as:

$$n'_{pl} = v_s \cdot b \cdot N_{pl} \text{ ; } n'_{sl} = v_s \cdot b \cdot N_{sl} \text{ (grain/sec.)} \quad (6.52)$$

The amount (n'_c), (n'_{pl}) and (n'_{sl}) for the grinding speed of 60 m/s and wheel width (b) of 15 will be 90900 grains/sec., 2667600 grains/sec. and 4962600 grains/sec., respectively. The rubbing and ploughing regimes produce a huge amount of heat in the contact zone. The basic idea of grinding wheel structuring is the reduction of the grains which do micro-ploughing and micro-rubbing in such a way that there are still enough grains for cutting. For the structured wheel, the ploughing and rubbing will be drastically decreased (depending on the amount of χ). On the other hand, as it was observed in the previous section of this chapter, the uncut chip thickness and uncut chip area of the structured wheel will be increased as compared to the conventional wheel, which causes a reduction of specific energy and the corresponding heat generation. It should be mentioned that a reduction of dynamic cutting edges also causes an increase in the roughness of work surface which can be a disadvantage.

Theoretical Aspects and Modelling

Using the similar calculation applied for conventional wheels, the ploughing, sliding and cutting edge densities for the structured wheel can be calculated. The results of the calculations for sliding and ploughing are presented in table 6.3. For this calculation, it is assumed that ξ in equation (6.7) is equal to 1. As it can be seen, there is a considerable reduction of the number of grains which plough or rub the workpiece material. This reduction of ploughing and rubbing causes a drastic decrease in grinding forces and grinding energy.

Table 6.3: Comparison of the number of grains which perform rubbing or ploughing at the definite grinding parameters for structured and conventional resin bond wheels according to the model and calculation

Grinding wheel : B126, C100, Resin		Grinding speed : $v_c=60$ m/s				
Wheel width : 15 mm		Feed rate : $v_a=2000$ mm/min				
Wheel diameter : 400 mm		Depth of cut : $a_c=20$ μ m				
Sliding/Ploughing Structuring percentage %	N_{sl} (mm^{-2})	N_{pl} (mm^{-2})	n_{sl}	n_{pl}	n'_{sl} (s^{-1})	n'_{pl} (s^{-1})
Conventional wheel (100% Layer)	5.514	2.964	103936	55870	4962600	2667600
Structured wheel with 75% layer	4.621	2.539	87103	47859	4158900	2285100
Structured wheel with 50% layer	3.592	2.036	67707	38378	3232800	1832400
Structured wheel with 25% layer	2.313	1.386	43599	26125	2081700	1247400

Based on the above mentioned model and related equations, the cutting edge density of the grains which plough N_{pl} , rub N_{sl} or cut N_{ch} the materials can be assumed to be:

$$\left(\frac{N_{pl-stru}}{N_{pl-conv}} \right) = \chi^\psi \quad \text{where } 0 < \psi < 1 \quad (6.53)$$

$$\left(\frac{N_{sl-stru}}{N_{sl-conv}} \right) = \chi^\eta \quad \text{where } 0 < \eta < 1 \quad (6.54)$$

Where the amounts of ψ and η depend on the grinding parameters and wheel specification. These parameters should be experimentally obtained. For the above mentioned example, it can be seen that they are about 0.6.

6.3 DYNAMIC ASPECTS AND CORRESPONDING MODELLING

The following section is going to describe the force and energy models applied to the grinding process, implicating the structured and conventional wheels, and explaining the theoretical reasons for the reduction of forces and specific energy seen with structured grinding wheels.

6.3.1 Introduction

Engagement of grains with the workpiece in grinding includes three phases of rubbing or sliding, ploughing and cutting (figure 6.11). The first phase is when the grain slides on the workpiece without any material transport or material removal. This phase is categorized as elastic deformation of the workpiece. The second phase is when the stress and corresponding strain is increased to push the material to the plastic deformation phase, where ploughing occurs along with sliding. The workpiece material is piled up in front and to the side of the grains in this phase. Beyond the plastic deformation regime, the material will be sheared under higher stress and chip removal will occur. This phase occurs simultaneously with the sliding process.

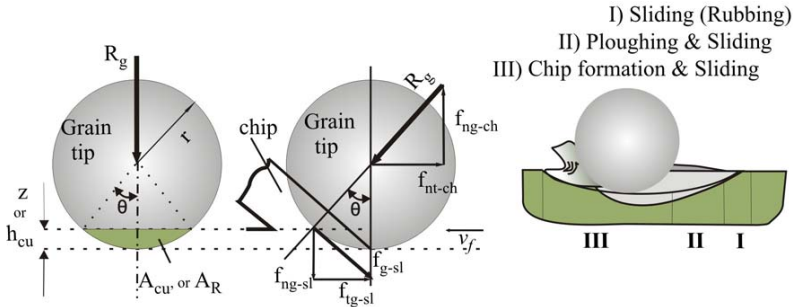


Figure 6.11: Schematic of the grinding forces and chip formation phases [Chen96a, Chen96b]

Based on these mechanisms, the specific energy as well as the forces applied in each stage can be distinguished as follows [Malk89]:

$$F_n = F_{n-ch} + F_{n-pl} + F_{n-sl} \quad (6.55)$$

$$F_t = F_{t-ch} + F_{t-pl} + F_{t-sl} \quad (6.56)$$

Theoretical Aspects and Modelling

$$e_c = e_{ch} + e_{pl} + e_{sl} \quad (6.57)$$

where F_t and F_n are the total tangential and normal forces and e_c is the total specific energy. The indices $_{ch}$, $_{pl}$ and $_{sl}$ indicate force components of the three above mentioned processes of chip formation of cutting, ploughing and sliding mechanisms, respectively. The normal and tangential forces seen in cutting, ploughing and sliding are related using constants k_{ch} , k_{pl} and k_{sl} , as follows:

$$F_{n-ch} = k_{ch} \cdot F_{t-ch} \quad ; \quad F_{n-pl} = k_{pl} \cdot F_{t-pl} \quad ; \quad F_{n-sl} = k_{sl} \cdot F_{t-sl} \quad (6.58)$$

$$e_{ch} = \frac{F_{t-ch} \cdot v_c}{v_w \cdot a_e \cdot b} \quad ; \quad e_{pl} = \frac{F_{t-pl} \cdot v_c}{v_w \cdot a_e \cdot b} \quad ; \quad e_{sl} = \frac{F_{t-sl} \cdot v_c}{v_w \cdot a_e \cdot b} \quad (6.59)$$

Based on Malkin's assumption, the chip formation energy for ductile materials is equal to the adiabatic melting energy of the workpiece [Malk89]. The chip formation specific energy for ferrous alloys is indicated to be 13.8 J/mm^3 . It can be observed that the forces due to cutting are generally dependent on the material removal rate and grinding speed. Based on this analogy, force and energy due to cutting are approximately constant for both conventional and structured wheels if the material removal rate and cutting speed is the same and there is no relation with the wheel topography.

The sliding and ploughing are the main mechanisms which occur when grain indentation on the workpiece is low, particularly before the critical indentation is reached, as was discussed in section 6.2.2. On the other hand, the amount of active grains which perform ploughing and rubbing is much higher than the amount of active grains which are able to perform micro-cutting. That is why in general, the ploughing and rubbing forces and corresponding specific energy are a considerable part of the total forces and energy seen in the grinding process.

In this section, to simplify the model applied for the process, the grain is assumed to be a sphere and the grain path on the workpiece surface (of geometrical contact length l_g) is considered uniform and proportional to the uncut chip thickness, as was illustrated in figure 6.4. The normal and tangential forces of each component can be written as the summation of normal and tangential forces of each active grain (either with or without chip formation) along the contact length. Considering the mean normal and tangential forces as \bar{F}_n and \bar{F}_t for the momentary number of the active grains, then:

$$\bar{F}_n = \sum_{j=1}^{\bar{N}_{mom}} F_{n,j} \approx \bar{F}_{ng} \cdot \bar{N}_{mom} \quad ; \quad \bar{F}_t = \sum_{j=1}^{\bar{N}_{mom}} F_{t,j} \approx \bar{F}_{tg} \cdot \bar{N}_{mom} \quad (6.60)$$

In the contact zone some of the active grains are only acting within phase one (sliding), some of them in phase two (ploughing and sliding) and the rest perform the third phase of cutting or chip formation along with sliding. The momentary number of the grains seen for each phase is different, but based on the stochastic nature of grain distribution, the average of each phase can be calculated with a reasonable approximation. In order to develop an appropriate model, each of the three different components of the forces (using momentary active grains) needs to be taken into consideration. Hereby, we begin with the sliding process and related forces and specific energy.

6.3.2 Implication on sliding forces and energy

The sliding process occurs when the grain comes to contact with the workpiece up to the time that it leaves contact. But the amount of the sliding force changes based on the elastic and plastic deformation, and chip formation mechanisms. However, the sliding components of those forces for a single abrasive grain is related to contact area between the grain and workpiece as well as workpiece hardness and friction coefficient between the abrasive and workpiece material [Shaw96]. At the first stage of contact of a grain with the workpiece, fully developed sliding occurs between the grain and workpiece and no material removal occurs. Then the indentation of the grain into the workpiece increases up to the point that contact stress is higher than the strength of the workpiece material, i.e. indentation reaches maximum elastic indentation and plastic deformation begin to occur. After this phase, grain penetration reaches its critical value for micro-cutting to occur. Therefore, the sliding force can be divided into three components. The first component of sliding is when the material is under elastic deformation and there is no chip formation. The second is when the material is under plastic deformation without chip formation and third component is when cutting and chip formation occurs. Figure 6.12 shows the elastic deformation (due to system stiffness), plastic deformation in the form of piled-up material in micro-ploughing, and finally chip formation as the last stage of the process. For the first component, assuming the loop stiffness of the machine is k and all other contact elements are rigid, then the normal force applied on the grain $F_{ng-sl-1}$ for the elastic deformation amount δ may be expressed as:

$$F_{ng-sl-1} = k \cdot \delta \quad ; \quad F_{fg-sl-1} = \mu \cdot k \cdot \delta \quad (6.61)$$

If the abrasive grit tip has a radius of r , the Hertzian contact stress can be determined to take into account the contact between two rollers, the first roller with a radius r and the second with a much larger radius, which can be assumed as infinity when comparing to the first. This contact stress was simplified by Ghosh et al [Ghos08] as:

$$\sigma_n = \frac{F_{ng-sl-1}}{r^2} \quad (6.62)$$

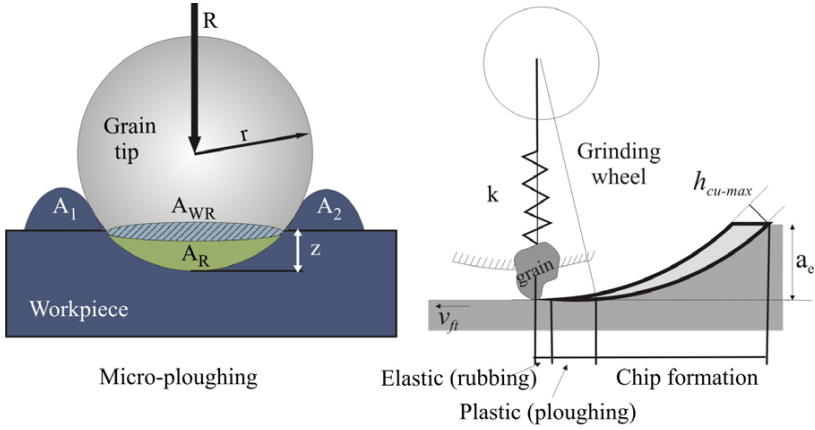


Figure 6.12: Schematic of micro-ploughing and rubbing due to system stiffness and chip formation

The loop stiffness is assumed to be constant and should be measured on the machine experimentally. Using equations (6.61) and (6.62), the maximum elastic deflection can be determined and the grain density of rubbing process can be calculated based on this value using the probability function of the grain distribution. Using equation (6.60)-(6.62), then:

$$\bar{F}_{n-sl-1} = \sigma_n \cdot r^2 \cdot \bar{N}_{mom-sl} \quad \text{and} \quad \bar{F}_{t-sl-1} = \mu \cdot \sigma_n \cdot r^2 \cdot \bar{N}_{mom-sl} \quad (6.63)$$

$$\text{and} \quad \bar{e}_{sl-1} = \bar{F}_{t-sl-1} \cdot \left(\frac{v_c}{a_e \cdot v_w \cdot b} \right) \quad (6.64)$$

The ratio of sliding force for the structured wheel to the conventional wheel using equation (6.54) can be expressed as:

$$\frac{(\bar{F}_{n-sl-1})_{stru}}{(\bar{F}_{n-sl-1})_{conv}} = \frac{(\bar{F}_{t-sl-1})_{stru}}{(\bar{F}_{t-sl-1})_{conv}} = \frac{(e_{stat-sl-1})_{stru}}{(e_{stat-sl-1})_{conv}} = \frac{(\bar{N}_{mom-sl-1})_{stru}}{(\bar{N}_{mom-sl-1})_{conv}} = \chi^\eta \quad (6.65)$$

The second sliding stage occurs along with ploughing, where there is an indentation with plastic deformation but without chip formation. The indentation of the active grains into the workpiece continues up to the critical value z_{crit} after which cutting occurs.

To have a mathematical model for the forces applied on an abrasive grain shown in figure 6.11, Chen and Row assumed the normal and tangential sliding forces for the up grinding case as follows [Chen96b]:

$$F_{ng-sl-2} = -\mu \cdot R_g \cdot \sin \theta \quad (6.66)$$

$$F_{fg-sl-2} = \mu \cdot R_g \cdot \cos \theta \quad (6.67)$$

where θ can be calculated from the grain geometry as:

$$\theta = \arccos\left(1 - \frac{z}{r}\right) \quad (6.68)$$

Then the average sliding forces on a single grain will be:

$$\bar{F}_{ng-sl-2} = \frac{I}{z_{crit}} \int_0^{z_{crit}} (\mu R \sin \theta) \cdot d(z) \quad (6.69)$$

$$\bar{F}_{fg-sl-2} = \frac{I}{z_{crit}} \int_0^{z_{crit}} (\mu R \cos \theta) \cdot d(z) \quad (6.70)$$

For a grain modelled as a sphere with rather large negative rake angle, Shaw was able to show that in fine grinding, the normal forces applied to the grain is similar to the forces seen in a Brinell hardness test [Shaw 96]. This implies that the normal force in cutting is proportional to the projected area of the indentation (A_{wg}), illustrated in figure 6.4, as well as hardness of the workpiece material (H), as follows:

$$R_g = K \cdot A_{wg} \cdot H \quad (6.71)$$

where K is a constant defined as the ratio of average pressure on the contact area to the uniaxial flow stress. In most cases K is about 1.0 [Shaw96]. So based on figure 6.4:

$$A_{wg} = \pi \cdot [r^2 - (r - z)^2] \quad (6.72)$$

At this stage $z \ll 2r$ and equation (6.72) can be written as:

$$A_{wg} \cong 2 \cdot \pi \cdot r \cdot z \quad (6.73)$$

The results of the integrals of equations (6.69) and (6.70) are equal for both structured and conventional wheels, as z_{crit} is the same for both wheel-workpiece systems. Therefore using equations (6.53)-(6.60) and the integral results, the ratio between the sliding force of structured wheel and the sliding force of the conventional wheel in this stage will be:

Theoretical Aspects and Modelling

$$\frac{(\bar{F}_{n-sl-2})_{stru}}{(\bar{F}_{n-sl-2})_{conv}} = \frac{(\bar{F}_{t-sl-2})_{stru}}{(\bar{F}_{t-sl-2})_{conv}} = \frac{N_{mom-stru}}{N_{mom-conv}} = \frac{N_{pl-stru}}{N_{pl-conv}} = \chi^{\psi} \quad (6.74)$$

Using following simplification, the sliding normal and tangential forces can be calculated. The average contact area can be found using:

$$\bar{A}_{wg} = \frac{l}{z_{crit}} \int_0^{z_{crit}} A_{wg} \cdot dz_{crit} \quad (6.75)$$

Then using equations (6.73) and (6.75):

$$\bar{A}_{wg} \cong \pi \cdot r \cdot z_{crit} \quad (6.76)$$

As $z \ll 2r$ that the following simplification can be used:

$$\sin \theta \approx \sqrt{\frac{2z}{r}} \quad \cos \theta = 1 - \frac{z}{r} \approx 1 \quad (6.77)$$

Therefore the integrals (6.69) and (6.70) can be solved to:

$$\bar{F}_{t-sl-2} \cong \frac{1}{2} \cdot \pi \cdot \mu \cdot K \cdot H \cdot r \cdot z_{crit} \cdot \bar{N}_{mom-sl-2} \quad (6.78)$$

$$\bar{F}_{n-sl-2} \cong \frac{2\sqrt{2}}{5} \cdot \pi \cdot \mu \cdot K \cdot H \cdot r^{\frac{1}{2}} \cdot z_{crit}^{\frac{3}{2}} \cdot \bar{N}_{mom-sl-2} \quad (6.79)$$

and using the equation (6.59), the specific energy for this stage becomes:

$$\bar{e}_{sl-2} = \bar{F}_{t-sl-2} \cdot \left(\frac{v_c}{a_e \cdot v_w \cdot b} \right) \quad (6.80)$$

The third stage of sliding occurs when cutting and chip formation begins. This stage will be studied together with chip formation later in section 6.3.4.

6.3.3 Implication on ploughing forces and energy

The ploughing force is mainly responsible for plastic deformation in the form of piled up material at the front and sides of the abrasive grain. Malkin assumed that the ploughing force

is constant for a given material removal rate, abrasive and workpiece material. This amount is considered by Malkin to be about $F'_{t-pl} = 1$ N/mm for steel as the specific tangential force due to ploughing, [Malk89]. The above mentioned assumption is basically acceptable if the topography of the wheel remains unchanged. But after a change in wheel topography, material removal rate is not the only parameter which influences the ploughing force, and instead the topography of the wheel has a direct influence on the interaction of grains with the workpiece and resulting plastic deformation, as it was seen in subsection 6.2.3.

To investigate the ploughing forces and energy, it is necessary to study a new term called relative chip volume f_{ab} which was defined by Zum Gahr [Zumg87] as the local ratio of the chip volume to the scratch volume on the workpiece (the transported volume), as illustrated in figure 6.12.

$$f_{ab} = \frac{A_R - (A_1 + A_2)}{A_R} = 1 - \frac{(A_1 + A_2)}{A_R} \quad (6.81)$$

$$f_{ab} = 0 \Rightarrow \text{Ideal ploughing}$$

$$f_{ab} = 1 \Rightarrow \text{Ideal cutting}$$

Giwerzew [Giwe03] showed that f_{ab} and specific energy in the case of a single grain scratching with low cutting speed, are reduced when the uncut chip thickness is increased. It is also shown that the results of scratching could be rather well confirmed in grinding experiments. Assuming that these results can be expanded to include grinding processes with higher grinding speed, generally, with increasing uncut chip thickness (or uncut chip area), the ploughing energy and corresponding ploughing forces will be reduced. The results of his work can be generally formulated as:

$$f_{ab} = k_1 \cdot h_{cu-max}^{k_2} \quad (6.82)$$

For the specific energy the results can be written in general form as:

$$e_c = \frac{k_3}{h_{cu-max}^{k_4}} \quad (6.83)$$

where k_1 , k_2 , k_3 and k_4 are positive constants and depend on the grinding parameters, workpiece properties and wheel specifications. Equation (6.83) is known as the influence of size effect on the specific energy. Equations (6.82) and (6.83) show that for the grains which do micro-cutting and produce chips, the ploughing specific energy is reduced with increasing chip thickness. In the case of wheel structuring there is exactly such a situation in which the uncut chip thickness is increased, as compared to the conventional wheel. So it can be estimated that even for the grains which do micro-cutting, the ploughing specific energy is

Theoretical Aspects and Modelling

reduced. But this energy portion is just a small part of the total energy consumed for ploughing, because there are lots of grains which perform micro-ploughing without chip formation. Hereby this component of the ploughing force and ploughing energy is investigated.

De Vathire et al. [Deva81] proposed that the scratch hardness can be defined as the ratio of the normal force during scratching to the bearing area. He developed his model for the ductile material based on a pyramid form of a grain and found the following equations for the average normal and tangential forces acting on a grain.

$$\bar{F}_{ng-pl} = H_s \cdot z_{crit}^2 \cdot \tan^2 \alpha \cdot (1 + \omega) \quad (6.84)$$

$$\frac{\bar{F}_{tg-pl}}{\bar{F}_{ng-pl}} = 1.8 - 0.02\alpha \quad (6.85)$$

$$H_s = (5.64 - 0.14\alpha + 0.001\alpha^2) \cdot H \quad (6.86)$$

$$\omega = 0.043 + 0.00514\alpha \quad (6.87)$$

where H_s is the scratch hardness, H is the workpiece hardness and α is the pyramid apex angle [Deva81].

Using equation (6.60), then :

$$\bar{F}_{n-pl} = \bar{F}_{ng-pl} \cdot N_{mom-pl} \quad \bar{F}_{t-pl} = \bar{F}_{tg-pl} \cdot N_{mom-pl} \quad (6.88)$$

and the specific energy can be written as:

$$e_{pl} = \frac{\bar{F}_{t-pl} \cdot v_c}{v_w \cdot a_c \cdot b} \quad (6.89)$$

Based on equation (6.84), the average ploughing force of grains up to the critical indentation level can approximately be constant for a given material and grain type, but the total ploughing force depends on the number of grains which do only micro-ploughing. This amount depends on the topography of the wheel. Besides it was observed that the number of such grains compared to the grains which do micro-cutting is extremely high, therefore it is inevitable that the main ploughing process was done by these grains which do not cut.

Using equations (6.9), (6.53) and (6.88), if the grinding parameters for both structured and conventional wheels are equal, then the ratio of the ploughing forces for the structured and conventional wheels can be expressed as:

$$\frac{(\bar{F}_{n-pl})_{stru}}{(\bar{F}_{n-pl})_{conv}} = \frac{(\bar{F}_{t-pl})_{stru}}{(\bar{F}_{t-pl})_{conv}} = \frac{N_{mom-stru}}{N_{mom-conv}} = \frac{N_{pl-stru}}{N_{pl-conv}} = \chi^{\psi} \quad (6.90)$$

6.3.4 Implication on cutting forces and energy

The sliding forces in the first and second stage, as well as main ploughing forces were modelled. Up to this stage of the total chip formation process there is no material removal, and theoretically so far the specific energy due to sliding and ploughing is infinity as the material removal is zero. To prevent this problem, the specific energies for sliding and ploughing modes were calculated using the total material removal rate which occurs in last stage of chip formation. This stage includes the final stage of the sliding process, as well as the chip formation component. Here, sliding and cutting occur simultaneously. To have a mathematical model for the forces applied on a grain, from figure 6.11, the normal and tangential forces for up-grinding are as follows [Chen96b]:

$$F_{ng-ch} = R_g \cdot \cos \theta \quad F_{ig-ch} = R_g \cdot \sin \theta \quad (6.91)$$

$$F_{ig-sl} = \mu \cdot R_g \cdot \cos \theta \quad F_{ng-sl} = -\mu \cdot R_g \cdot \sin \theta \quad (6.92)$$

So far, the specific energy due to cutting and sliding can be written as:

$$e_{g-ch} = \frac{R_g \cdot \sin \theta}{A_{cu}} \quad e_{g-sl} = \frac{\mu \cdot R_g \cdot \cos \theta}{A_{cu}} \quad (6.93)$$

The specific energy for each part can be defined as:

$$e_{ch} = \frac{l}{h_{cu-max}} \cdot \int_0^{h_{cu-max}} \frac{F_{ig-ch}}{A_{cu}} \cdot dh_{cu} \quad , \quad e_{sl-3} = \frac{l}{h_{cu-max}} \cdot \int_0^{h_{cu-max}} \frac{F_{ig-sl}}{A_{cu}} \cdot dh_{cu} \quad (6.94)$$

Using equations (6.14), (6.71), (6.73), (6.93) and with some simplifications based on $h_{cu} \ll r$, the result of integrals in equation (6.94) for sliding and cutting at the stage of chip formation (after rubbing and ploughing) will be:

$$e_{ch} \cong \frac{3\sqrt{2}}{2} \cdot \pi \cdot K \cdot H \quad (6.95)$$

Theoretical Aspects and Modelling

$$e_{sl-3} = \frac{3\sqrt{2}}{2} \cdot \pi \cdot \mu \cdot K \cdot H \cdot \left(r^{\frac{1}{2}} \cdot \bar{h}_{cu}^{-\frac{1}{2}} - \frac{4}{3} r^{\frac{1}{2}} \cdot \bar{h}_{cu}^{\frac{3}{2}} \right) \quad (6.96)$$

In equation (6.96), as $\left(r^{\frac{1}{2}} \cdot \bar{h}_{cu}^{-\frac{1}{2}} \gg \frac{4}{3} r^{\frac{1}{2}} \cdot \bar{h}_{cu}^{\frac{3}{2}} \right)$ this equation can be approximated as:

$$e_{sl-3} \cong \frac{3\sqrt{2}}{2} \cdot \pi \cdot \mu \cdot K \cdot H \cdot r^{\frac{1}{2}} \cdot \bar{h}_{cu}^{-\frac{1}{2}} \quad (6.97)$$

Then using equations (6.59), (6.91), (6.92), (6.95) and (6.97), the following results for the forces will be achieved:

$$\bar{F}_{t-ch} \cong \frac{3\sqrt{2}}{2} \cdot \pi \cdot K \cdot H \cdot v_c^{-1} \cdot v_w \cdot a_e \cdot b \quad (6.98)$$

$$\bar{F}_{t-sl-3} \cong \frac{3\sqrt{2}}{2} \cdot \pi \cdot \mu \cdot K \cdot H \cdot r^{\frac{1}{2}} \cdot \bar{h}_{cu}^{-\frac{1}{2}} \cdot v_c^{-1} \cdot v_w \cdot a_e \cdot b \quad (6.99)$$

$$\bar{F}_{n-ch} \cong \frac{3\sqrt{2}}{2} \cdot \pi \cdot K \cdot H \cdot r^{\frac{1}{2}} \cdot \bar{h}_{cu}^{-\frac{1}{2}} \cdot v_c^{-1} \cdot v_w \cdot a_e \cdot b \quad (6.100)$$

$$\bar{F}_{n-sl-3} \cong -\frac{3\sqrt{2}}{2} \cdot \pi \cdot \mu \cdot K \cdot H \cdot v_c^{-1} \cdot v_w \cdot a_e \cdot b \quad (6.101)$$

Using equation (6.28) as well as equations (6.95), (6.98) and (6.101) the force and specific energy ratio for the corresponding terms of the structured and conventional wheels will be:

$$\frac{\left(\bar{F}_{n-sl-3} \right)_{stru}}{\left(\bar{F}_{n-sl-3} \right)_{conv}} = \frac{\left(\bar{F}_{t-ch} \right)_{stru}}{\left(\bar{F}_{t-ch} \right)_{conv}} = \frac{e_{ch-struc}}{e_{ch-conv}} = 1 \quad (6.102)$$

So far using equation (6.28) as well as equations (6.97), (6.99) and (6.100) the force and specific energy ratio for the structured and conventional wheels will be:

$$\frac{\left(\bar{F}_{t-sl-3} \right)_{stru}}{\left(\bar{F}_{t-sl-3} \right)_{conv}} = \frac{\left(\bar{F}_{n-ch} \right)_{stru}}{\left(\bar{F}_{n-ch} \right)_{conv}} = \frac{\left(e_{sl-3} \right)_{stru}}{\left(e_{sl-3} \right)_{conv}} = \left(\frac{\bar{h}_{cu-stru}}{\bar{h}_{cu-conv}} \right)^{-1} = \chi^{10^{\frac{3}{5}}} \quad (6.103)$$

The total tangential and normal force, as well as total specific energy will be the summation of each of the above mentioned components of sliding, ploughing and cutting. The reduction

of forces as well as specific energy are proven, as the parameters of ζ , ψ and η have positive values. The amount of the reduction as well as validation of the model will be discussed in chapter 7.

6.3.5 Validation of the force and energy models

The validation of the force and energy models is presented in this section. Hereby the two most important parameters in the grinding process, i.e. tangential grinding force and grinding specific energy, will be the focus of investigation for validation of the force and energy models. Validation was done for a conventional grinding wheel with 100% contact layer, and for a structured grinding wheel with conditioned abrasive layer of just 25%. In this section, the target is to show how closely the model results and the experimental results compare. The explanation of why the tangential grinding forces or specific energy change due to reduction of contact area will be described in more detail in the next chapter.

Table 6.4 illustrates the input parameters considered for the study.

Table 6.4: Test conditions for vitrified bond CBN grinding wheel

Grinding wheels	Vitrified bond CBN grinding wheel, B126 C125; Ø400 mm x 15 mm
Grinding conditions	Feed speed v_{fi} = 500-2500 mm/min; Cutting speed v_c = 60 m/s; Depth of cut a_c = 0.005-0.025 mm; No Coolant (Dry grinding)
Workpiece	100Cr6; Hardness = 60 HRC, 2.18 GP _a Dimension = 100x60x30 (mm x mm x mm);
Dressing conditions	Dressing cutting speed v_{cd} = 60 m/s; Dressing infeed a_{ed} = 5 μ m; Dressing ratio: q_d =-0.9; Dressing feed : v_{fad} =153 mm/min; Total dressing depth: a_d = 10 μ m

A vitrified bond grinding wheel was dressed using a diamond disc roller with the conditions presented in the table 6.4, and then the special structure was produced using another diamond disc dresser (average width of 0.5 mm and inclined angle of 60°), as was outlined in section 5.2. The resulting wheel structure with 25% contact layer was compared with a similar grinding wheel having a conventional 100% contact layer. The elastic deformation of the wheel-workpiece system is considered to be 1 μ m. The critical indentation is considered 3.78

Theoretical Aspects and Modelling

μ as was discussed in chapter 6. Using the same calculations demonstrated in table 6.3, the rubbing, ploughing and cutting edges are calculated.

Figures 6.13 to 6.15 illustrate a comparison of the model results and experimental results for specific grinding energy as well as for specific tangential grinding force.

Grinding wheel	: B126, C125, Vitrified	Grinding speed	: $v_c = 60$ m/s
Wheel width	: 15 mm	Feed rate	: $v_{ft} = 0.5-2.5$ m/min
Wheel diameter	: 400 mm	Depth of cut	: $a_c = 15$ μ m
Material	: 100Cr6, 60 HRC	Grinding type	: Dry grinding

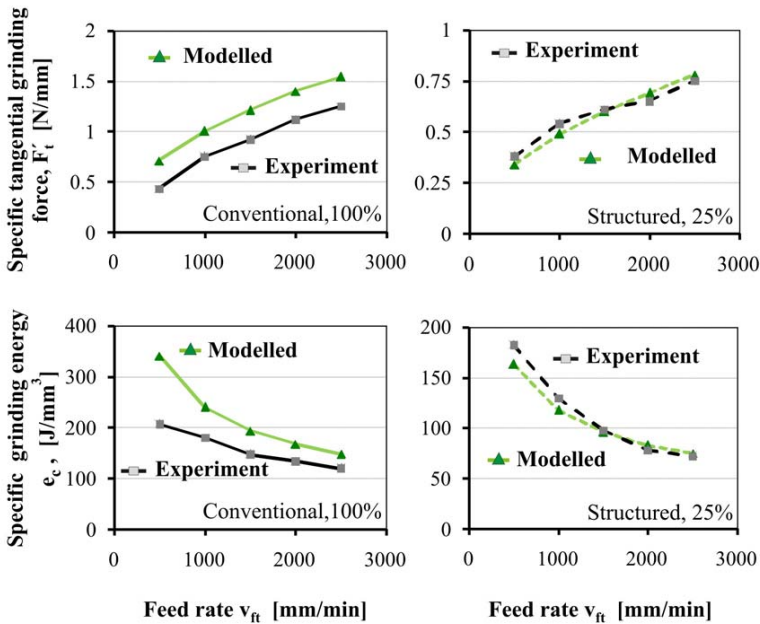


Figure 6.13: Comparison of the predicted and measured specific tangential grinding force and specific grinding energy versus feed rate for conventional and structured wheel

A global overview of the figures shows a close trend between the modelled and experimental results. However it is generally observed that the model is more closely matched for the structured wheel as compared with the conventional wheel.

Grinding wheel	: B126, C125, Vitrified	Grinding speed	: $v_c = 40-60$ m/s
Wheel width	: 15 mm	Feed rate	: $v_{ft} = 1.5$ m/min
Wheel diameter	: 400 mm	Depth of cut	: $a_e = 15$ μm
Material	: 100Cr6, 60 HRC	Grinding type	: Dry grinding

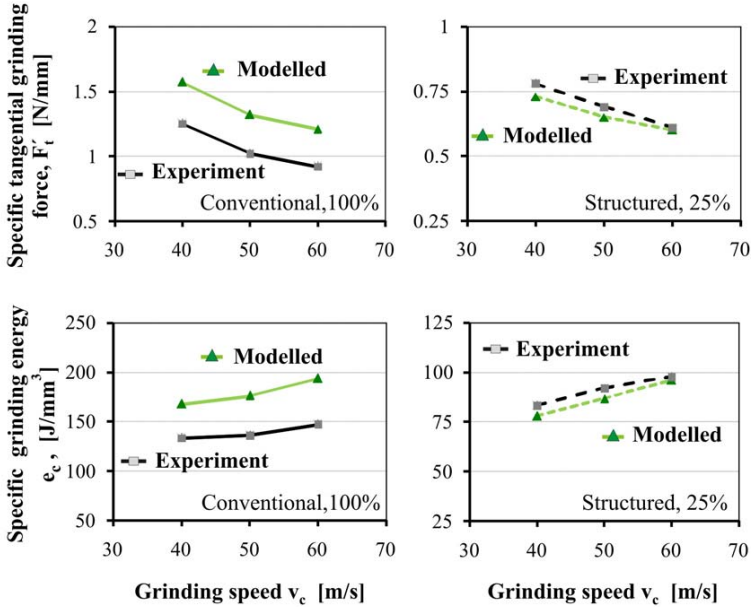


Figure 6.14: Comparison of the predicted and measured specific tangential grinding force and specific grinding energy versus grinding speed for conventional and structured wheel

Figure 6.13 highlights the results of comparison at a constant depth of cut of 15 μm and constant grinding speed of 60 m/s. At the upper side of the figure, the tendency of the variation of specific tangential force versus feed rate is similar to the model results. Considering the lower side of the figure, where the specific energy of the model results are compared with experiments, a similar close estimation of specific grinding energy, especially in the case of the structured wheel, is achieved using the developed model. As it was predicted with increasing feed rate at constant grinding speed and depth of cut, the tangential grinding force is increased and the specific grinding energy is decreased.

Figure 6.14 presents results for specific tangential grinding force and specific grinding energy versus grinding speed, at constant depth of cut of 15 μm and constant feed rate of 1.5 m/min.

Theoretical Aspects and Modelling

The reduction of grinding forces with increasing grinding speed can also be observed in both model and experimental results. The tendency is again similar for both cases, however, the structured wheel with 25 % abrasive layer shows better conformity with the model results than that of the conventional wheel. At constant feed rate, the specific energy is slightly increased with increasing grinding speed. Hereby the tendency for both the model and experiments are also similar. As it can be observed, the modelling results are nearer to the experimental results in the case of the structured wheel.

Grinding wheel	: B126, C125, Vitrified	Grinding speed	: $v_c = 60$ m/s
Wheel width	: 15 mm	Feed rate	: $v_{ft} = 1.5$ m/min
Wheel diameter	: 400 mm	Depth of cut	: $a_c = 10-25$ μm
Material	: 100Cr6, 60 HRC	Grinding type	: Dry grinding

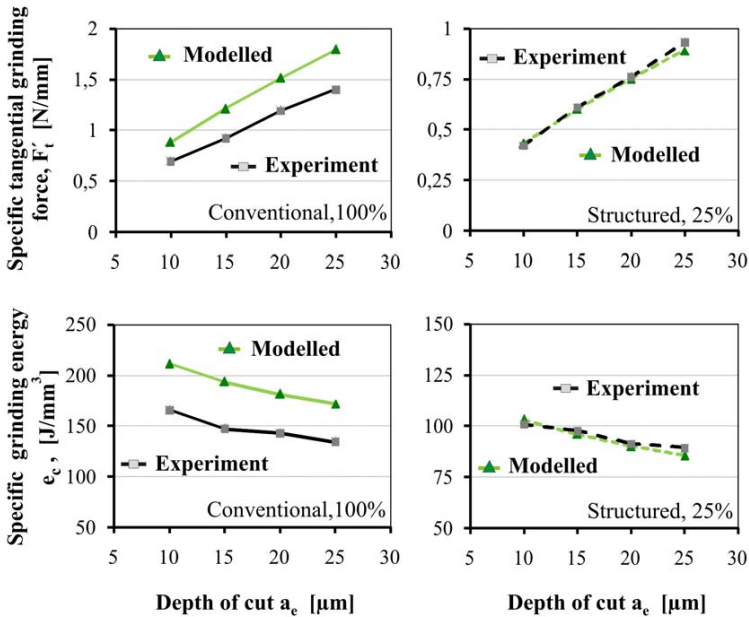


Figure 6.15: Comparison of the predicted and measured specific tangential grinding force and specific grinding energy versus depth of cut for conventional and structured wheel

In figure 6.15, modelled and experimental specific grinding energy and specific tangential grinding force are shown versus depth of cut. The depth of cut is varied at a constant grinding speed of 60 m/s and constant feed rate of 1.5 m/min. The left side of the figure presents the

comparison for the conventional wheel and the right side demonstrates the results for the structured wheel with 25% contact layer. With increasing the depth of cut, the grinding force also increases and the specific grinding energy is reduced. The tendency of the both model results and experiments are very similar as in the previous figures. Hereby better conformity between model and experiments is also observed in the case of using the structured wheel.

Considering the error between the modelled and experimental results which can be calculated in general form as:

$$Error = \sqrt{\sum \left(\frac{X_{mod} - X_{exp}}{X_{exp}} \right)^2} \frac{1}{n} \times 100\% \quad (6.104)$$

Where X_{mod} is the value calculated using model, X_{exp} is the value achieved by experiment and n is the number of experimental data . By calculation, the amount of error for the structured wheel with 25% contact layer is about 5% and for the conventional wheel error is about 23%. The main source of this difference between the model and experimental results is due to the simplification and assumptions which were considered in the development of model.

As it can be seen in all cases, the modelling results are closer to the experimental results for the structured wheel with 25% contact layer as compared to the conventional grinding wheel. The reason is perhaps due to the fact that the amount of grains which do rubbing and ploughing is considered nearer to the real case. It means that the model is more sensitive to the effects of rubbing and ploughing. Finally, it is necessary to mention that a more accurate model is needed in future regarding the grinding process which provides more uniform results for any type of wheel topography.

6.4 THERMAL ASPECTS AND CORRESPONDING MODELLING

Thermal analysis has greatly clarified the importance of various physical processes involved in grinding [Rowe01b]. High specific energy of the grinding process causes high temperature in the grinding zone that can affect surface integrity of the workpiece as well as wear of the grinding wheel. The high negative rake angle of the abrasive and small chip size in grinding processes, as an undefined cutting edge process, comparing to the processes with defined cutting edges such as turning or milling, generates considerable rubbing between the abrasive and workpiece [Tawa06]. Moving heat source theory is usually the basis of the thermal analysis of the grinding processes and the related temperature which rises on the workpiece surface. The total grinding energy is considered to be converted partially into heat in the grinding contact length. The fraction of the total heat transported to the workpiece is a critical parameter needed to calculate the process temperature. The aim of this section is to investigate the effect of wheel structuring on the thermal aspects of the process.

6.4.1 Implication on heat generation and heat partitioning

The heat generated in the contact zone is assumed to be conducted to the workpiece, grinding wheel, chips and coolant. In general cases, the amount of the heat which flows into the workpiece depends on many parameters such as workpiece material, abrasive material, grinding parameters, wheel specification, cooling efficiency, etc. Figure 6.16 presents a global view of the percentage of each portion of transferred heat [Brin04].

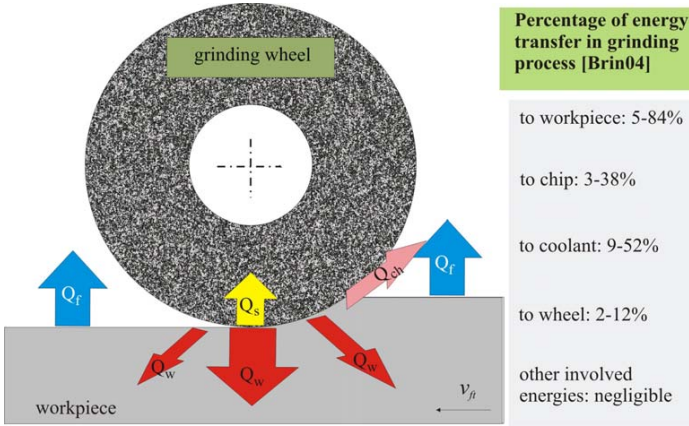


Figure 6.16: Schematic of the heat partitioning in the grinding process

To calculate more accurate values for the heat flow into the workpiece, a model is considered based on the works of Rowe and Stephenson [Rowe01b, Step03]

Assuming that the total power and energy consumed in the contact zone is changed to heat (because the other involved energies such as chip kinetic energy, residual strain energy of the workpiece, etc. are considered negligible in comparison), the total heat power Q is expressed as:

$$Q = Q_w + Q_s + Q_{ch} + Q_f \tag{6.105}$$

where Q_w , Q_s , Q_{ch} and Q_f are the heat power transferred to the workpiece, wheel, chips and coolant respectively.

In the case of dry grinding, as there is no coolant and the heat conducted by air is negligible, $Q_f \approx 0$. Therefore the total heat flux q_t can be partitioned based on equation (6.105) and the related area of each term as:

$$Q_t = q_w \cdot A_w + q_s \cdot A_s + q_{chip} \cdot A_{chip} \quad (6.106)$$

Considering the total contact area, the heat flux will be calculated as:

$$q_t = \frac{Q_t}{A} = q_w + q_s \cdot \frac{A_s}{A} + q_{chip} \cdot \frac{A_{chip}}{A} \quad (6.107)$$

$$\text{with } A = A_w = l_g \cdot b \quad (6.108)$$

where A_s is the total grain contact area with the workpiece in the contact zone, and q_w , q_s , and q_{chip} are the heat flux flows into the workpiece, wheel and chips, respectively; and q_t is the total heat flux .

The heat flux into the chips can be written as [Step03]:

$$q_{chip} = e_{chip} \cdot \frac{a_e \cdot v_w}{l_g} \quad (6.109)$$

$$\text{with } e_{chip} = \rho_w \cdot c_w \cdot T_{ch} \quad (6.110)$$

where e_{chip} is the specific energy of the chips, ρ is the density of workpiece material, c_w is the specific heat capacity, and T_{chip} is the chip temperature which can reach the melting point [Jin02, Step03]. Malkin [Malk06] assumed that the chips reach the melting point and calculated the approximate value of 6 J/mm^3 for specific energy of chips for ferrous materials.

The total heat flux q_t can be defined as [Jin02]:

$$q_t = e_c \cdot \frac{a_e \cdot v_w}{l_g} \quad (6.111)$$

where e_c is the specific grinding energy, a_e is the depth of cut, v_w is the feed rate and l_g is the contact length.

It was seen in the last section that the specific grinding energy can be considerably reduced in the case of using a structured wheel. So by equation (6.111), if other parameters a_e , v_w and l_g

Theoretical Aspects and Modelling

are considered to be equal for both the structured and conventional wheels, it can be concluded that:

$$\frac{q_{t-stru}}{q_{t-conv}} = \frac{e_{c-stru}}{e_{c-conv}} \quad (6.112)$$

As it was seen in the previous section, the specific energy is reduced by structuring, therefore the equation (6.112) shows that the total heat flux is also reduced when using the structured wheel, so it can be estimated that the temperature on the workpiece surface will be reduced as well or:

$$q_{t-stru} < q_{t-conv} \quad \text{and} \quad T_{\max-stru} < T_{\max-conv} \quad (6.113)$$

The heat flux into the grains and workpiece are changed by structuring. To obtain the heat flux flow to the workpiece and to the wheel, the “grain-workpiece contact analysis” of Hahn [Hahn62] is considered in this study. Based on this model, if a grain slides on the surface of the workpiece and the heat flux which flows into the workpiece is q_{wg} , and heat flux flowing into the grain is q_g , the heat fluxes and the temperature at the grain-workpiece contact T_{gw} can be expressed as:

$$q_g = h_g \cdot T_{gw} \quad (6.114)$$

$$q_{wg} = h_{wg} \cdot T_{gw} \quad (6.115)$$

Generally a workpiece-wheel partition ratio R_{ws} can be considered to divide the partial heat flux which flows into the workpiece as:

$$R_{ws} = \frac{q_{wg}}{q_{wg} + q_g} = \frac{h_{wg}}{h_{wg} + h_g} \quad (6.116)$$

In a steady state condition, if the contact shape is assumed to be circular, R_{ws} can be written as [Rowe96a, Mari04, Malk07]:

$$R_{ws} = \left(1 + \frac{0.97\lambda_g}{\sqrt{\lambda_w \cdot \rho_w \cdot c_w \cdot \sqrt{r_o \cdot v_s}}} \right)^{-1} \quad (6.117)$$

where λ_g and λ_w are the heat conductivities of the grain and workpiece, respectively, ρ_w is the density of the workpiece, c_w is the specific heat capacity of the workpiece and r_o is the

effective radius of the abrasive grain in contact with the workpiece, which can be assumed as the grain tip radius based on the spherical model for the grain tip shown in figure 6.4.

The heat conducted to the workpiece is generated by the abrasive grains during the time that each single grain is in contact with workpiece, and flows into the workpiece through each individual grain contact area. Therefore, if the heat transfer to the surrounding is considered negligible, then:

$$q_w \cdot A = q_{wg} \cdot A_s \quad (6.118)$$

$$Q_s = q_g \cdot \sum_1^{N_{mom}} A_{wg} = q_s \cdot A_s \quad (6.119)$$

where q_{wg} is the average heat flux which conducts to the workpiece across the contact area between grain and workpiece, q_g is the average heat flux which conducts to the grain at the same contact area, and \bar{A}_{wg} is the projection of the contact area of the grain and workpiece as illustrated in figure 6.4; and therefore :

$$A_s = \sum_1^{N_{mom}} A_{wg} \approx \bar{N}_{mom} \cdot \bar{A}_{wg} \quad (6.120)$$

Considering the parameter R as the ratio of the total heat flux flowing into the wheel to the total heat flux flowing into the workpiece, it can be observed from equations (6.116)-(6.120) that:

$$R = \frac{q_s}{q_w} = \left(\frac{1}{R_{ws}} - 1 \right) \frac{A}{\bar{N}_{mom} \cdot \bar{A}_{wg}} \quad (6.121)$$

To compare this ratio for structured and conventional wheels, as it can be seen from equation (6.117), the value of R_{ws} depends on the material properties of the grain and workpiece, radius of the grain tip, and grinding speed. This parameter is approximately equal for both structured and conventional wheels under the same grinding conditions (the wheel wear is not considered in calculation).

The workpiece-wheel contact area A is also constant based on equation (6.108), therefore the parameter R for structured (R_{stru}) and conventional (R_{conv}) wheels can be written as:

$$\frac{R_{stru}}{R_{conv}} = \frac{\bar{N}_{mom-conv}}{\bar{N}_{mom-stru}} \cdot \frac{\bar{A}_{wg-conv}}{\bar{A}_{wg-stru}} \quad (6.122)$$

Theoretical Aspects and Modelling

Using equation (6.76), and considering the proportional relation of mean uncut chip thickness and grain indentation, the ratio of the average projection of contact area of a grain in the case of the structured and conventional wheels will be:

$$\frac{\bar{A}_{wg-stru}}{\bar{A}_{wg-conv}} \cong \frac{\bar{z}_{cu-stru}}{\bar{z}_{cu-conv}} = \frac{\bar{h}_{cu-stru}}{\bar{h}_{cu-conv}} \quad (6.123)$$

Using equations (6.8), (6.16) and (6.26), for the part of chip formation in grinding processes, then:

$$\frac{\bar{N}_{mom-stru}}{\bar{N}_{mom-conv}} = \frac{\bar{A}_{cu-conv}}{\bar{A}_{cu-stru}} \cong \frac{\bar{z}_{conv}}{\bar{z}_{stru}} = \frac{\bar{h}_{cu-conv}^{\frac{3}{2}}}{\bar{h}_{cu-stru}^{\frac{3}{2}}} \quad (6.124)$$

and using equations (6.121) – (6.124):

$$\frac{R_{stru}}{R_{conv}} \cong \left(\frac{\bar{z}_{stru}}{\bar{z}_{conv}} \right)^{\frac{1}{2}} \cong \left(\frac{\bar{h}_{cu-stru}}{\bar{h}_{cu-conv}} \right)^{\frac{1}{2}} \quad (6.125)$$

Equation (6.125) shows that the ratio of the heat flux into the grains and heat flux into the workpiece is proportional to grain indentation (and in the case of chip formation, to mean uncut chip thickness). As for the structured wheel, this indentation is higher, thus obviously R_{stru} is greater than R_{conv} . This ratio can be calculated, in each phase, using cutting edge density of each phase of the grinding process based on the grain distribution function explained in section 6.2.3.

6.4.2 Implication on workpiece temperature

In the previous section heat partitioning of the grinding process was studied. The mathematical calculation to determine the portion of the heat which flows into the workpiece is necessary to calculate the temperature of the workpiece. Most of the models for calculating temperature are based on the work of Jaeger and Carslaw [Jaeg42, Cars59] for a moving heat source. Their approach was developed for a two dimensional heat source which moves with a constant velocity along the surface of a semi-infinite solid (workpiece). For this model, which is illustrated in figure 6.14, the temperature rise in two dimensional cases $T(X,Z)$ can be written as [Brin06, Mari04]:

$$T(X,Z) = \frac{2 \cdot \alpha_w \cdot q_w}{\pi \cdot \lambda_w \cdot v_w} \cdot \int_{X-L}^{X+L} e^{-u} \cdot K_\theta \cdot \left(\sqrt{u^2 + Z^2} \right) \cdot du \quad (6.126)$$

where K_0 is the modified Bessel function of the second kind of order zero, and α_w is the thermal diffusivity of the workpiece. X , Z , L and u are the dimensionless parameters expressed as follows:

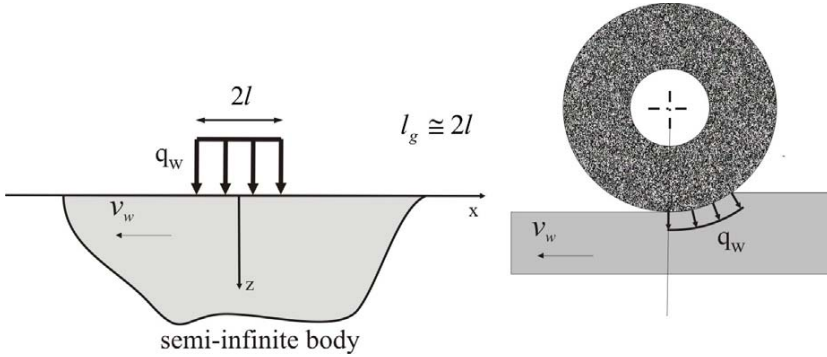


Figure 6.17: Thermal modelling based on a moving heat source on a semi infinite solid

$$X = \frac{v_w \cdot x}{2 \cdot \alpha_w}; \quad Z = \frac{v_w \cdot z}{2 \cdot \alpha_w}; \quad L = \frac{v_w \cdot l_g}{4 \cdot \alpha_w}; \quad u = \frac{v_w \cdot (x - x_0)}{2 \cdot \alpha_w} \quad (6.127)$$

$$\alpha_w = \frac{\lambda_w}{\rho_w \cdot c_w} \quad (6.128)$$

where x and z are the directions as defined in figure 6.17, and l_g is the geometrical contact length. The assumptions which must be considered for proper use of equation (6.126) are according to Marinescu et al [Mari04]:

- The temperature field in the workpiece is quasi-stationary
- The thermal properties of the workpiece are not changed due to changing temperature
- The body of the workpiece is assumed semi-infinite
- All of the heat energy is transferred to the workpiece
- The heat flux is perpendicular to the feed rate

As the computation of the above mentioned integral equation is rather complex, some of the authors introduced other simplified solutions which can be applied with a good approximation for temperature. The maximum temperature is expressed by Rowe and Marinescu et al. [Rowe01a, Mari04] as:

Theoretical Aspects and Modelling

$$T_{\max} = \frac{C \cdot q_w}{\sqrt{\lambda_w \cdot \rho_w \cdot c_w}} \sqrt{\frac{l_g}{v_w}} \quad (6.129)$$

The parameter C is a constant which depends on the heat source distribution and so-called Peclet number which is shown in table 6.5. Peclet number is defined as [Mari04]:

$$Pe = \frac{v_w \cdot l_g}{4 \cdot \alpha_w} \quad (6.130)$$

Table 6.5: Relation of temperature factor C with Peclet number for a triangular heat flux [Mari04]

Peclet number (Pe)	C
Pe > 10	1.06
0.2 < Pe < 10	$\frac{0.95}{\pi} \cdot \sqrt{2\pi + \frac{Pe}{2}}$
Pe < 0.2	0.76

A similar expression was developed by Malkin and Guo [Malk07, Guo94]. For a triangular heat source, the maximum temperature is given by:

$$T_{\max} = \frac{(1.06) \cdot q_w \cdot \alpha_w^{0.5} \cdot a_e^{0.25} \cdot d_e^{0.25}}{\lambda_w \cdot v_w^{0.5}} \quad (6.131)$$

The above mentioned equations result when the Peclet number is greater than 5, although both equations are also fairly accurate for a Peclet number greater than 1 [Malk07]. Takazawa [Taka66] developed the following function for the temperature rise at a depth of z under the workpiece surface by:

$$T(z) = \frac{2 \cdot q_w \cdot \alpha_w}{\pi \cdot \lambda_w \cdot v_w} \cdot (3.1) \cdot L^{0.53} \cdot e^{-0.69L^{-0.37z}} \quad (6.132)$$

In chapter 7, the above mentioned models will be applied to calculate grinding temperatures, comparing the results with experimental measured temperatures for both conventional and structured grinding wheels.

6.5 PREDICTION OF PROCESS USING ARTIFICIAL NEURAL NETWORK

As it was described in chapter 2, the neural network method is one of the powerful tools used to predict and model a phenomenon, especially if the factors which influence the phenomena are too complicated to be analytically described. Neural network consists of a number of interconnected processing elements called neurons. The neurons calculate the sum of the computed weighted inputs and then apply a linear or non-linear function called transfer function to determine the outputs. The network is fed with a large amount of training data that represent the pattern attempting to be modelled. The weights are computed by an iterative method during the training process. Neural networks process consists of two main stages which are training and verification. During the training process, specific inputs together with the corresponding solve outputs are introduced to the system. A learning algorithm is implemented to adjust the weights between neurons in a way that the error between neural system outputs and targets becomes minimum. The application of ANN model for prediction of machining processes is used widely by researches however until now there have been no clear rules that could serve as a basis to be followed in producing a perfect model.

For this study, it was desired to create neural networks for the off-line prediction of grinding process results in flat surface dry grinding of hardened steel specimens. These predictions could later be used to design and optimize process conditions in similar operations. Existing experimental data which facilitated the study included four different input parameters; these were the grinding wheel surface structure, grinding speed, feed rate, and depth of cut. Output data were measured normal and tangential grinding forces, workpiece surface roughness, and the occurrence of grinding burn. The RBF (Radial Basis Function) network architecture was selected because of its previous successful employment in grinding prediction, although this had been for an on-line detection system using AE (Acoustic Emissions) and power signals [Wang01]. It was thus decided to compare this network architecture with the more common back propagation network using LM (Levenberg-Marquardt) training, that which had been successfully employed by E. Brinksmeier [Brin98] for a similar off-line grinding prediction system, and also by T. Özel and Y. Karpat [Özel05] for their comprehensive study of hard turning prediction by neural network method. The goal was to determine the most suitable network type for this research, using the Matlab Neural Network Toolbox application.

After careful consideration of the network details seen in the three main papers previously mentioned, it was decided to create three types of networks; one for the simultaneous prediction of tangential and normal grinding forces, another for the surface roughness parameters R_z and R_a , and a third for the prediction of grinding burn. Networks were created using both RBF and LM-back-propagation network types for comparison. Two different data sets were used: one with measurements only taken from the 25% contact layer, and another using complete data taken from all CBN contact layers (i.e. 25, 50, 75, and 100%). Table 6.6

Theoretical Aspects and Modelling

listed the combinations of prediction type, network type, and dataset type employed for this study.

Available data included 240 different input combinations; 60 of these were for the 25% CBN contact layer. Training data were selected to represent as many potential scenarios as possible without overtraining the network. Half of the existing data were thus grouped into a training set, and the other half was used to test each resulting network. The number of neurons in the hidden layer had to be specified for the LM networks, while this parameter was automatically optimised by RBF networks during training. Each of the four LM network types in table 6.6 were also slightly different because of the nature of the interaction between chosen input parameters, of selected training data and of the desired outputs.

Table 6.6: Test conditions with vitrified bond CBN wheel

#	Network type		Prediction type			CBN-layer database		Network type
	RBF	LM	Forces	Roughness	Burn	25%	All	Structure
1	X		X			X		4-29-2
2		X	X			X		4-4-2
3	X		X				X	4-117-2
4		X	X				X	4-40-2
5	X			X		X		4-13-2
6		X		X		X		4-4-2
7	X				X		X	4-111-2
8		X			X		X	4-3-1

The grinding test condition using resin bond CBN wheel is presented in table 6.7. The number of hidden layer neurons was selected for each network to produce the most repeatable and accurate results. Network training parameters such as learning rate (for LM) and function spread (for RBF) were optimized to produce best results and these remained unchanged to facilitate the comparison of network performance.

The grinding wheel was dressed with diamond roll with the conditions being presented in table 6.7 and then the special structure was produced with a CVD diamond profile dresser as discussed in chapter 5. Wheel surface structures with 25%, 50% and 75% CBN contact layer were applied for comparison with the conventional 100% layer. Both tangential and normal grinding forces were measured. The network results presented in figures 6-18 and 6-19 and table 6.8 provide a comparison between RBF and LM network types, highlighting only those for a cutting speed of 60 m/s.

Table 6.7: Test conditions with vitrified bond CBN wheel

Grinding wheels	Resin bond CBN grinding wheel, B126 C100; Ø400 mm x 15 mm
Grinding conditions	Workpiece: 100Cr6, 60 HRC; Feed speed $v_{ff}= 500-2500$ mm/min; Cutting speed $v_c= 60$ m/s; Depth of cut $a_e= 0.005-0.025$ mm; No coolant (Dry grinding)
Dressing conditions	Dressing cutting speed $v_{cd}= 60$ m/s; Dressing infeed $a_{ed}= 5$ μ m; Dressing ratio: $q_d=-0.9$; Dressing feed : $v_{fad}=153$ mm/min; Total depth of dressing: $a_e= 10$ μ m

Figure 6.18 demonstrates the comparison of LM method with RBF method based on the prediction of normal and tangential forces by dry grinding.

It is seen that both methods predict the forces during dry grinding with a very good accuracy. For both predicted and experimental value, the tangential and normal grinding forces are increased with a very close trend when the depth of cut increased at the constant grinding speed and constant feed rate. A similar situation can be observed when the feed rate is increased at the constant grinding speed and constant depth of cut. The error in worst situation is less than 3% which shows a very good prediction by neural network analysis.

Figure 6.19 illustrates the comparison of RBF and LM neural networks results for prediction of workpiece surface roughness (Rz and Ra). The accuracy of these results is not as good as that of grinding forces. This may reflect the inaccurate measurement of roughness by roughness tester which has a normal 20% variation in the measurement of different regions of the ground surface. Numerical roughness values are also very small and numerically very close, making it more difficult to establish a defined pattern by neural network method.

Although the prediction of roughness by neural network method could not provide very accurate results comparing to the prediction of forces, it is still a rather valuable tool since the error between the experimental values and predicted values is less than 20%, which is quite acceptable in many applications.

Theoretical Aspects and Modelling

Grinding wheel	: B126, C100, Resin	Grinding speed	: $v_c = 60$ m/s
Wheel dim.	: 15 mm X 400 mm	Feed rate	: $v_{ft} = 0.5-2$ m/min
Wheel type	: Structured 25%	Depth of cut	: $a_c = 5-25$ μm
Material	: 100Cr6, 60 HRC	Grinding type	: Dry grinding

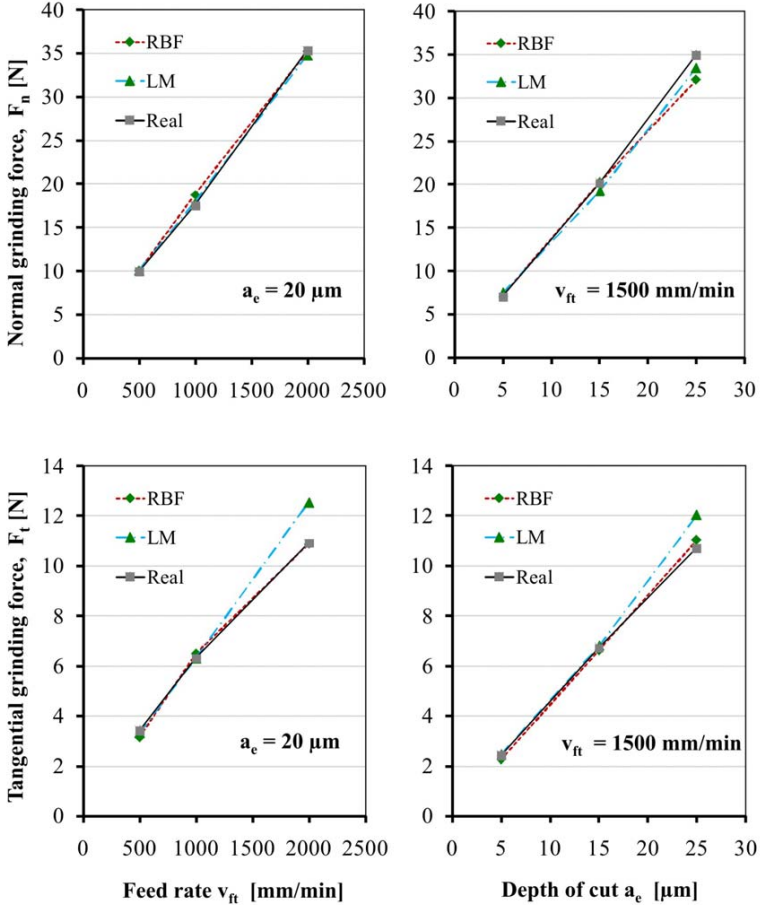


Figure 6.18: Measured and predicted grinding forces for 25% CBN contact layer

Table 6.8 shows the results of burn prediction by neural network analysis, comparing with experiments. The results demonstrate that burn prediction accuracy is very good. Among 120 input combinations tested on each network, only a total of 16 RBF predictions and 15 LM predictions were false, illustrating comparable and accurate results for both, with at least 87% accuracy, and both network types demonstrated good repeatability.

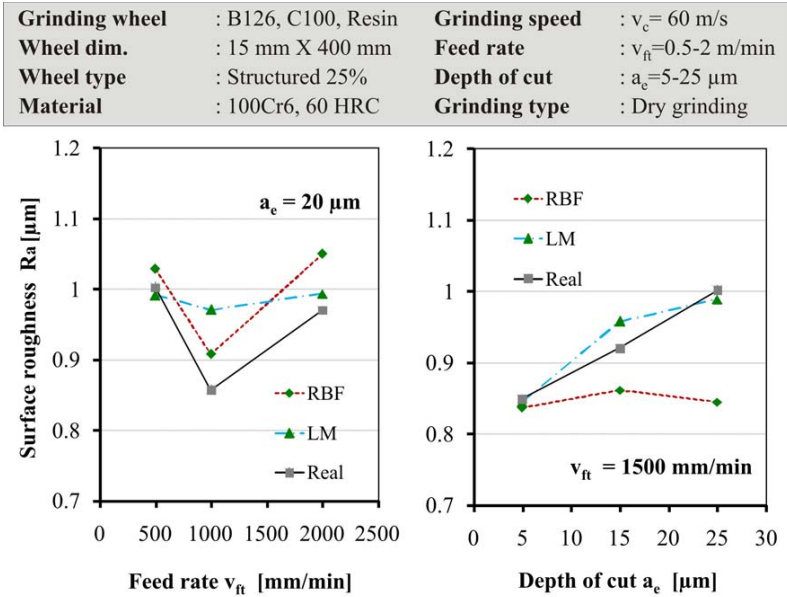


Figure 6.19: Measured and predicted surface roughness for 25% CBN contact layer

It should be noted that neural networks are normally initialized with random value weights for all neurons, so the same initialization parameters actually produced slightly different results with each identical trial, since the various random weights had to be adjusted differently during network training. This phenomenon was especially notable for LM networks; so although some of the most accurate LM results are presented, such results were not achieved at every trial and some trials even produced very poor results. Accurate results from RBF networks were generally more repeatable than of LM networks, which could be attributed to the fundamental differences between the training behaviour of each network type.

As a short summary and interpretation of this section, it can be noted that RBF and LM network types are both capable of producing very accurate results for surface grinding prediction, however, careful attention must be paid to network selection and training parameters. Each network type is mathematically different and thus some types are better suited for certain applications than other types of networks. The RBF network seen here demonstrated the most repeatable and generally very accurate results for grinding prediction. While the LM network results were sometimes more accurate, that network uses different network training methods which do not always show good repeatability, and sometimes do not converge to a good result at all. The LM network thus seems better suited for roughly

Theoretical Aspects and Modelling

linear applications, such as in the study of hard turning previously mentioned. The resulting RBF network is thus a most convenient tool for dry grinding process prediction, which has an inherently more complicated input-output relationship. Further optimisation of network parameters and investigation of different combinations could yield even more accurate results in future experiments.

Table 6.8: A sample of burn prediction results; ‘1’ means burn and ‘0’ means no burn (false prediction shown also in *italic*)

Network inputs (4)				Network output (1)		
% Contact layer	Cutting speed: v_c (m/s)	Feed speed: v_{ft} (m/min)	Depth of cut: a_e (mm)	Grinding burn, Experiment	RBF burn prediction	RBF burn prediction
25	60	1500	0.005	0	0	0
25	60	1500	0.015	0	0	0
25	60	1500	0-025	0	0	0
25	60	2000	0.010	0	0	0
25	60	2000	0.020	0	0	0
25	60	2500	0.005	0	0	0
25	60	2500	0.015	0	0	0
25	60	2500	0.025	0	0	0
50	60	1500	0.005	0	0	0
50	60	1500	0.015	1	1	0
50	60	1500	0.025	1	1	1
50	60	2000	0.010	0	<i>1</i>	0
50	60	2000	0.020	1	1	0
50	60	2500	0.005	0	0	0
50	60	2500	0.015	1	1	0
50	60	2500	0.025	1	1	1
100	60	1500	0.005	0	0	0
100	60	1500	0.015	1	1	1
100	60	1500	0.025	1	1	1
100	60	2000	0.010	0	<i>1</i>	0
100	60	2000	0.020	1	1	1
100	60	2000	0.005	0	0	0
100	60	2500	0.015	1	1	1
100	60	2500	0.025	1	1	1

Chapter 7

7 EXPERIMENTAL ANALYSIS

In this chapter, the effect of grinding speed, depth of cut, feed rate as well as structuring of the wheel on the grinding forces and energy, surface roughness, surface integrity, grinding temperature, chip size and wheel wear will be studied. To compare the effect of the structuring on the above mentioned parameters a wide range of systematic tests were applied using common grinding wheels, both structured and conventional, mentioned in chapter five. In order to compact the discussions, in each section of this chapter only the results of one or two types of wheels are presented. The goal is here to compare the conventional wheel with the structured wheel in terms of productivity and quality of workpiece.

7.1 STRUCTURING EFFECT ON GRINDING FORCES

The grinding forces are one of the most important parameters of the grinding process which represents fundamental information regarding the dynamic of the process. A reduction of tangential grinding forces shows particularly a reduction of heat generated in the contact zone, i.e. cooler grinding. The grinding forces also influence the wear characterisation of the wheel. Higher grinding forces cause a generally higher rate of wheel wear. The grinding forces for a specific wheel and workpiece combination are generally determined by wheel topography, depth of cut, grinding speed and feed rate. In the following section the effects of these parameters on grinding forces based on the applied tests will be taken into overall consideration.

The grinding test conditions using a vitrified CBN grinding wheel are illustrated in table 7.1. The vitrified bond grinding wheel was dressed with a diamond wheel and the conditions presented in table 7.1, then the special structure was produced with another diamond disc dresser (average width of 0.5 mm and inclined angle of 60°), as discussed in section 5.2. The structure having 25% contact layer was used for most of the tests comparing with the conventional 100% layer. Both tangential and normal grinding forces were measured by a piezoelectric dynamometer positioned under the workpiece clamping system.

Table 7.1: Test conditions with vitrified bond CBN wheel

Grinding wheels	Vitrified bond CBN grinding wheel, B126 C125; Ø400 mm x 15 mm
Grinding conditions	Workpiece: 100Cr6, 60 HRC; Feed speed $v_{ft}= 500\text{-}2500$ mm/min; Cutting speed $v_c= 60$ m/s; Depth of cut $a_e= 0.005\text{-}0.025$ mm; No coolant (Dry grinding)
Dressing conditions	Dressing cutting speed $v_{cd}= 60$ m/s; Dressing infeed $a_{ed}= 5$ µm; Dressing ratio: $q_d= -0.9$; Dressing feed : $v_{fad}=153$ mm/min; Total depth of dressing: $a_e= 10$ µm

Figures 7.1 to 7.5 demonstrate some of the most important results regarding the effect of the variation on the grinding parameters as well as structuring on the grinding tangential and normal forces.

Grinding wheel	: B126, C125, Vitrified	Grinding speed	: $v_c= 60$ m/s
Wheel width	: 15 mm	Feed rate	: $v_{ft}=2$ m/min
Wheel diameter	: 400 mm	Depth of cut	: $a_e=5\text{-}25$ µm
Material	: 100Cr6, 60 HRC	Grinding type	: Dry grinding

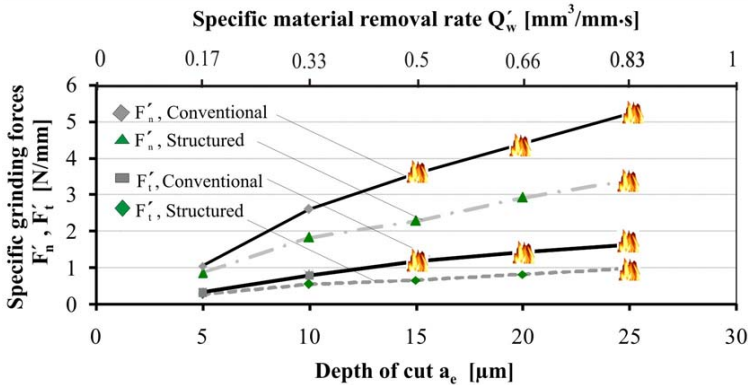


Figure 7.1: Grinding forces vs. depth of cut; The effect of structured wheel on the reduction of grinding forces in comparison with the conventional wheel at the same grinding speed and feed rate (the fire symbol indicates grinding burn conditions)

Experimental Analysis

In figure 7.1, the specific grinding forces (tangential and normal) are compared for varying depth of cut for a 25% contact layer grinding wheel as well as full contact layer wheel, at a constant cutting speed of 60 m/s and feed rate of 2 m/min. Hereby the considerable reduction of specific grinding forces by use of a structured wheel with 25% contact layer may be interpreted to show a reduction in energy and heat generated between grinding wheel and workpiece.

Discoloration conditions (burning) were noted in tests using the conventional wheel with 100% contact layer (indicated by a fire symbol) which damaged the workpiece at a depth of cut of 0.015 mm or more. The discoloration became stronger with increasing depth of cut. Grinding at the same depth of cut using the 25% layer structured wheel caused no visual thermal damage, up to a depth of cut of 0.025 mm. It should be mentioned that after burning of the workpiece material, the workpiece material properties are changed, especially the surface hardness, which may cause softening of the material and resulting in a decrease of grinding forces. This may cause an inaccuracy in grinding force measurements. However, as the aim of the comparison is to determine the force tendency for the two grinding wheels, this potential for inaccuracy was not considered.

Increasing normal and tangential forces with the increasing of the depth of cut is due to the fact that with increasing depth of cut, the geometric and kinematic contact length as well as number of momentary dynamic cutting edges (in the contact length) will be increased. The reason for lower grinding forces in the case of a structured wheel as compared to the conventional wheel is the reduction of dynamic cutting edges and increasing the mean uncut chip thickness as was discussed theoretically in chapter 6.

Figure 7.2 illustrates specific grinding forces vs. feed rate for the constant depth of cut of 0.02 mm and cutting speed of 60 m/s. In this case, also, the grinding forces seen with a 25% contact layer are significantly lower than those with a 100% layer. The discoloration points shown are for a feed rate of 1 m/min and more; however, there was no sign of such discoloration up to the feed rate of 2.5 m/min when the structured wheel was used.

The results also indicate that the grinding forces are increased along with the increasing feed rate. The reason for this tendency is actually the higher mean uncut chip thickness achieved by each active grain due to increasing the feed rate and simultaneously increasing number of dynamic cutting edges in the contact zone. However the reasons for reduction in grinding forces in the case of structured wheel (25% layer) compare to the conventional wheel (100% layer) in a defined feed rate, are the reduction of the number of dynamic cutting edges and the increase of the total mean uncut chip thickness of the process and the resulting reduced rubbing and ploughing action.

Grinding wheel	: B126, C125, Vitrified	Grinding speed	: $v_c = 60$ m/s
Wheel width	: 15 mm	Feed rate	: $v_{ft} = 0.5-2.5$ m/min
Wheel diameter	: 400 mm	Depth of cut	: $a_c = 20$ μ m
Material	: 100Cr6, 60 HRC	Grinding type	: Dry grinding

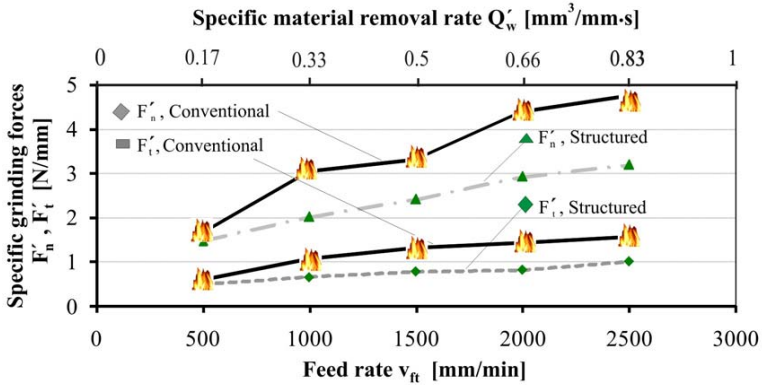


Figure 7.2: Grinding forces vs. feed rate; The effect of structured wheel on the grinding forces in comparison with the conventional wheel at the same grinding speed and depth of cut (the fire symbol indicates grinding burn conditions)

Figure 7.3 illustrates grinding forces versus grinding speed for the constant depth of cut of 0.02 mm and constant feed of 2000 mm/min, which makes a constant specific material removal rate of 0.67 $mm^3/mm.s$. The reduction of grinding forces can also be observed by comparing the conventional and special conditioned wheels. However, it indicates that an increase in grinding speed has a low influence on the grinding forces for both cases of structured and conventional wheels. Thermal damage is again observed when using the conventional wheel; however, no burn was observed when using the structured wheel with 25% contact layer. Hereby the reduction of forces by increasing the grinding speed at constant material removal rate is due to the slight reduction of dynamic cutting edges and mean uncut chip thickness of each grain. Besides, the material can also be softened due to higher specific energy and higher resulting heat generation at the contact zone, therefore the forces are decreased.

The effect of depth of cut and feed rate were investigated and presented in figures 7.1 and 7.2 and it was observed that a higher depth of cut and higher feed rate cause higher grinding forces but the only way to increase the material removal rate, as the most important parameter of productivity, is to increase either feed rate or depth of cut or both; with the constraint that the favorable workpiece quality is achieved in terms of surface integrity, dimensional accuracy and roughness.

Experimental Analysis

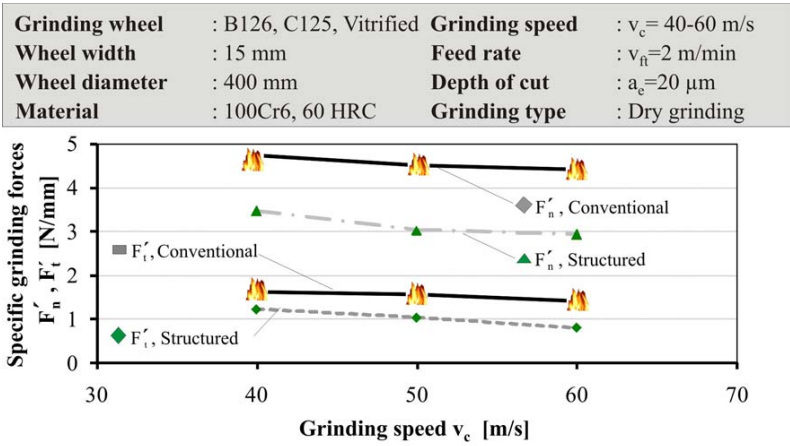


Figure 7.3: Grinding forces vs. grinding speed; The influence of a conventional and structured grinding wheel on the grinding forces (the fire symbol indicates grinding burn conditions)

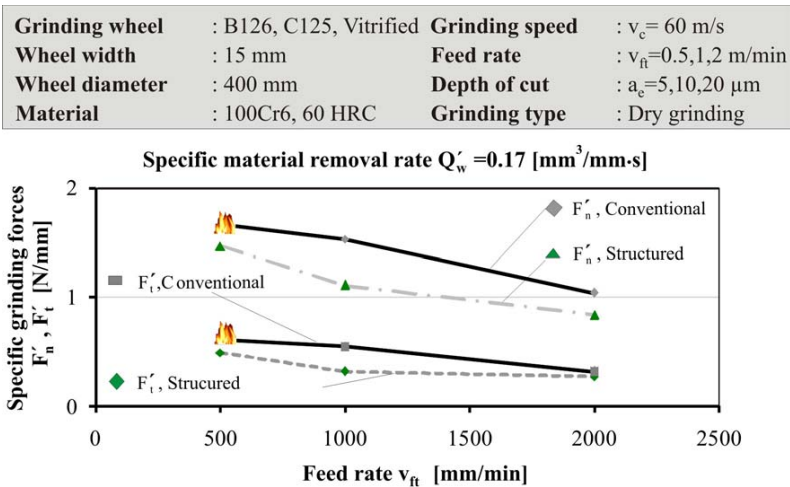


Figure 7.4: Grinding forces vs. feed rate and depth of cut at constant material removal rate and constant grinding speed for the structured and conventional vitrified CBN wheels

The question is that a variation of which parameters (between depth of cut and feed rate) causes lower grinding forces and consequently lower heat generation? To answer this question, the grinding forces versus depth of cut and feed rate at the constant material removal rate for structured wheel with 25% contact layer and conventional wheel are illustrated in figure 7.4. It can be seen that the effect of increasing feed rate has obviously better results. The reason is that an increase in feed rate has a great influence on the reduction of the dynamic cutting edges due to lower contact length at the constant material removal rate. If the material removal rate and grinding speed are constant, decreasing the number of dynamic cutting edges causes an increase in uncut chip thickness, as well as more micro-cutting action and less micro-ploughing action [Zepp05]. The same phenomena is achieved if the wheel is structured i.e. the lower dynamic cutting edges decreases grinding forces and makes the process more efficient. Figure 7.5 shows tangential grinding force versus depth of cut for 25%; 50%, 75% and 100% contact layers at constant cutting speed of 60 m/s and feed rate of 1 m/min.

Grinding wheel	: B126, C125, Vitriified	Grinding speed	: $v_c=60$ m/s
Wheel width	: 15 mm	Feed rate	: $v_{ft}=1$ m/min
Wheel diameter	: 400 mm	Depth of cut	: $a_c=5-25$ μm
Material	: 100Cr6, 60 HRC	Grinding type	: Dry grinding

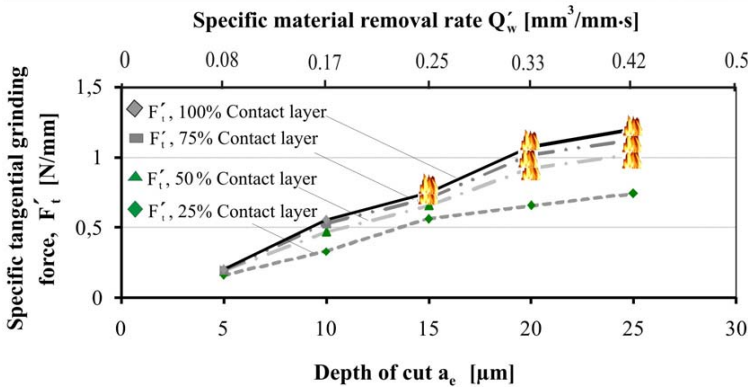


Figure 7.5: Tangential force vs. depth of cut; Influence of the 25%, 50%, 75% and 100 % contact layers on measured grinding forces (the fire symbol indicates grinding burn conditions)

The 25% contact layer shows the best results in terms of grinding forces. Hereby it can be seen that the tendency of increasing tangential grinding forces is one of the criteria of grinding specific energy and grinding power. The grinding forces are increased with increasing percentage of contact layer. In other words, heat generated in the contact zone is going to be reduced when fewer cutting edges are in contact with the workpiece.

Experimental Analysis

As a short summary of this section, the considerable reduction of grinding forces in the case of using a structured wheel should be mentioned. It can also be observed that, at a constant material removal rate, the feed rate has a positive effect in decreasing grinding forces. The effect of grinding speed in decreasing the grinding force can also be mentioned, however increasing the grinding speed causes higher power induced in the process and consequently stronger heat generation and possible higher temperature, as well as thermal damage on the workpiece. In general form, process optimization should be done individually based on the workpiece material properties and component condition in terms of desired quality and tolerances.

7.2 STRUCTURING EFFECT ON SURFACE ROUGHNESS

Surface roughness is another important output parameter in terms of the quality of the machined component. To compare the structuring effect on the surface roughness some of the results are illustrated in figures 7.6 to 7.8. Figure 7.6 shows the measured workpiece surface roughness parameters Ra and Rz vs. depth of cut. Hereby, it is clear that the finer surface finish will be achieved using the conventional grinding wheel (100% contact layer) comparing to the structured wheel (25% contact layer).

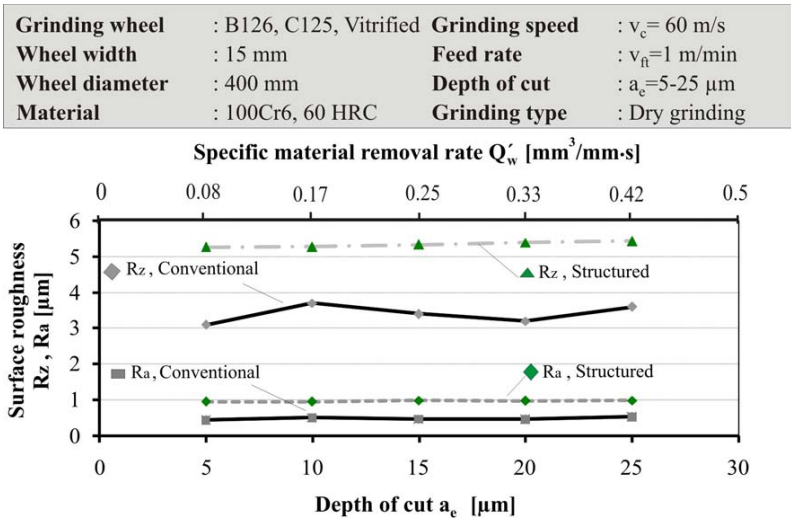


Figure 7.6: Measured workpiece surface roughness vs. depth of cut; An increase of roughness by structured wheel in comparison with the conventional wheel.

The higher surface roughness is caused by the lower number of static and dynamic cutting edges seen in a structured wheel surface, since the micro-rubbing mechanism which can actually improve surface roughness is reduced. The micro-rubbing process causes a polishing process which has a great effect on producing the finer surface. This is due to more grains which are in contact with workpiece during the process and more rubbing action in the case of using conventional wheel.

Figure 7.7 shows the surface roughness parameters Ra and Rz versus feed rate at a constant depth of cut and grinding speed. The finer surface achieved by the conventional wheel with 100% contact layer is compared to the structured wheel with 25% contact layer, similar to previous figure.

Grinding wheel	: B126, C125, Vitrified	Grinding speed	: $v_c = 60$ m/s
Wheel width	: 15 mm	Feed rate	: $v_{ft} = 0.5-2.5$ m/min
Wheel diameter	: 400 mm	Depth of cut	: $a_c = 10$ μ m
Material	: 100Cr6, 60 HRC	Grinding type	: Dry grinding

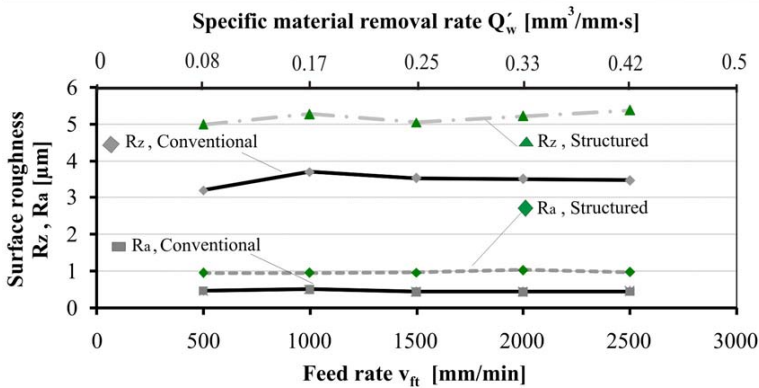


Figure 7.7: Measured workpiece surface roughness vs. feed rate; The effect of the structured wheel on workpiece roughness in comparison with that of the conventional wheel

Figure 7.8 shows the surface roughness Ra and Rz versus grinding speed at constant depth of cut and feed rate for structured (25% contact layer) and conventional wheel. The same situation as the last two figures was observed when comparing the structured and conventional wheels. As it can be observed in all the figures related to measured workpiece roughness parameters, the effects of grinding speed, feed rate and depth of cut are not so large in the domain of each parameter. The main reason for such a situation may be that in dry grinding the thermal effect is what dominates the grinding process, and concerning surface roughness it was reported also by Marinescu et al. [Mari04]. The spherical chips from the

Experimental Analysis

grinding process which will be presented in the next sections shows the effect of high temperature at the time of chip formation.

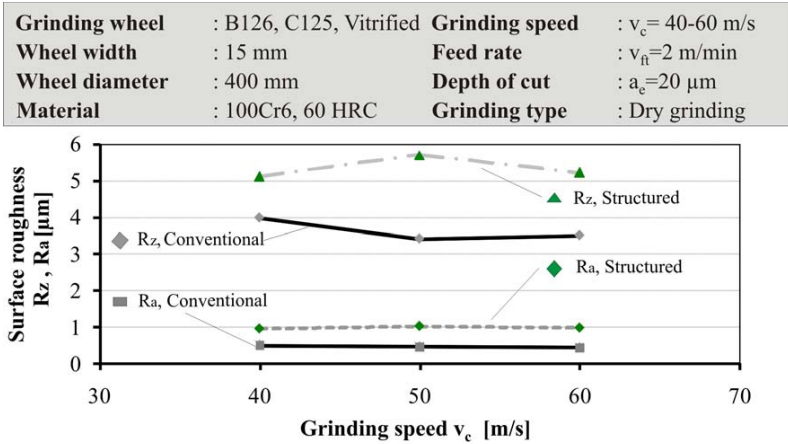


Figure 7.8: Measured workpiece surface roughness vs. grinding speed; The influence of a conventional and structured wheel on surface roughness parameters Ra and Rz

On the other hand, for all cases the structured wheel produces a rougher workpiece surface finish. This can be a disadvantage of the new concept of structuring but in many industrial applications the achieved surface roughness even by a structured wheel with 25% contact layer is acceptable. It should be mentioned that all the tests were done by applying a single grinding pass to the workpiece. Another grinding wheel pass over the workpiece surface may be used without additional depth of cut, also known as a spark-out pass, to further improve the surface roughness. However, this may be a disadvantage in terms of process time and economical aspects.

7.3 STRUCTURING EFFECT ON GRINDING ENERGY

A machining process is more efficient when the energy consumption for removing the material is reduced. It means with lower specific energy the higher efficiency is achieved. The specific energy can be defined as [Kloc05a]:

$$e_c = \frac{F'_t \cdot v_c}{a_e \cdot v_{ft}} \quad (7.1)$$

where e_c is the specific energy in J/mm^3 . To investigate the efficiency of the new grinding wheel concept compared with the conventional wheel, the terms of the specific energy should be taken into consideration. It is significant because the specific energy has a direct relation with the heat generated in the contact zone and temperature rise. Rowe et al. [Rowe97] have shown that the specific energy is reduced by increasing the depth of the penetration or indentation of the grain in the workpiece. This effect refers to the size effect in grinding terminology. Chen [Chen89] related specific energy to a mean uncut chip area and demonstrated a strong size effect for grinding ceramics. The effect of the uncut chip thickness on the cutting regime in terms of micro-cutting, micro-ploughing and micro-rubbing is the main reason for its direct influence on the specific energy, and thus efficiency of the grinding process.

The new concept wheels are basically developed to increase the grain penetration (size effect) and to reduce the amount of the grains which have a lower penetration into the workpiece. Lower penetration in grinding causes the grains to do more rubbing and ploughing causing heat generation without material removal.

In order to study the size effect on the specific energy, a term of equivalent uncut chip thickness can generally be considered [Mari04], as follows:

$$h_{eq} = \frac{a_e \cdot v_{ft}}{v_c} = \frac{Q'_w}{v_c} \quad (7.2)$$

Using equation (7.1) and (7.2) the specific energy can be defined as:

$$e_c = \frac{F'_t}{h_{eq}} \quad (7.3)$$

As it can be seen the equivalent chip thickness for a particular wheel is a term which fully depends on the grinding parameters and not the wheel specification. That is why this parameter can be used to compare the conventional and structured wheels. However, the grinding specific energy also depends on the uncut chip thickness and material removal rate [Mari04].

In this section, the influence of the size effect and the specific energy is studied for both structured and conventional grinding wheels to investigate the efficiency of the new concept and to compare the effect of grinding parameters on the specific energy. Figure 7.9 shows the specific energy versus equivalent chip thickness at constant grinding speed for structured (with 25% contact layer) and conventional wheel. As it can be seen in this figure, the specific energy is reduced with increasing equivalent chip thickness. Hereby the reduction of the

Experimental Analysis

specific energy using a structured wheel can also be noted. Besides with increasing the feed rate at a constant material removal rate the specific energy will be decreased.

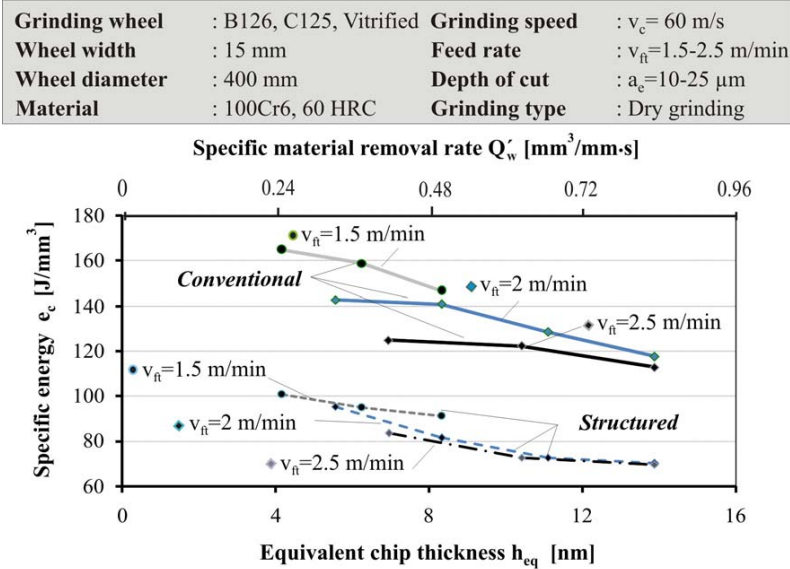


Figure 7.9: Specific energy vs. equivalent chip thickness at constant grinding speed; Considerable reduction of specific energy in the case of the structured wheel in comparison with the conventional wheel

The first result shows the positive influence of the size effect in case of structured wheels. The greater penetration, the larger the chip size and uncut chip thickness, and the lower the specific energy. The effect of feed rate may also be noted for both conventional and structured wheels. It can be noted that at a constant equivalent chip thickness or material removal rate, an increase of the feed rate (and consequently reduction of the depth of cut) causes a reduction in the specific energy. The reason for this phenomenon can be explained by increasing uncut chip thickness. As a matter of fact the uncut chip thickness is reduced with decreasing depth of cut but at the same time increased with increasing feed rate. But as it is discussed in chapter 6, the effect of the feed rate on the uncut chip thickness dominates over the depth of cut (by power of two) and these results in greater uncut chip thickness and lower specific grinding energy. In the case of the structured wheel, the reduced cutting edges cause the same condition by increasing the uncut chip thickness and consequently reducing specific energy.

Figure 7.10 demonstrates the grinding specific energy versus equivalent chip thickness at constant material removal rate. Changing the equivalent chip thickness can be achieved by varying the grinding speed. Hereby it can also be observed that the specific energy is reduced with increasing equivalent chip thickness. The considerable reduction of the specific energy in the case of using the structured wheel compared to the conventional wheel is also apparent.

Grinding wheel	: B126, C125, Vitrified	Grinding speed	: $v_c = 40-60$ m/s
Wheel width	: 15 mm	Feed rate	: $v_{f1} = 1, 2$ m/min
Wheel diameter	: 400 mm	Depth of cut	: $a_c = 10, 20$ μ m
Material	: 100Cr6, 60 HRC	Grinding type	: Dry grinding

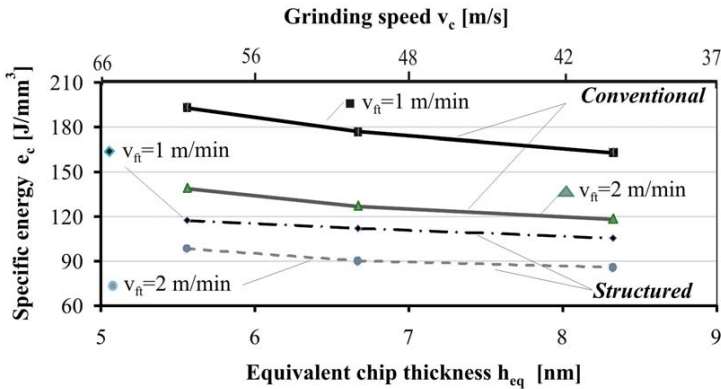


Figure 7.10: Specific energy vs. equivalent chip thickness at constant material removal rate; Considerable reduction of specific energy in the case of the structured wheel in comparison with the conventional wheel

The reason for this is fully discussed by the explanation of the last figure. But here the interesting matter is the speed effect on the specific grinding energy and the efficiency of the process. As it can be seen the increasing wheel speed does not reduce the specific energy, but actually increases it. It has been seen in figure 7.3 that with increasing grinding speed, the grinding forces are reduced which alone cause a decrease in the specific energy. But on the other hand, increasing the wheel speed reduces the mean uncut chip thickness and increases the specific energy. Based on equation (7.3) these two parameters control the grinding specific energy when they change simultaneously. In the case of dry grinding, with the above mentioned test parameters, the final results were increasing specific energy with increasing wheel speed for both cases of the structured and conventional wheels. It must be also mentioned that a higher grinding speed gives less chance for heat to conduct to the workpiece as reported by Tawakoli [Tawa93] in the case of HEDG, causing less thermal damage. Therefore it is rather complicated to evaluate the efficiency and thermal characteristic of the

Experimental Analysis

process in terms of increasing the grinding speed. But it is obvious that for process optimisation, the grinding speed should be considered in interaction with the other grinding parameters. In general, in the grinding process, it may be concluded that improvement in efficiency can be achieved not just by increasing the grinding speed but at the same time with increasing the material removal rate, as in case of HEDG.

7.4 STRUCTURING EFFECT ON GRINDING TEMPERATURE

As it was discussed in chapter 6, almost all the mechanical energy which causes the elastic and plastic deformations, friction and surface generation, is converted to heat in the contact area. As a matter of fact, all components which take part in the chip formation process are affected by the thermal loads. In dry grinding, as there is no coolant, heat energy is distributed to the workpiece, grinding wheel and chips. The most important criterion for an acceptable workpiece quality is to avoid thermal damage in the workpiece by reduction of the heat transferred to it. However, the most difficult problem is that the thermal conductivity of the workpiece is often higher than that of the other components which participate in chip formation, and therefore the majority of heat energy is transferred into the workpiece. The reduction of heat generated in the contact zone is thus a critical aim for avoiding thermal damage. In this section it is shown how the wheel structuring reduces heat generation by measuring the tendency of the temperature change in both cases of structured and conventional grinding wheel usage. The measurements were carried out while varying the grinding parameters for structured (with 25% contact layer) and conventional wheels. The measured results are also compared with the temperature models discussed in chapter 6. In order to calculate the temperature based on the analytical models, the material data of 100Cr6 is presented in table 7.2.

Table 7.2: Properties of the workpiece

DIN	Material-No.	λ_w (W/mK)	ρ_w (kg/m ³)	C_w (J/kgK)	β_w (J/m ² sK)	α_w (m ² /s)
100Cr6	1.3505	39.6	7810	461	11941	1.1E-5

To calculate R_w it is necessary to define two other parameters λ_g as well as r mentioned in equation (6.117). The thermal conductivity of CBN λ_g was reported in a rather vast variety of values from 200 Wm/K [Maie08] up to 1300 Wm/K [Mari04]. The grain tip radius (with wear) for CBN is also reported from 5 μm [Jin02] to 25 μm [Maie08]. In this work the amount of 290 was considered for λ_g which was reported by Jin and Stephenson [Jin02] and for the value of r the average amount of 13 μm was supposed.

Figure 7.11 shows the maximum temperature versus depth of cut at the constant feed rate and constant grinding speed based on the analytical modelling developed by Malkin (equation (6.131)) [Malk07] and Marinescu et al. (equation (6.128)) [Mari04].

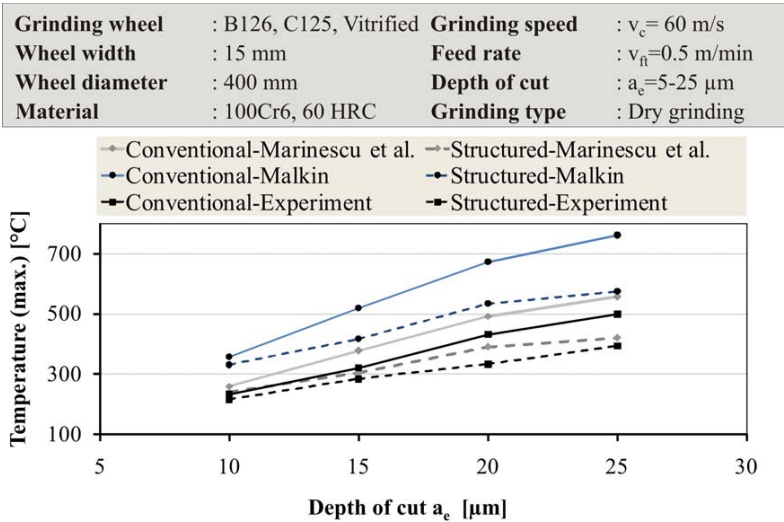


Figure 7.11: Workpiece surface temperature versus depth of cut for the structured and conventional grinding wheels

The results show that for all cases the maximum surface temperature of the workpiece is lower in the case of structured wheels as compared to the conventional wheel. However the experimental measurement demonstrates a temperature which is below the calculated analytical temperature. This result is not surprising by considering the response time of the temperature sensors and the possible errors encountered with extrapolation explained in chapter 4. Besides there are other sources of error such as changing the media properties between sensors and workpiece which changes the emission factor, electrical noise, reflection (although the side of material was painted in black), system calibration and set up. In spite of the existence of such inaccuracies, the tendency of temperature changes is similar to the results of the analytical models and a proportional correlation can be found between the maximum temperature determined analytically and those obtained experimentally.

The analytical results illustrate that the Malkin’s equation is rather overestimated compared to the other analytical model and the experiments. The results of other grinding conditions also show the overestimated value for the temperature in the case of using Malkin’s equation. The reason is perhaps the lower Peclet number in all the test conditions than the suggested value of Peclet number in the Malkin analysis (a Peclet number more than 5).

Experimental Analysis

The higher temperature reached by increasing the depth of cut for both wheels is simply due to the load, energy and power applied to the workpiece with increasing depth of cut as well as increased material removal rate.

As observed for almost all test cases, the same tendency of overestimated temperature resulted from the Malkin's equation; the results of Malkin's approach will not be presented in next figures of this section. Figure 7.12 shows the maximum temperature versus grinding speed for the structured and conventional type wheels.

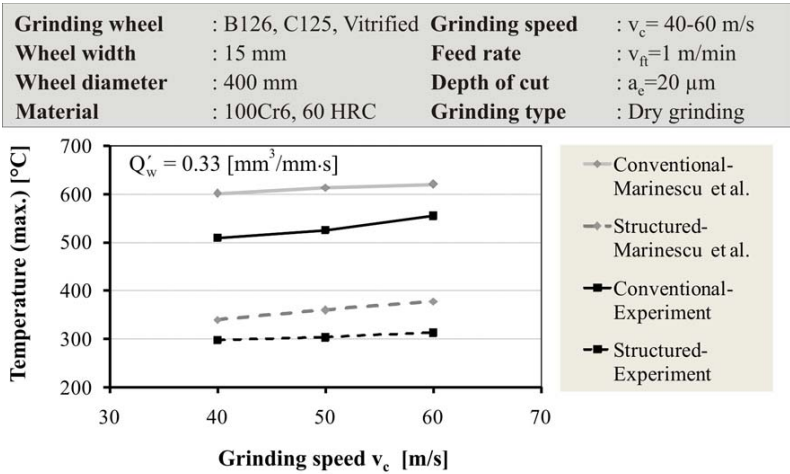


Figure 7.12: The maximum grinding temperature vs. grinding speed for structured and conventional wheels

Here, a good correlation also exists between the analytical and experimental results. The results demonstrate a lower temperature in the case of using a structured wheel compared to the conventional wheel.

On the other hand, it can be seen that the effect of the grinding speed in this test domain is not very considerable (a rather small increase in temperature) in comparison with the effect of depth of cut. The reason for this was explained in the section of grinding specific energy. Actually the two opposite effects of grinding speed in the grinding process causes such results. From one side, with an increase in the grinding speed the grinding force is decreased and also there is less time for heat to penetrate into the workpiece, but on the other hand the power and specific energy will be increased due to smaller uncut chip thickness. These two opposite effects influence the process and in the case of dry grinding the increasing specific

energy dominates the process heat transfer resulting in a slight increase in the temperature at the contact zone.

Figure 7.13 demonstrates the maximum temperature at the workpiece surface versus one of the most important parameters mentioned in all the physical modelling approaches of the temperature, i.e. the time during which the moving heat source are on workpiece surface contact zone or l_c/v_{ft} . This time is presented in milliseconds as in the figure 7.13.

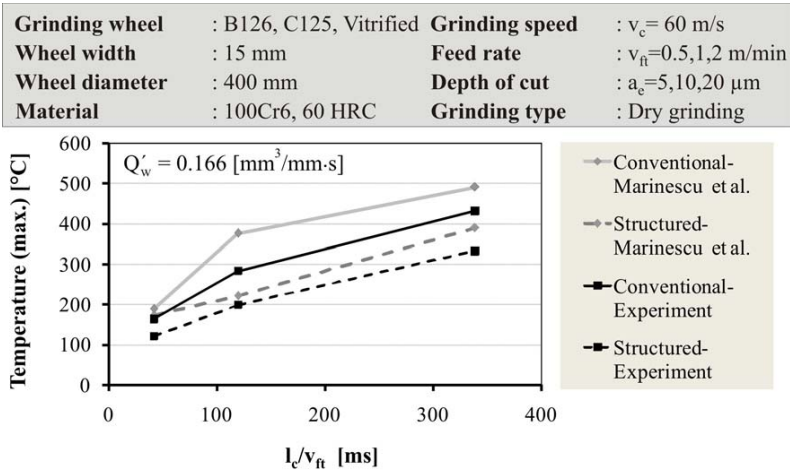


Figure 7.13: The maximum temperature versus heat source contact time with workpiece (l_c/v_{ft}) for structured and conventional wheel

During constant material removal rate, increasing the feed rate causes a reduction in the depth of cut and therefore it reduces the contact length and the contact time (the effect of the feed rate increasing the contact length can be neglected due to a very high amount of speed ratio). By reduction of the contact time, the heat source which is produced in the contact zone has less time to penetrate to the workpiece, therefore a considerable reduction in workpiece temperature can be achieved. This phenomenon can be seen in both cases of the structured and conventional wheels.

The reduction of grinding temperature in the case of the structured wheel compared to the conventional wheel can be observed for both analytical and experimental results. Hereby an increase in the uncut chip thickness and corresponding reduction of the tangential forces, in the case of the structured wheel, is the reason for such a reduction in surface temperature.

As a summary of this section, the following points need to be mentioned:

Experimental Analysis

- The structured wheel produces lower heat causing lower surface temperature.
- The experimental measurement and analytical calculation have a good correlation, however such infrared sensors are not accurate enough to indicate the precise temperatures.
- The effect of grinding speed in dry grinding is not very considerable.
- The contact time of the moving heat source with the workpiece, as well as feed rate, have a great influence on grinding surface temperature.

More research work in terms of temperature measurement in the dry grinding process should be done to study the effect of changing material properties by varying the grinding temperature, i.e. to study the role of the grinding wheel characteristics as well as grinding parameters on elevating temperature.

7.5 STRUCTURING EFFECT ON SURFACE INTEGRITY

Excessive temperatures in dry grinding can cause thermal damage to the ground surface. Grinding burn is a directly visible or invisible type of workpiece thermal damage. This can be observed by etching of the surface, but in this thesis, it refers to discoloration of the workpiece surface which can be distinguished by naked eye. Grinding burn changes the properties of the workpiece surface material and hence, component performance. Shaw attributes the discoloration associated with burn to interference phenomena arising from the presence of oxide layers [Shaw96].

In the steel grinding process, due to heat generation in the contact zone and the resulting temperature increase, thermal damage may occur resulting in metallurgical transformations which may cause micro-cracks, hardness alteration, tensile residual stress, or distortion and corrosion.

In general form, the characteristics of the workpiece surface layer (including burning) in terms of mechanical properties, residual stress and material microstructure are referred to surface integrity. In this section, characteristics of the ground surface in terms of surface microstructure, residual stress and hardness will be studied and the effect of grinding wheel structuring on the above mentioned terms will be presented.

7.5.1 Investigation of the microstructure

Two primary types of thermal damage in steel are widely referred to as re-hardening in form of white layer, which increases the hardness of the metal workpiece surface, and tempering which decreases the hardness of the metal workpiece surface.

Previous research has shown that re-hardening by grinding process mostly causes the microstructure of tetragonal martensite [Brin94, Brin95]. As it is concerned, requirements for such a structure are the high thermal load to increase process temperature to the austenitizing temperature (about 800 °C for steel) as well as rapid cooling so that the martensite can be produced (at a rate greater than the critical cooling rate of martensite)[Avne74]. The rapid heating (high temperature of workpiece surface in a short period of time) increases the austenitizing temperature, but in contrast mechanical pressure and load can decrease this critical temperature [Maie08]. In grinding processes, both of the above mentioned phenomena occur, i.e. mechanical load and high rate of temperature increase. So in general, if the heat generation in the contact zone and the mechanical forces are low, the possibility of generating the white layer will be decreased. Maier [Maie08] showed that for cylindrical grinding of steel the thickness of this re-hardening layer is increased if the material removal rate becomes higher. In this study, the re-hardening white layer in the case of the conventional electroplated wheel is compared with that of the structured electroplated wheel to prove the existence of a lower heat affected zone for the structured wheel. Furthermore, a similar micro-structural study for grinding with resin bonded wheels, where no white layer is observed, will be presented. The workpiece material is 100Cr6 with the composition shown in table 7.3 and Grinding test conditions for the electroplated CBN wheel are illustrated in table 7.4.

Table 7.3: Chemical composition of 100Cr6, by percent (%)

DIN	Material-No.	C	Si	Mn	P	S	Cr
100Cr6	1.3505	0.90 – 1.05	0.15 – 0.35	0.25 – 0.45	<0.3	<0.025	1.35 – 1.65

Table 7.4: Test conditions with electroplated bond CBN wheel

Grinding wheels	Electroplated bond CBN grinding wheel, B126; Ø400 mm x 15 mm 1) Conventional wheel (100% contact layer) 2) Structured wheel (22% contact layer)
Grinding conditions	Workpiece: 100Cr6, 48 HRC; 100X60X30 Feed speed: $v_f= 2000$ mm/min; Cutting speed: $v_c= 100$ m/s; Depth of cut: $a_e= 0.02, 0.04, 0.06, 0.08, 0.1$ mm No coolant (Dry grinding)

Figure 7.14 shows grinding burn and the discoloration of the workpiece following grinding with the conventional electroplated wheel. The above mentioned white layer followed by a darker layer and bulk material structure can be clearly seen. By increasing the material removal rate to $Q'_w = 3.33$ mm³/mm·s, an obvious burn was seen on the workpieces ground by structured and conventional wheels alike.

Experimental Analysis

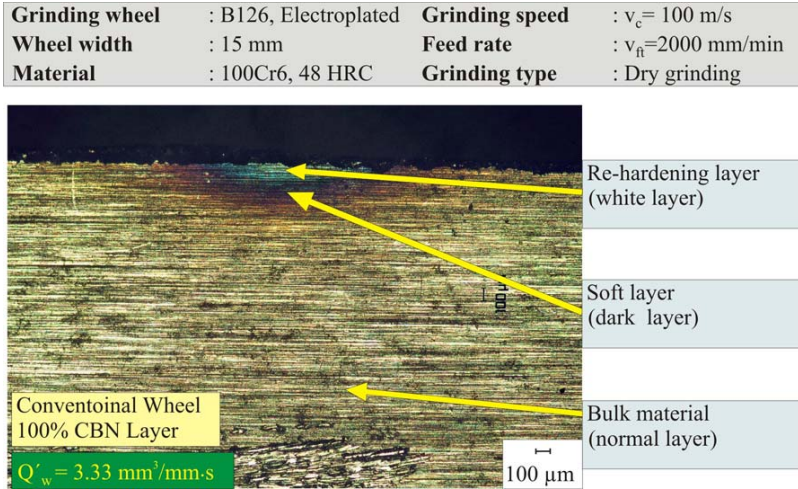


Figure 7.14: Different layers of workpiece grinding burn after grinding with a conventional electroplated wheel

This result shows that the temperature of the workpiece surface ground by the structured wheel reaches the critical austenitisation temperature of the material, so that the phase transformation to martensite could occur. Increased temperature by increasing the material removal rate is due to more specific energy required for material removal, and higher process forces, which were studied in previous chapters. This critical re-hardening temperature depends on the grinding parameters.

Figure 7.15 shows metallographic pictures of the ground workpieces in order to study the effect of material removal rate on the extent of thermal damage and also to compare the structured and conventional wheels. With the material removal rate of $Q'_w = 2 \text{ mm}^3/\text{mm}^3\text{-s}$ during grinding, the workpiece ground with the conventional wheel began to burn.

No burn was found with the same condition using the structured wheel. However, increasing the material removal rate to $Q'_w = 2.66 \text{ mm}^3/\text{mm}^3\text{-s}$ produced some discoloration. The workpiece which was ground by conventional wheel was clearly burnt.

Rowe [Rowe95] measured the workpiece temperature of ferrous materials using thermocouples and found the start of discoloration in grinding processes to be in the temperature range of 450-500 °C. It is estimated that the workpiece surface temperature in the case of the structured wheel should be also in this range. Extrapolation analysis of the

experimental temperature measurement by infrared measurement system shows the same temperature range under the workpiece surface, in the case of discoloration.

Grinding wheel	: B126, Electroplated	Grinding speed	: $v_c = 100$ m/s
Wheel width	: 15 mm	Feed rate	: $v_{ft} = 2000$ mm/min
Material	: 100Cr6, 48 HRC	Grinding type	: Dry grinding

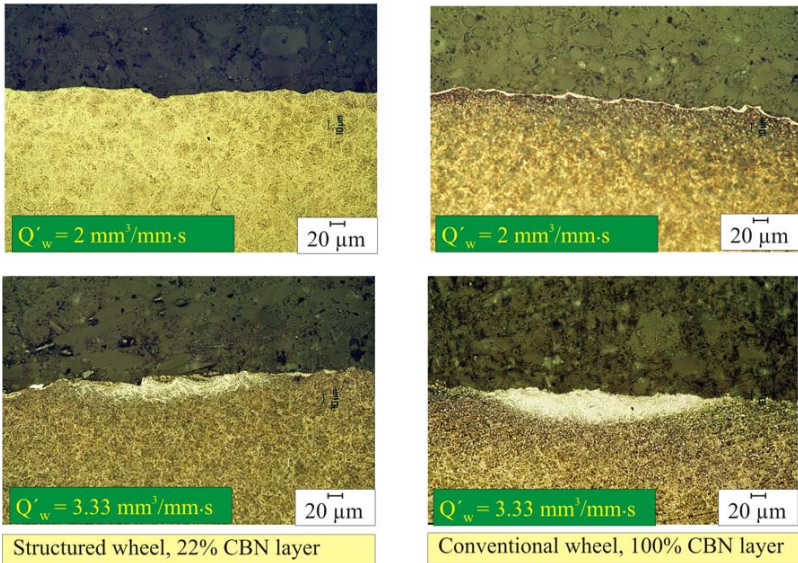


Figure 7.15: Microstructure of the workpiece and grinding burn after grinding with structured and conventional grinding wheels with different MRRs.

It should be noted that the thickness of the white layer in the case of the structured wheel is less than the thickness of this layer when grinding with conventional wheel. Figure 7.16 shows the result of measurement of the re-hardening layer for both cases, the maximum thickness of this layer is about 33 µm when grinding with the structured wheel and is about 38 µm when using the conventional wheel. The lower white layer thickness in the first case proves less heat generation in the grinding process, as compared to the grinding with conventional wheel. The micro-hardness test of the workpieces of figure 7.16 also shows that the white layer has a hardness of 1000 HV compared to the bulk material which had a hardness of about 600 HV. It must be noted, however, that higher hardness amounts were found only at the points at which there was a white layer, and not in the entire workpiece surface.

Experimental Analysis

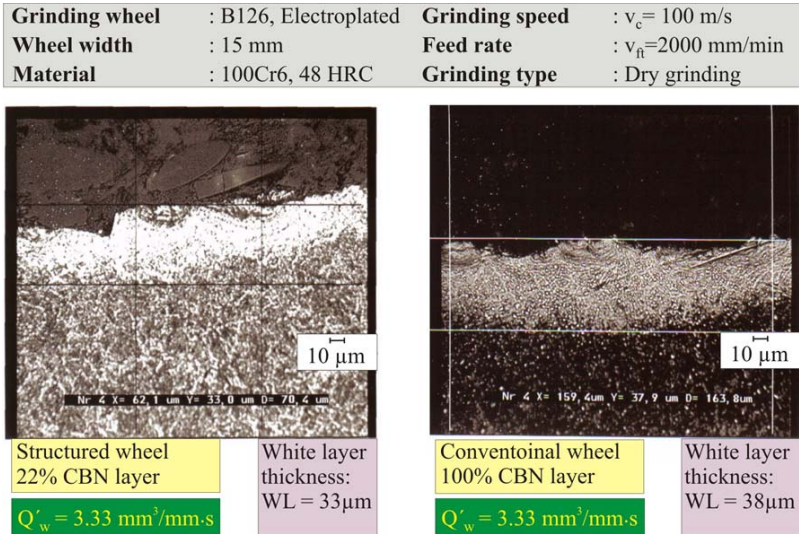


Figure 7.16: Measurement of the re-hardening layer after grinding of steel workpieces with structured and conventional wheels

As was previously discussed, the martensitic transformation occurs when the temperature and the rate of cooling are high. In dry grinding processes, the rate of cooling highly depends on the feed rate. The contact length between grinding wheel and workpiece contains the area of heat generation. The heat source in the contact zone moves over the workpiece surface at a speed corresponding to the feed rate. When the feed rate is increased at a constant grinding speed and depth of cut, two phenomena happen simultaneously. Due to the higher feed rate at constant depth of cut, the material removal rate and the number of dynamic cutting edges are increased, which causes higher heat generation. On the other hand, due to higher feed rate, the heat generated in the contact zone remains on a definite point of the workpiece for a shorter period of time, therefore the cooling rate is going to be higher. It theoretically means that if the feed rate is high, then the possibility of a martensitic transformation will be increased. However at the constant material removal rate, increasing the feed rate causes a decreasing on the specific energy, therefore lower heat generation in the contact area which decrease the possibility of martensite transformation.

The resin bond grinding wheel was structured by special conditioning using a CVD single point stationary dresser, as explained in chapter 5. Hereby, the structure with 25% contact layer with special conditioning was applied as a comparison with the conventional wheel with 100% layer.

Figure 7.17 shows the effect of grinding burn on the workpiece. Near the surface layer of the workpiece, the effect of the heat is so high that it completely changes the microstructure of the steel compared to a depth of 3.5 mm under the surface in which the heat is actually dissipated.

Grinding wheel	: B126, C100, Resin	Grinding speed	: $v_c = 60$ m/s
Wheel width	: 15 mm	Depth of cut	: $a_c = 0.025$ mm
Material	: 100Cr6, 60 HRC	Grinding type	: Dry grinding

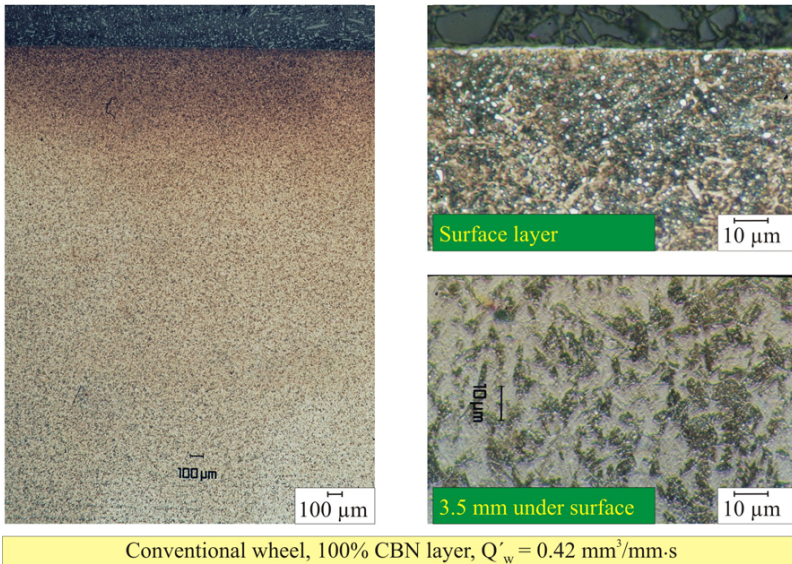


Figure 7.17: Microstructure of tempering layer after grinding with conventional wheel

Figure 7.18 shows the microstructure of 100Cr6 workpiece which was ground at a low feed rate by resin-bonded structured and conventional CBN grinding wheels. It can be seen that the workpiece microstructure is changed due to the high heat generation when using the conventional wheel. This is compared to the structured wheel tests in which no re-hardening layer in microstructure was found. The micro hardening test on the material shown in the figures 7.17 and 7.18 shows that the hardness of the ground material by conventional wheel, where it is not burnt, is between 800 to 868 HV and the hardness at the burnt points are between 455- 625 HV. So far the hardness of the ground material using the structured wheel is similar to the hardness of the existing bulk material.

Experimental Analysis

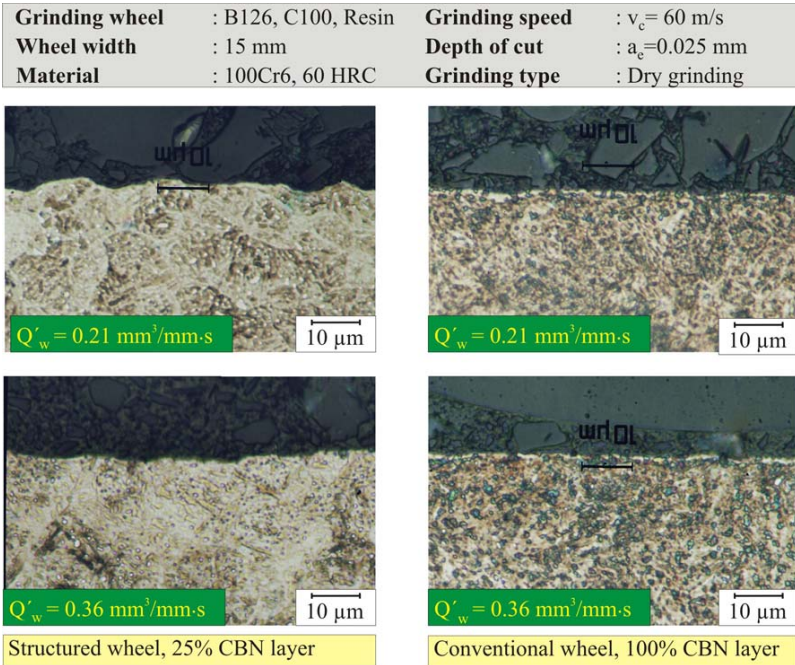


Figure 7.18: Microstructure of the workpiece surface layer after grinding with conventional and structured resin-bonded wheels

7.5.2 Investigation of residual stresses

One of the most important criteria for assessing the quality of machined components is residual stress, especially in the case of components which are severely loaded or under high fatigue condition. During the grinding process, plastic deformation under mechanical loading as well as plastic deformation due to high temperatures can alter the stress state of a workpiece. The mechanical load in grinding typically causes compressive residual stresses. As it was discussed in previous chapters, the workpiece is, on the other hand, heated in the arc of the contact length by a moving heat source. The passage of a heat source followed by rapid cooling (either by coolant, or in dry grinding by air) generally causes a tensile residual stress in the workpiece. The resulting residual stress state is tensile or compressive depending on which of the above mentioned two actions dominates the process [Brin82a, Shaw96]. Process variables such as machine setting, grinding parameters, coolant type, dressing conditions, workpiece material, grinding method, and wear behaviour of the grinding wheel, as well as the characteristic of grinding wheel micro and macro-topography in terms of the grit type, grit

size, bond and bond hardness and macro-structure, can determine the residual stresses on the workpiece. Any reduction of the heat generated in the contact zone causes reduced tensile residual stress in the workpiece. It is also known that CBN abrasive wheels produce less heat since they are sharper than conventional abrasive, and they convey larger quantities of heat away from contact zone because of their higher thermal conductivities [Tawa93]. Brinksmeier et al. [Brin82b, Brin94] mentioned that finer wheel dressing causes finer surface roughness, but greater thermal loading and hence greater chance for tensile residual stress. Shaw [Shaw96] discussed that the burn associated with un-tempered martensite causes tensile residual stress.

The grinding test conditions using an electroplated CBN wheel illustrated in table 7.4 were used prior to residual stress measurement of the ground workpiece surface. Both conventional and structured wheels were used at the same grinding condition. The residual stresses in the grinding direction and also perpendicular to the grinding direction were measured. The results are demonstrated in figures 7.19 and 7.20.

In figure 7.19, the upper curve compares the residual stresses parallel to the grinding direction for the structured and conventional wheels. It can be seen that residual stresses in the case of the structured wheel are compressive up to material removal rate of $Q'_w = 2 \text{ mm}^3/\text{mm}\cdot\text{s}$, and beyond this material removal rate it becomes tensile. The material removal rate of $Q'_w = 2.66 \text{ mm}^3/\text{mm}\cdot\text{s}$ is the beginning of workpiece burn in terms of discoloration of the material. A similar trend can be seen in the case of conventional wheel use, however it is clear that the tensile residual stress begins at the lower removal rate of $Q'_w = 2 \text{ mm}^3/\text{mm}\cdot\text{s}$. For this wheel, as Q'_w is decreased, the residual stress along the grinding direction decreases in value and subsequently transforms from a tensile state to a compressive state. The highest residual tensile stress of about 600 MPa was observed in the sample ground at $Q'_w = 3.33 \text{ mm}^3/\text{mm}\cdot\text{s}$ while the highest residual compressive stress of about -440 MPa was observed in the sample ground at $Q'_w = 0.66 \text{ mm}^3/\text{mm}\cdot\text{s}$. In the case of using the structured wheel, the maximum tensile residual stress of about 290 MPa at the $Q'_w = 3.33 \text{ mm}^3/\text{mm}\cdot\text{s}$ and the maximum compressive stress of about -340 MPa at the $Q'_w = 0.66 \text{ mm}^3/\text{mm}\cdot\text{s}$ were observed. This means that both tensile stress and compressive stress were lower when using the structured wheel.

The lower tensile residual stresses prove also that the thermal loading when using the structured wheel, is less than thermal loading of the same grinding situation with the conventional wheel is used. It also shows that the mechanical loading dominates the residual stress regime up to the material removal rate of $Q'_w = 2 \text{ mm}^3/\text{mm}\cdot\text{s}$

Experimental Analysis

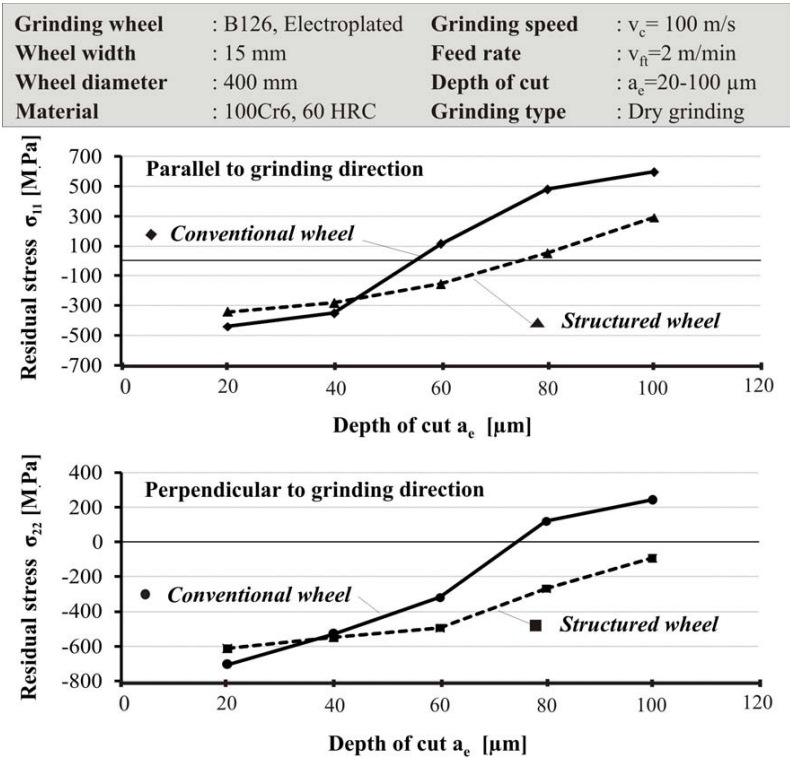


Figure 7.19: Residual stress vs. depth of cut for conventional and structured wheels measured parallel (upper curve) as well as perpendicular (bottom curve) to the grinding direction.

The bottom curve of figure 7.19 shows the residual stress measured perpendicular to the grinding direction. Here it can be seen that the tensile residual stresses of the workpiece which was ground by the structured wheel are less than that of the same material under grinding with the conventional wheel. Actually in this direction, up to the material removal rate of $Q'_w = 3.33 \text{ mm}^3/\text{mm}\cdot\text{s}$, the residual stress when using the structured wheel is compressive, but in the case of the conventional wheel it is compressive just up to the material removal rate of $Q'_w = 2 \text{ mm}^3/\text{mm}\cdot\text{s}$. Above this material removal rate, the residual stress is in the form of a tensile stress. Figure 7.20 compares the residual stresses in two directions; both parallel and perpendicular to grinding direction

Grinding wheel	: B126, Electroplated	Grinding speed	: $v_c = 100$ m/s
Wheel width	: 15 mm	Feed rate	: $v_{ft} = 2$ m/min
Wheel diameter	: 400 mm	Depth of cut	: $a_e = 20-100$ μm
Material	: 100Cr6, 60 HRC	Grinding type	: Dry grinding

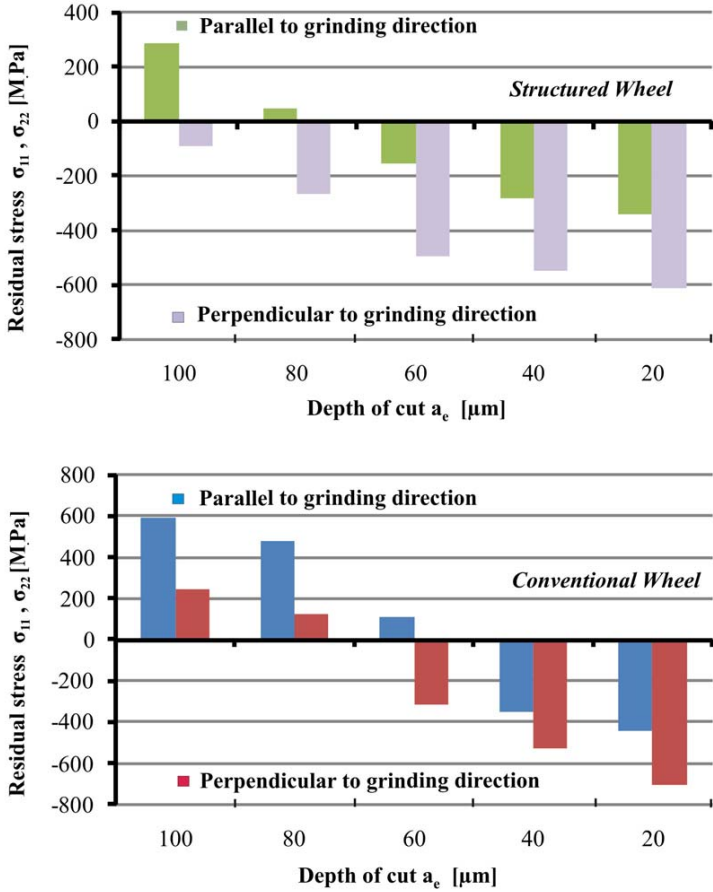


Figure 7.20: Residual stress vs. depth of cut. A comparison of the residual stresses both parallel and perpendicular to the grinding direction for both conventional and structured wheels

As was expected and reported in many researches [Brin82a, Töns83, Wern86, Tawa93], the residual stress values recorded for the measurements done perpendicular to the grinding direction are more compressive as compared with the residual stress value measured parallel

Experimental Analysis

to the grinding direction. This situation was observed for both cases of structured and conventional grinding wheels.

The reason why the residual stresses are more compressive in the perpendicular direction was discussed by Toenschhoff and Brinksmeier as well as Tawakoli [Töns83, Tawa93]. They mentioned that during chip removal from the surface of the workpiece, a part of residual stress in the grinding direction is removed by the chip. Besides, the temperature at the root of the chip drops steeply at the sides as compared to the front of the chip, which causes lower tensile residual stresses in the direction perpendicular to grinding. The other point which can be added to the above mentioned interpretation is that the chip formation occurs with micro ploughing which shows itself as piled up materials on the sides of grit indentation into the workpiece (of course not for all of the grits but for most of them). The micro ploughing process, as it was discussed in chapter 6, is rather a mechanically plastic deformation regime compared to the chip formation at the front side of the grit movement (parallel to the grinding direction). This mechanical loading, as it was explained, makes a rather more compressive residual stress, however the severe thermal loading may dominate the residual stress regime in the case where extreme thermal damage is seen.

While the number of tests carried out for residual stresses were too small to enable general statements to be made which are valid in all cases, the results, however justify the following conclusions:

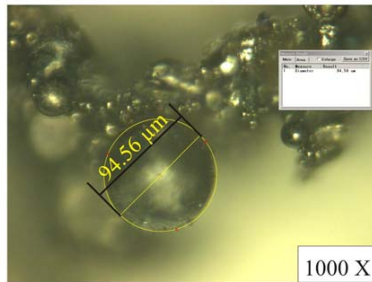
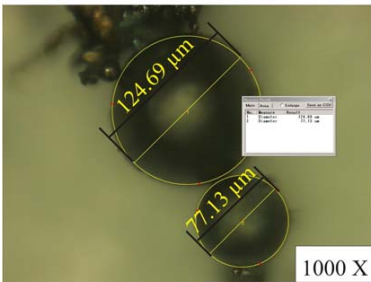
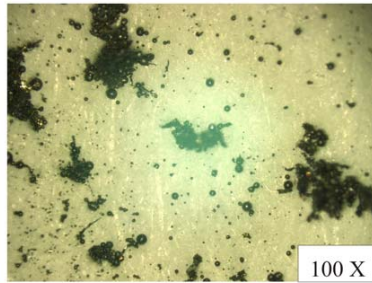
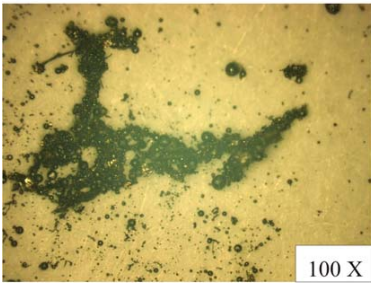
- The structured wheel produces less thermal loading and consequently less tensile residual stresses.
- Increasing the material removal rate (i.e. by increasing depth of cut) causes increased tensile residual stresses because of the thermal effect.
- Burn points are, in most of the cases seen, the sign of tensile residual stresses on the workpiece surface
- The residual stress in the direction parallel to grinding direction is more tensile compared to the residual stresses perpendicular to the grinding direction, which are more compressive.

7.6 STRUCTURING EFFECT ON CHIP SIZE

Individual chips are insufficient evidence of thermal damage to the workpiece since the temperature at the grain-chip interface is very localized [Mari04]. However the form and the size of the chip give information regarding the nature of the grain indentation into the workpiece material, as well as uncut chip thickness h_{cu} . One of the most important parameters which influences the chip size is the topography of the wheel in terms of the grain size and grain separation distance, or wheel concentration.

Figure 7.21 shows the chips after grinding of the workpiece material 100Cr6 at a grinding speed of $v_c = 80$ m/s and feed rate $v_{ft} = 2000$ mm/min.

Grinding wheel	: B126, Electroplated	Grinding speed	: $v_c = 80$ m/s
Wheel width	: 15 mm	Feed rate	: $v_{ft} = 2000$ mm/min
Wheel diameter	: 400 mm	Depth of cut	: $a_c = 0.08$ mm
Material	: 100Cr6, 48 HRC	Grinding type	: Dry grinding



Structured wheel, 22% CBN layer

Conventional wheel, 100% CBN layer

Figure 7.21: Increased chip size shown after grinding with the structured wheel, comparing with smaller chips produced by the conventional wheel

The structuring of the grinding wheel influences the maximum chip thickness and corresponding chip size. As it was previously discussed in chapter 6, the maximum chip thickness is typically dependent on the dynamic cutting edges and these depend directly on the static cutting edges. Therefore any change in topography has a direct effect on the chip size. The other parameters which influence the chip size are the material removal rate, grinding speed, grinding speed ratio and equivalent wheel diameter. Reduction of the static cutting edges causes an increase in the uncut chip thickness and the chip size, if the other grinding conditions are considered constant. Increasing the material removal rate while the

Experimental Analysis

other parameters are unchanged also causes larger chip sizes. Increasing the grinding speed, grinding ratio and equivalent wheel diameter reduces the chip size in general form.

Dry surface grinding tests were carried out with two electroplated grinding wheels with the same B126 grit size. One of the wheels was structured with about 22% contact layer and the other was a conventional wheel with 100% contact layer. The chips were gathered using a magnet installed in front of the wheel where the chips were easily attracted.

As it can be seen, chips are in the form of a sphere which proves high temperature at the time of chip formation. The high temperature causes the chips to be in a molten state, as mentioned by Malkin [Malk89]. He suggested that the energy needed for chip formation can be achieved based on the energy which is necessary to melt the chips. The random measurement of more than 80 chips from both cases shows that the average diameter of the chips produced by the structural wheels is about 1.4 times greater than the chips produced by the conventional wheels. One of these measurements for electroplated bond wheel is demonstrated in figure 7.21 (bottom). The same trend of varying chip size can be found for the resin bonded grinding wheels of structured and conventional type. In all cases, reduction of the CBN contact layer causes an increase in the chip size.

7.7 STRUCTURING EFFECT ON WHEEL WEAR

The characteristic of the grinding process depends on many factors among which the topography of the wheel in terms of the active grains, grain spacing and grain sharpness are greatly affected by the wheel wear. Grinding wheel wear in terms of attrition, grain fracture and grain pullout can affect the grinding forces, grinding power, roughness of the ground surface and part surface integrity. It was reported in many researches that attritious wear causes dulling of the abrasive grains, causing an increase in the number of active grains on the wheel surface and resulting in increased forces, grinding power and vibration [Shi06, Upad07, Oliv08]. However it was also found that grain pullout by electroplated wheel slightly decreases the active grain density and therefore the reverse effect occurs [Shi06]. In such cases, the grinding forces are reduced with wheel wear. The same situation can also occur in the case of grain fracture, in which new sharp edges created due to partial fracture of the grain may reduce the grinding forces and energy. Both matters can increase the grinding efficiency during a definite grinding condition, so-called self sharpening which is a favourable grinding condition.

Among different bonds the electroplated bond, as a single-layer bond, is the only bond type that could not be normally dressed and thus the effect of wear is more critical because there is almost no chance to attain a sharp wheel topography such as that of the new wheel. There is also no self-sharpening effect in terms of grain pull out for this bond because only one grain layer is available on the wheel surface, and the bond type holds the grains so strongly that

grain pullout doesn't usually occur. So in general form the behaviour of the electroplated wheel under wear is rather different from other types of grinding wheels, and perhaps more important, as there is no way to re-produce the primary condition of the wheel after wear begins.

In this section, a comparison between the wear of the structured wheel and of the conventional wheel is presented. Radial wheel wear versus the specific material removal for two types of vitrified and electroplated wheels is studied. In addition, the effects of wear on the grinding forces and workpiece roughness are also investigated for the electroplated bond wheel. Figure 7.22 presents the radial wear of the conventional vitrified bond CBN wheel as well as the wear characteristic of the same wheel type, but structured by special conditioning. The depth of cut of 0.01 mm was considered to ensure there is no burning or material softening for both wheels. Clearly the wheel wear of the specially conditioned wheel is more than that of the normal wheel. The G-ratio of about 663 for this wheel, at specific material removal of 5000 mm³/mm, compared to the G-ratio of 995 for the conventional wheel at the same specific material removal shows better wear resistance of the conventional wheel.

Grinding wheel	: B126, C125, Vitrified	Grinding speed	: $v_c = 60$ m/s
Wheel width	: 15 mm	Feed rate	: $v_{ft} = 1$ m/min
Wheel diameter	: 400 mm	Depth of cut	: $a_c = 10$ μ m
Material	: 100Cr6, 60 HRC	Grinding type	: Dry grinding

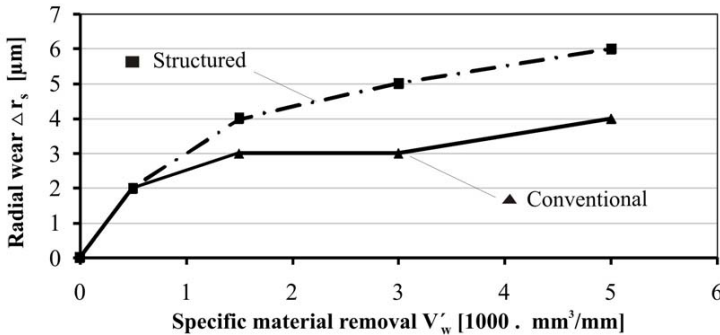


Figure 7.22: Wear characteristics of the structured and conventional wheel vs. specific material removal for vitrified bonding

Figure 7.23 shows the radial wear of the conventional electroplated CBN wheel in contrast with that of the structured CBN wheel. As it can be seen the wheel wear of the structured wheel has the same trend as for the vitrified wheel; i.e. the wear in the case of the conventional wheel is less than for the structured wheel. The G-ratio of about 785 for the structured wheel at specific material removal of 14400 mm³/mm, compared to the G-ratio of

Experimental Analysis

1413 for the conventional wheel at the same specific material removal, shows longer wheel life of the conventional wheel type.

Grinding wheel	: B126, Electroplated	Grinding speed	: $v_c = 80$ m/s
Wheel width	: 15 mm	Feed rate	: $v_{ft} = 2$ m/min
Wheel diameter	: 400 mm	Depth of cut	: $a_c = 40$ μ m
Material	: 100Cr6, 48 HRC	Grinding type	: Dry grinding

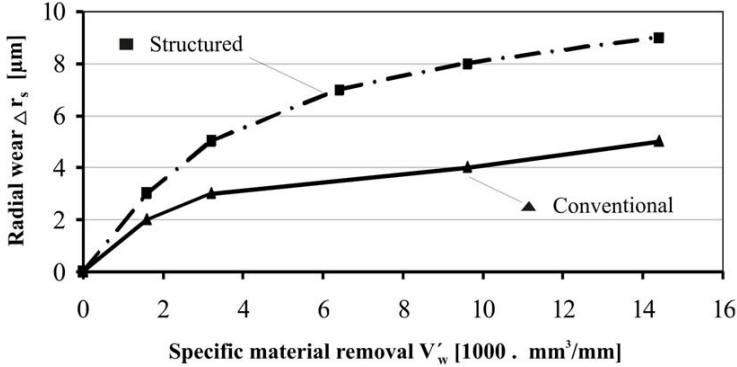


Figure 7.23: Wear characteristics of the structured and conventional wheels vs. specific material removal rate for electroplated bonded grinding wheels

The reason for increased wear in the case of the structured (or specially conditioned) wheel is that fewer CBN grits are in contact with workpiece and these grits perform the material removal. However they do perform more cutting (instead of ploughing) during process but they are under higher loading (both mechanical and thermal) and subsequently it can be estimated that more wear occurs for the active grains. The rate of wheel wear for both wheels at the beginning of the grinding is greater, because CBN grits are rather sharp and brittle when the wheel is new and they will wear at a faster rate. Besides, some of the grains, which are not tightly kept by bond, will be pulled out easily. In later stages of wheel life as the grains become duller, they are also geometrically less sharp and therefore the rate of wheel wear is decreased.

Figure 7.24 shows attritious wear of the conventional electroplated wheel after testing for the purpose of measurement. The 3D photography using a digital microscope provides a clear picture of attrition of the grains. The wheel was under investigation after grinding 100Cr6 material with a hardness of 48 HRC. The total specific material removal was $14400 \text{ mm}^3/\text{mm}$.

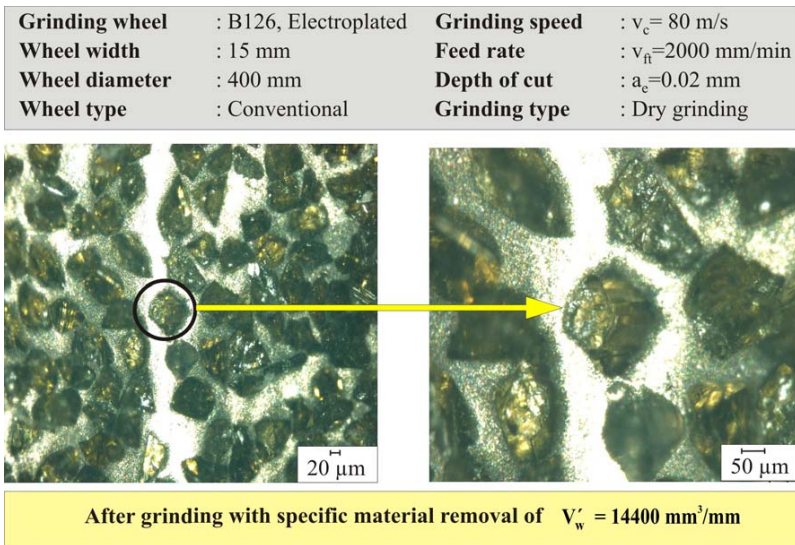


Figure 7.24: Attritious wear of the electroplated bonded wheel in dry grinding mode

Figure 7.25 presents again the attritious grain wear, this time on the structured electroplated wheel. In dry grinding as there is no high force applied to the grains due to thermal damage restrictions, it is assumed that attritious wear dominates the wear mechanism and the other two types of grain fracture and grain pullout will rarely occur (unless at the beginning of working with a new wheel). This matter was experimentally observed as well.

If the attritious wear dominates the wear mechanism, it can be predicted that the wear flat area will be increased by increasing the radial wear and consequently the grinding forces should be increased. The reason of such phenomena is that with increasing the wear flat area, the dynamic cutting edges will be increase. By increasing the wear flat area the share of rubbing and ploughing regimes in grinding process will be increased. These matters cause an increase in grinding forces and grinding energy. More grinding energy causes more heat generation which itself increases the wear of the grains and more wear flat area. So it can be estimated that, in such situation, a higher grinding wheel wear occurs. On the other hand, it is also possible that grains can not withstand high force due to the wear flat and either are broken or pulled out. In case of vitrified bond grinding wheels, the possibility of self sharpening are more that electroplated wheel.

Experimental Analysis

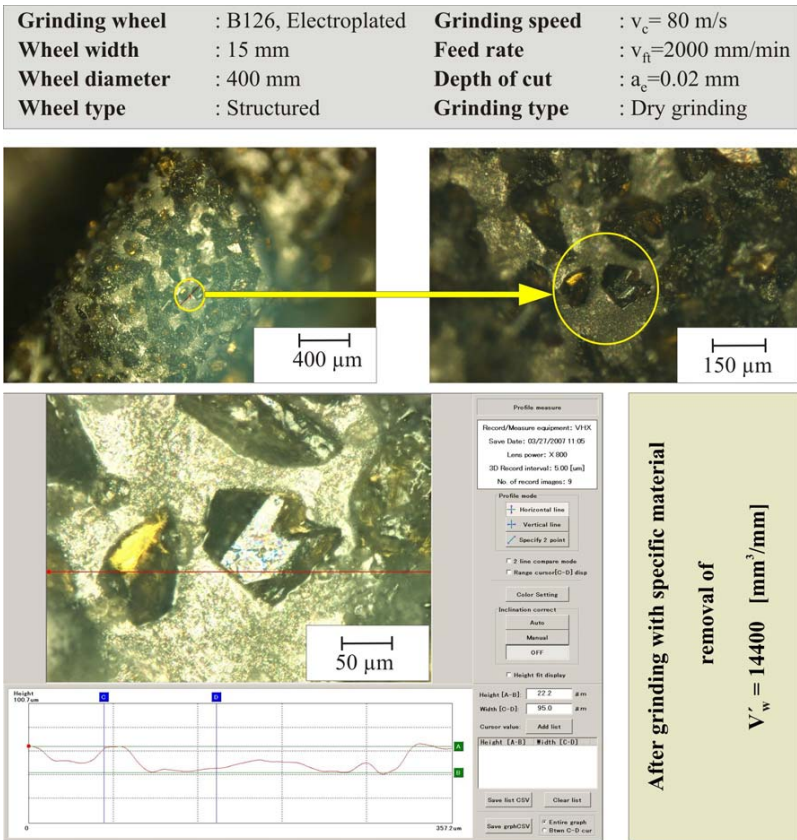


Figure 7.25: 3D digital microscopy and measurement of attritious wear on the electroplated bonded wheel in dry grinding mode

Figure 7.26 demonstrates the change in force and roughness during grinding up to a specific material removal of about $7000 \text{ mm}^3/\text{mm}$ for the electroplated CBN wheel, both conventional and structured. The forces are slightly increased with the increasing material removal in the case of the conventional wheel, but more sharply increased in the case of using the structured wheel. The roughness, in contrast to the forces, has a slight reduction tendency with increasing specific material removal.

Grinding wheel	: B126, Electroplated	Grinding speed	: $v_c = 80$ m/s
Wheel width	: 15 mm	Feed rate	: $v_{ft} = 2$ m/min
Wheel diameter	: 400 mm	Depth of cut	: $a_c = 40$ μ m
Material	: 100Cr6, 60 HRC	Grinding type	: Dry grinding

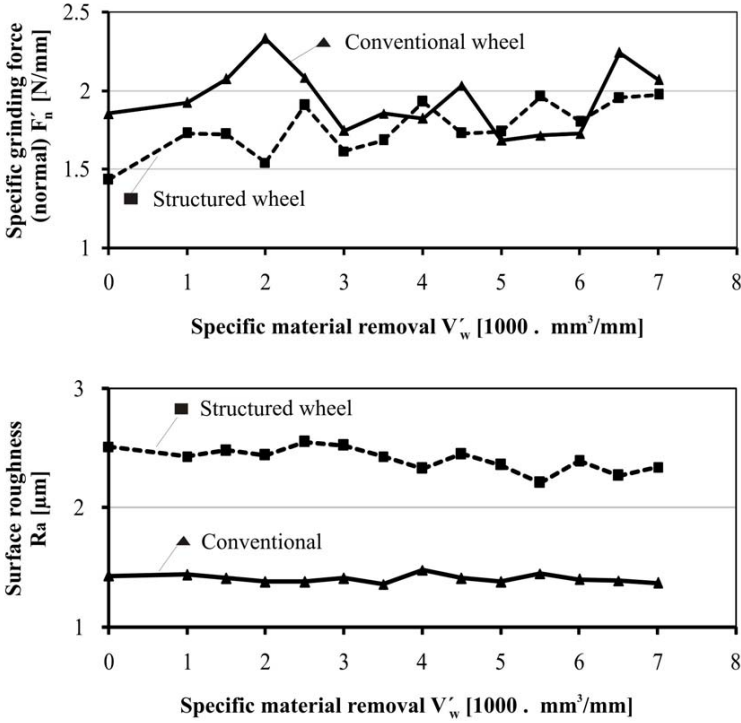


Figure 7.26: Influence of wear on normal grinding forces and surface roughness in the case of the conventional and structured electroplated bonded wheels

An increase in grinding forces is due to two reasons; first, as previously discussed, is because of attritious wear of the superabrasive, and the second reason is wheel loading during the process (as there is no coolant to transport the chips). Both phenomena also cause more heat generation in the contact zone [Ghos08]. Wheel loading is one of the critical phenomena which may further increase the specific energy in grinding. The probability of undesired wheel loading is increased under the following conditions:

- If chip volume is greater than the inter-grain space or chip pocket,
- If the chip length is greater than the circumferential pitch between adjacent grains,

Experimental Analysis

- Affinity of work material towards the grain material and bond material,
- Workpiece material is soft and ductile.

Among the above mentioned conditions, it can be observed that the spacing between the grains and grain size are the parameters that can be controlled. In the case of the structured wheel, the average space between the grains are in fact greater than that of the conventional wheel, however, on the other hand, chip size is also rather greater. Therefore the problem of undesired loading occurs in both types of wheels. Figure 7.27 shows the loading problem on the wheel surface for the electroplated bonded structured wheel, as well as laser structured vitrified wheel by SEM microscopy. In case of the electroplated wheel the chips are somehow welded to the bond and cannot be easily removed.

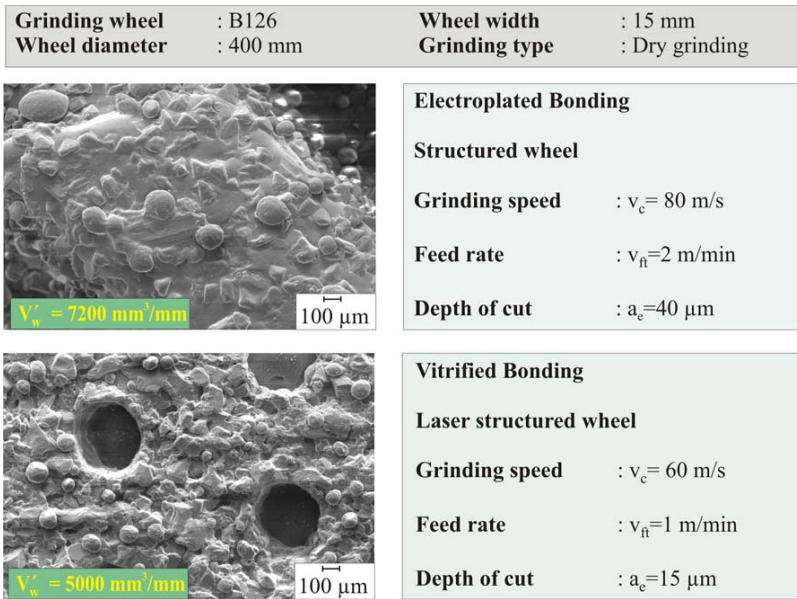


Figure 7.27: SEM microscopy image of the structured loaded wheels (electroplated and vitrified bonded types)

In both cases the chips stick to the wheel surface so that they appear rather in a black color after a short period of working. These accumulated chip particles will be in contact with workpiece and rub against the workpiece, which may cause a thermo-mechanical bonds to become established due to metal-metal contact, resulting in more friction and heat. These bonds are established and broken often during the grinding process, meaning extra grinding energy is required. With increasing material removal rate, the loading and loading effect of

the wheel will be increased. The reason is that, in dry grinding, there is no coolant to removed the chips from the grinding wheel surface so the accumulation of chips on the wheel surface decreases the chip pocket. Figure 7.28 shows the increasing wheel loading with increasing material removal.

Grinding wheel	: B126, Electroplated	Grinding speed	: $v_c = 80$ m/s
Wheel width	: 15 mm	Feed rate	: $v_{ft} = 2$ m/min
Wheel diameter	: 400 mm	Depth of cut	: $a_c = 40$ μ m
Wheel type	: Conventional	Grinding type	: Dry grinding

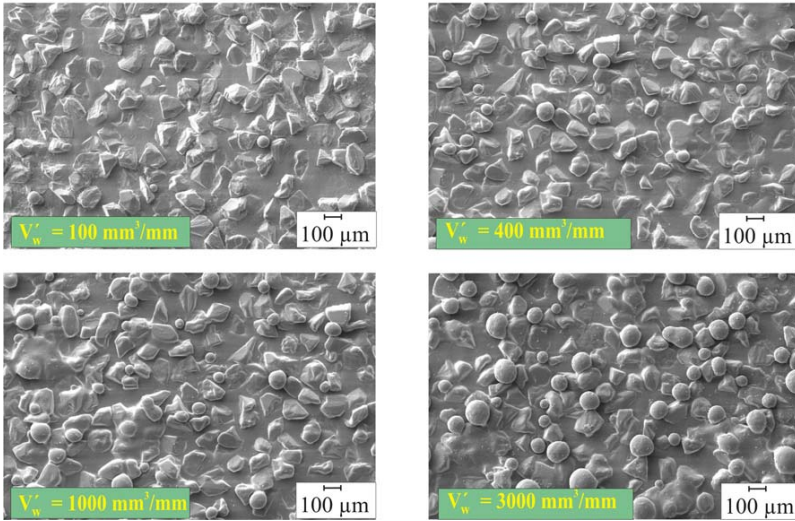


Figure 7.28: Increasing loading effect by increasing material removal in grinding with an electroplated bonded wheel

A common and practical method for sharpening the wheel, which was also used in this work for the dry grinding process, is the sharpening process using a vitrified bonded aluminum oxide block which is fed into the rotating grinding wheel. Schleich [Schl82] studied the sharpening process and developed a model, resulting that in the sharpening process, it is more efficient to apply an extreme load on the wheel by higher depth of cut and feed rate to open the wheel surface. The sharpening process was applied by three passes of the wheel on the aluminum oxide block (250x60x25 mm³) with depth of cut of 2 mm, feed rate of 5000 mm/min and wheel speed of 80 m/s. The grinding forces before sharpening and after sharpening were measured. After sharpening the specific normal grinding force was decreased from 2.2 N/mm to 1.9 N/mm, so there was about a 14% reduction in grinding force after sharpening.

Experimental Analysis

As a short summary of this section, it can be noted that grinding wheel wear is increased by using the novel structured wheels and this can be a disadvantage especially in the case of the electroplated wheel where there is no chance to dress the wheel, in order to re-produce the optimal micro-topography on the wheel. This disadvantage comparing to the other advantages of the novel wheel (such as less thermal damage, lower residual stress, etc.) should be taken into consideration and to a compromise to be made. The problem of wheel loading is more critical in dry grinding. This is a matter which should be investigated more in future work, and more efficient ways of decreasing or minimizing wheel loading during dry grinding processes should be examined.

Chapter 8

8 CONCLUSION AND SUMMARY

This research study was undertaken to investigate the dry grinding process using some innovative structured grinding wheels. The target of the study was to increase the material removal rate without changing the grinding condition. Experiments were carried out for the surface grinding of 100Cr6 steel workpieces over a wide range of operating parameters. Special grinding wheel structuring techniques were used to test grinding wheels with reduced contact layer. Different structured grinding wheels used with different contact area, and these were compared with a conventional grinding wheel. The scope of the experimental measurements encompassed grinding forces, workpiece roughness, radial wheel wear, and workpiece surface integrity in terms of residual stresses, micro-structural changes and thermal damages, as well as modelling of chip thickness, forces and specific energy.

The effects of grinding wheel structuring on grinding forces and specific energy were investigated and it was found that using a structured wheel, the grinding forces and specific energy are reduced mainly due to the size effect. The reduction of forces is decreased in some cases more than 35% for a structured wheel with 25% contact layer compared to the conventional wheel. Besides, under the range of the process parameters studied, the effects of depth of cut and feed rate for conventional and structured wheels were investigated. Increasing each of the mentioned parameters causes an increase in material removal rate and grinding forces. But under constant material removal rate, with increasing feed rate (decreasing depth of cut), a decrease in grinding forces is observed. Besides, it was found that by increasing the grinding speed, grinding forces slightly decreased but specific energy slightly increased when using both conventional and structured grinding wheels.

The energy analysis performed in this work indicates that the most energy expended in grinding is associated mainly with ploughing and rubbing action and, using the structured wheel, this portion of rubbing and ploughing energy is significantly reduced, thereby the grinding temperature and the risk of thermal damages are also reduced. This is a key point of the application of structured wheels in the grinding process. A reduction of more than 40% on the specific grinding energy was observed using the structured wheel with 25% contact layer.

Thermal aspects in grinding were also addressed in this work. The calculated and measured surface temperatures showed a decrease in grinding temperature during use of the structured wheels as compared to the conventional wheels. The grinding temperature is extremely sensitive to the ratio of the contact length to the feed rate, which is an indicator of contact time. Experimental and theoretical analysis showed that increasing contact time causes an increase in grinding temperature. Using the structured wheel, the contact time is reduced. Within the range of the process parameters of this work, decreasing the grinding speed causes a slight reduction in grinding temperature. On the other hand, it should be noted that the observed temperature and the predicted temperature using calculation are rather different, although their tendency is similar. This uncertainty suggests a need for further research both in temperature measurement and corresponding mathematical modelling.

Workpiece surface roughness is another output which was studied. The surface roughness depends directly on the dynamic cutting edges and, at least in the domain of this research work, is insensitive to grinding parameters. In addition, experimental analysis shows that the surface roughness decreases with increasing wheel wear. It was found that the surface roughness actually increases when using the structured wheel, as compared to the conventional wheel. It was also found that the surface roughness is progressively decreased with increasing the wheel contact layer. Very low surface roughness is achieved using the conventional 100% contact layer grinding wheel, but at cost of heat generation and increased process requirements in the grinding process. Tighter control or process optimization are a way of reducing process demands without sacrificing workpiece surface roughness.

The surface integrity of the ground workpiece was another characteristic studied in this research. Visual burn is found to accompany either softening or re-hardening of the workpiece surface. Softening often occurred when low visual burn was present and mostly for very hard bulk material (i.e. about 60 HRC in this study). Re-hardening was most often found where there was rather higher visual burn and when the workpiece hardness is not so high (i.e. about 48 HRC or less). The micro-structural change seen by re-hardening was an apparent white etching layer, where in contrast by softening there was found carbon precipitation from a martensitic microstructure.

The residual stresses of the ground surface were investigated both parallel and perpendicular to the grinding direction by x-ray diffraction method. The residual stresses are mostly compressive in the case of grinding with the structured wheels, compared to conventional wheels where the residual stresses are mostly tensile. The compressive residual stress is also accompanied with mechanical interaction where tensile residual stresses are mainly due to thermal loads. It was also found that the residual stress values recorded for the measurements that were made perpendicular to the grinding direction were more compressive, as compared with the residual stress values measured parallel to the grinding direction. This situation was observed for both cases of structured and conventional grinding wheels.

Conclusion and Summary

Wheel wear was studied over a long period of grinding steel specimens. Wheel wear causes an increase in grinding forces and power due to the wheel dulling. The wheel wear of the structured wheels are higher than conventional ones, due to the higher load applied on each individual grain. The wear of the CBN grains was found to be rather high at the beginning of the process due to grain pull-out as there are some grains which are held weakly in the bond material either by the previous dressing process or by electroplating. In later stages the wheel wear was observed to be lower and mostly attritious in nature.

A model used to predict the grinding forces and grinding specific energy was also presented. To develop the model, first the dynamic cutting edge density was calculated using a normal distribution of grain heights and based on the static grain density. Based on this model the chip thickness and the deformation area of a single grain can be calculated. The interaction of single grains with the workpiece and the different modes of rubbing, ploughing and cutting regimes in terms of forces and specific energy were also modelled. Then by combination of these two models the grinding forces and specific energy were determined. The effects of wheel structuring on tangential grinding forces and specific energy, in comparison with application of a conventional wheel, were theoretically and experimentally studied. In addition, models for mean uncut chip area and mean uncut chip thickness were presented and the effect of structuring on both parameters was studied. An increase in chip thickness was predicted and in the observations was proven. A neural network analysis of forces, roughness and grinding burn was developed to support the prediction of the process by empirical means as well.

Wheel loading is perhaps the most important challenge in dry grinding. Increased loading was found in the form of embedded workpiece material by vitrified bond wheel and adhering workpiece material for the electroplated bond wheel. Increased grinding forces and power by wheel loading was observed in experiments mainly due to increasing friction from chip material that remains on the workpiece surface. Loading problems, especially in dry grinding, is a matter which should be investigated more in future work, and more efficient ways of decreasing or minimizing wheel loading during processes should be examined. The main recommendations for future research in addition to the conclusions mentioned before is more investigation and modelling in the field of residual stresses and grain interaction with the workpiece.

The grinding wheel wear changes the wheel topography and consequently the dynamic cutting edge density. A model used to describe changes in grinding wheel wear over time should also be developed to predict the grinding outputs such as forces, energy, surface roughness etc. The effect of grain tip, grain shape and grain type is another matter which can be considered in terms of interaction with different materials to investigate the different modes of rubbing, ploughing and cutting to support the models and extend the physical understanding of the grinding process. The simulation of material removal is another

interesting research work. Structuring with micro-structuring in such a way that the grains have maximum cutting with minimum ploughing and rubbing should be researched as well. The micro-structural changes due to high grinding temperatures are another matter which can be more systematically studied to have better control of workpiece surface integrity. Other types of cooling systems such as cooled air or cryogenic systems used with grinding wheel structuring also have potential to be investigated. While this research focused mainly on surface grinding techniques, the results can serve as a strong basis for the study of wheel structuring in other grinding methods as well.

ZUSAMMENFASSUNG

Die bei Zerspanungsverfahren mit geometrisch definierter Schneide wie Drehen oder Fräsen relativ gut eingeführte Technologie der Trockenbearbeitung konnte bisher aus mehreren Gründen nicht auf Zerspanungsverfahren mit geometrisch undefinierter Schneide übertragen werden [Tawa06]. Trotzdem ist das Interesse von Forschung und Industrie an der Realisierung der Trockenbearbeitung beim Schleifen sehr groß. Zum Einen müssen die ökonomischen Aspekte wie die anteiligen Kosten für die Beschaffung, Aufbereitung, Zuführung, Filterung und Reinigung des Kühlschmierstoffs sowie die Verunreinigung von Maschinen und Anlagen durch den Einsatz von Kühlschmierstoff berücksichtigt werden. Zum Anderen spielen Schleifschlamm, Sondermüll, die Gefahr der Verunreinigung des Grundwassers oder der Luft und die Begrenzung der natürlichen Erdölvorkommen als ökologische Aspekte in Zukunft eine sehr große Rolle [Kloc00].

Die Ursachen dafür, dass die Trockenschleiftechnologien bis jetzt nicht so gut angewendet werden können, liegen in der Natur des Schleifprozesses und den Anforderungen an die Qualität der Oberflächenschichten. Die Zerspanung mit geometrisch undefinierter Schneide ist ein sehr energiereicher Prozess, bei welchem die zugeführte Energie zum größten Teil in Mikropflügen so wie Mikropflügen und damit in Wärmeenergie umgewandelt wird. Daher sind zur Reduzierung der Wärme und der Temperatur meist erhebliche Mengen an Kühlschmierstoff (KSS) notwendig.

Wegen der zufälligen Anordnung von Spanflächen einzelner Schleifkörner sowie deren unterschiedlichen Eingriffstiefen ist in einem Schleifprozess in der Regel ein geringer Teil der Körner an der Mikrospanung beteiligt. Um einen möglichst kühlen Schliff zu erzeugen, müssen die Schleifparameter und die Schleifscheibenspezifikationen so sein, dass möglichst die Anteile der Mikrospanung erhöht werden. Hiermit führt die Erhöhung der Eingriffstiefe zu einer Vergrößerung der einzelnen Späne. Dies erfordert einen entsprechend großen Porenraum zur Aufnahme der Späne. Der Begriff Makrotopographie kann durch die Kornplatzierung auf der Schleifscheibenoberfläche, die Kornverteilung so wie die Porenraumform, den Leerraum, wo kein Kontakt zwischen Werkzeug und Werkstück auftritt, die Schneiden-Bindung-Porenverteilung und die Geometrie und Kontur der Schleifscheibe definiert werden [Tawa08a]. Bei den strukturierten Schleifscheiben sind Veränderungen der Makrotopographie und dadurch eine Reduzierung des Reibungsanteils und der Wärme und eine Erhöhung des Spanbildungsprozesses möglich. Mit der strukturierten Schleifscheibe konnte ein Trockenschleifprozess mit höherem Zeitspanvolumen ohne thermische Probleme realisiert werden.

In dieser Arbeit wurde der Effekt der Strukturierung auf den Trockenschleifprozess ermittelt. Das Ziel war eine industrielle, praktische Einführung des Trockenschleifens und eine Erhöhung der üblichen Zeitspanvolumen ohne thermische Schädigung auf dem Werkstück. Die praktischen Untersuchungen erfolgten an Werkstückproben aus gehärtetem 100Cr6. Zum Einsatz kamen die kunstharzgebundene, keramisch gebundene und galvanisch gebundene CBN-Schleifscheibe der Korngröße B126. Zur Strukturierung wurden verschiedene Geometrien und Methoden verwendet. Um den Einfluss der Stellgrößen bei der Trockenschleifbearbeitung mit strukturierter Schleifscheibe beurteilen zu können, ist ein Vergleich mit der konventionellen (nicht strukturierten) Schleifscheibe erforderlich. Dazu

wurden Schleifkräfte, Werkstückrauheit, Radial-Verschleiß der Schleifscheibe und Temperatur beim Flachsleifen gemessen. Die Oberflächegüte und Randzonenschäden in Form von Mikrostruktur, Mikrohärtigkeit und Eigenspannungen wurden berücksichtigt und verglichen. Für Spannungsdicke, Schleifkräfte und bezogene Energie wurden die physikalischen und empirischen Modelle ermittelt. Die Modelle wurden mit den experimentellen Resultaten verifiziert bzw. verglichen.

Eine enorme Reduzierung der Schleifkräfte beim Einsatz der strukturierten Schleifscheibe (teilweise über 35% Verringerung der Kräfte) im Vergleich zum Einsatz der konventionellen Schleifscheibe resultiert aus den kleineren dynamischen Schneiden. Bei den Untersuchungen wurden die Zustellung, die Vorschubgeschwindigkeit und die Schnittgeschwindigkeit als Prozessparameter variiert. Die Ergebnisse zeigen, dass unter konstanten Zeitspannungsvolumen die Erhöhung der Vorschubgeschwindigkeit im Vergleich zur Steigung der Zustellung kleinere Schleifkräfte entstehen lassen. Bei der Erhöhung der Schnittgeschwindigkeit mit den konstanten Zeitspannungsvolumen werden die Schleifkräfte reduziert. Bei steigenden Schnittgeschwindigkeiten steigt auch die Anzahl der Schneiden, die mit dem Werkstück in Kontakt kommen. Dadurch reduziert sich die Schneidendicke und erhöht sich die Reibungswärme ebenso wie die umgesetzte Energie. Eine höhere Schnittgeschwindigkeit kann sich erst in Verbindung mit steigenden bezogenen Zeitspannungsvolumen positiv auswirken.

Die strukturierte Schleifscheibe hat im Vergleich zu der nicht strukturierten Scheibe einen höheren Oberflächenrauheitswert. In vielen Fällen sind die relativ höheren Rauheitswerte akzeptabel und gut genug. Die Oberflächenrauheitswerte können aber nach Bedarf durch Ausfeuern verfeinert werden. Die geringfügig höhere Rauheit bei der strukturierten Schleifscheibe wird bedingt durch kleinere dynamische Schneidenzahlen so wie einer größeren Spannungsdicke. Die Parameter Zustellung, Vorschubgeschwindigkeit und Schnittgeschwindigkeit haben geringen Einfluss auf die Oberflächenrauheit in den Untersuchungsbereichen.

Die Energieanalyse in dieser Arbeit zeigt, dass die Hauptteile der Prozessenergie durch Mikroreiben und Mikropflügen in Wärme umgewandelt werden und beim Einsatz der strukturierten Schleifscheibe diese Teile drastisch reduziert werden. Die Reduzierung bis über 40% der bezogenen Energie war ein bedeutendes Resultat der Benutzung der neuen Konzepte.

Sowohl die Modellberechnung als auch die versuchsweise Messung zeigen eine geringere Prozesstemperatur auf der Kontaktzone beim Einsatz der strukturierten Schleifscheibe im Vergleich mit einer nicht strukturierten Schleifscheibe. Die Resultate zeigen, dass die Temperatur in höchstem Maß abhängig vom Verhältnis der Kontaktlänge zur Vorschubgeschwindigkeit, d.h. Kontaktzeit ist. Die Unterbrechungen auf der Kontaktfläche der strukturierten Schleifscheibe ermöglichen einen kurzen Kontakt zwischen der Schleifscheibe und dem Werkstück. Nach Kontakt und Materialabtrag erfolgt immer eine kurze Unterbrechung. In dieser kontaktlosen Zeit hat die erzeugte Wärme Zeit, sich zu verteilen und die Werkstückoberflächentemperatur reduziert sich dadurch. Außerdem bleiben genügend Räume in den kontaktfreien Flächen für die zwanglose Aufnahme der Späne.

Die Randzonengefügeveränderungen wurden beim Schleifprozess untersucht. Die Brandmarken zeigen die thermischen Schädigungen. Diese Schädigungen wurden am häufigsten beim Einsatz der nicht strukturierten Schleifscheibe gesehen. Eine thermische

Zusammenfassung

Schädigung (weiße Schicht unter dem Mikroskop) mit einer punktuellen höheren Härte als das Grundmaterial wurde schon nach dem Schleifen des 100Cr6 mit einer Härte von 48 HRC bei galvanisch gebundenen Schleifscheiben berücksichtigt. Im Gegensatz dazu wurde nach dem Schleifen des 100Cr6 mit einer Härte von 60 HRC mit kunstharzgebundener Schleifscheibe eine deutliche Reduzierung der Härte mit beschädigten Werkstückoberflächen festgestellt. Die Gefügebeeinflussung durch den Schleifprozess hängt von den Werkstoffeigenschaften und dem zeitlichen und örtlichen Verlauf der Wärmequelle und der Temperatur auf der Kontaktzone ab.

Die Eigenspannungen beim Einsatz der strukturierten Schleifscheibe traten - im Vergleich mit nicht strukturierten Schleifscheiben - am häufigsten als Druckeigenspannungen auf, wobei nicht strukturierte Schleifscheibe sich am meisten als ungünstige Zugeigenspannungen zeigten. Außerdem wurde sowohl für die konventionelle als auch die strukturierte Schleifscheibe eine unterschiedliche Eigenspannung in der Richtung parallel zur Schleifbahn und senkrecht zu dieser Richtung festgestellt. Die Ursachen der eventuell entstandenen Eigenspannungen beim Schleifprozess liegen zum einen in der mechanisch induzierten Druckspannung und zum anderen in der ungünstigeren thermisch induzierten Zugspannung.

Zur Ermittlung und zum Vergleich des Verschleißverhaltens der strukturierten Schleifscheibe im Gegensatz zur nicht strukturierten Schleifscheibe wurden Untersuchungen mit keramisch und galvanisch gebundener Schleifscheibe durchgeführt. Beim Einsatz der strukturierten Schleifscheibe tritt im Vergleich zur konventionellen Schleifscheibe ein höherer Verschleiß auf. Allerdings ist dieser Verschleiß nicht so hoch, dass man die Wirtschaftlichkeit des Prozesses in Frage stellen muss. Hier sollte ein Kompromiss zwischen niedriger Wärmeentwicklung, niedriger Oberflächentemperatur des Werkstücks und höherem Verschleiß der Scheibe berücksichtigt werden.

Die Schleifscheibenzusetzung ist wahrscheinlich das größte Problem beim Trockenschleifen. Eine Steigung der Schleifscheibenzusetzung bei der Erhöhung des bezogenen Zerspanungsvolumens beeinflusst die Prozesskräfte so wie die Wärmeerzeugung. Ohne einen optimalen Schärfprozess kann die Schleifscheibe beim Trockenschleifen nicht lange Zeit verwendet werden. Eine optimale Methode zum Schärfen beim Trockenschleifprozess soll in den zukünftigen Forschungen berücksichtigt werden.

Um ein Prozessverständnis aufzubauen, wurden in theoretischen Betrachtungen (zunächst unter Vernachlässigung des Verschleißes) und unter einigen geometrischen Vereinfachungen die Spannungsdicke, die Prozesskräfte und die bezogene Energie modelliert. Aufbauend auf einer statistischen Analyse der Schleifscheibentopographie und der Betrachtung der kritischen Eingriffstiefe eines Korns in die metallischen Werkstoffe wurde zuerst ein Modell zur Berechnung der mittleren Spannungsdicken erstellt. Weiterhin wurden physikalische Modelle entwickelt, um die Eingriffskräfte und die Energie von einem Korn in verschiedenen Phasen von Mikroreibung, Mikropflügen und Mikrospanen ermitteln zu können. Diese Modelle wurden mit der statistischen Verteilung der Körner kombiniert, um die Prozesskräfte und die bezogene Energie für den ganzen Schleifprozess (mehrere Körner) zu ermitteln. Diese Modelle wurden mit den experimentellen Untersuchungen verifiziert bzw. verglichen. Außerdem wurde ein empirisches Modell zur Vorhersagung von Brandmarken, Rauheit und Prozesskräften mit einem neuronalen Netzwerk entwickelt. Die Ergebnisse des Modells zeigen eine akzeptable Übereinstimmung mit den Resultaten der Experimente.

REFERENCES

- [Auri03] Aurich, J.C.; Braun, O.; Warnecke, G.: Development of a superabrasive grinding wheel with defined grain structure using kinematic simulation, *Annals of the CIRP*, Vol. 52/1, (2003), pp. 275–280.
- [Avne74] Avner, H.M: Introduction to physical metallurgy, Glenco/Mc Graw Hill, 2nd edition., (1974).
- [Brau08] Braun, O.: Konzept zur Gestaltung und Anwendung definiert gesetzter CBN-Schleifscheiben, Dissertation, University of Kaiserslautern, (2008).
- [Brin82a] Brinksmeier, E.: Randzonenanalyse geschliffener Werkstücke, Dissertation, University of Hannover, (1982).
- [Brin82b] Brinksmeier, E.; Cammett, J.T.; König, W.; Leskovar, P.; Peter, J.; Tonshoff, H.K.: Residual stress - measurement and causes in machining processes, *Annals of the CIRP*, Vol. 31/2, (1982), pp. 491-510.
- [Brin94] Brinksmeier, E.; Brockhoff, T.: Randschicht-Wärmebehandlung durch Schleifen, *Härtereitechnische Mitteilungen*, 49. (1994), pp. 327-330.
- [Brin98] Brinksmeier, E.; Tönshoff, H.K.; Czenkusch C.; Heinzl, C.: Modelling and optimisation of grinding processes, *Journal of Intelligent Manufacturing*, Vol. 9-(4), (1998), pp. 303–314.
- [Brin99] Brinksmeier, E.; Heinzl, C.; Meyer, L.: Friction, Cooling and Lubrication in Grinding, *Annals of the CIRP*, Vol. 48/2, (1999), pp. 581-598.
- [Brin03] Brinksmeier, E.; Wilke, T.: Influence of process design on residual grinding stresses, 1st European Conference on Grinding, Fortschritt-Bericht VDI, No. 643, Aachen, Germany, Nov. (2003), pp. 15.1-15.27.
- [Brin04] Brinksmeier, E.; Heinzl, C.; Meyer, L.; Wittman, M.: Bewertung der Effektivität der Kühlschmierstoffzufuhr beim Schleifen, *Jahrbuch Schleifen, Honen, Läppen und Polieren*, 61. Ausgabe, (2004), pp. 2–16.
- [Brin05] Brinksmeier, E.; Heinzl, C.; Bleil, N.: Randschichtverfestigung durch Nutzung des Größeneffekts beim Schleifen, *Jahrbuch Schleifen, Honen, Läppen und Polieren*, 62. Ausgabe, (2005), pp. 21–37
- [Brin06] Brinksmeier, E.; Aurich, J.C.; Govekar, E.; Heinzl, C.; Hoffmeister, H.W.; Klocke, F.; Peters, J.; Rentsch, R.; Stephenson, D.J.; Uhlmann, E.; Weinert, K.; Wittmann, M.: Advances in modelling and simulation of grinding processes, *Annals of the CIRP*, Vol. 55/2, (2006), pp.667-696.
- [Broc99] Brochhoff, T.: Schleifprozesse zur martensitischen Randschichthärtung von Stählen, Dissertation, University of Bremen, (1999).
- [Burk01] Burkhard.G.: Spannen mit definiert angeordneten Hartstoffkörnern, Dissertation, ETH Zurich, (2001).

- [Burk02] Burkhard, G.; Rehsteiner F.; Schumacher B.: High efficiency abrasive tool for honing, *Annals of the CIRP*, Vol. 51/1, (2002), pp. 271-274.
- [Brun98] Brunner, G.: Schleifen mit mikrokristallinem Aluminiumoxid, Dissertation, University of Hannover (1998).
- [Cape02] Capello, E.; Semeraro, Q.: Process parameters and residual stress in cylindrical grinding, *Journal of Manufacturing Science and Engineering*, Vol. 124, (2002), pp 615-623.
- [Cars59] Carslaw, H.; Jaeger, J.C.: *Conduction of heat in solids*, Oxford Science Publications, Oxford University Press, (1959).
- [Chen89] Chen, C.; Jung, Y.; Inasaki, I.: Surface, Cylindrical and Internal Grinding of Advanced Ceramics: Grinding Fundamentals and Applications, *Journal of Engineering for Industry*, Vol. 39, (1989), pp. 201–211.
- [Chen96a] Chen X.; Rowe W.B.: Analysis and Simulation of the Grinding Process Part I: Generation of the Grinding Wheel Surface, *International Journal of Machine Tools and Manufacture*, Vol. 36, (1996), pp. 871–882.
- [Chen96b] Chen, X.; Rowe, W.B.: Analysis and Simulation of the Grinding Process Part II: Mechanics of Grinding, *International Journal of Machine Tools and Manufacture*, Vol. 36, (1996), pp. 883–896.
- [Chen96c] Chen, X.; Rowe, W.B.; Mills, B.; Allanson, D.R.: Analysis and simulation of the grinding process Part III: Comparison with experiment, *International Journal of Machine Tools and Manufacture*, Vol. 36(8), (1996), pp. 897–906.
- [Chen98] Chen, X.; Rowe, W.B.; Mills, B.; Allanson, D.R.: Analysis and simulation of the grinding process Part IV: Effects of wheel wear, *International Journal of Machine Tools and Manufacture*, Vol. 38(1/2), (1998), pp. 41–49.
- [Chen02] Chen, X.; Rowe, W.B.; Cai, R.: Precision grinding using CBN wheels, *International Journal of Machine Tools and Manufacture*, Vol. 42(5), (2002), pp. 585-593.
- [Chen04a] Chen, X.; Feng, Z.; Pashby, I.: Study on laser cleaning Al₂O₃ grinding wheel, *Key Engineering Materials*, Vol. 257-258, (2004), pp. 359-364.
- [Chen04b] Chen, X.; Feng, Z.; Pashby I.: Comparison of Laser Cleaning of Al₂O₃ and CBN Grinding Wheels, *Key Engineering Materials*, Vol. 257-258, (2004), pp. 365-370.
- [Choi86] Choi, H.Z.: Beitrag zur Ursachenanalyse der Randzonbeeinflussung beim Schleifen, Dissertation, University of Hannover (1986).
- [Choi01] Choi, H.Z.; Lee, S.W.; Jeong, H.D.: A comparison of the cooling effects of compressed cold air and coolant for cylindrical grinding with a CBN wheel, *Journal of Materials Processing Technology*, Vol. 111, (2001), pp. 265–268.
- [Cina95] Cinar, M.: Einsatzvorbereitung und Verschleissentwicklung keramisch gebundener CBN-Schleifscheibe, Dissertation, University of Bremen, (1995).

- [Dasi07] Da Silva, L.R.; Bianchi E.C.; Fusse, R.Y.; Catai, R.E.; França, T.V.; Aguiar, P.R.: Analysis of surface integrity for minimum quantity lubricant-MQL in grinding, *International Journal of Machine Tools and Manufacture*, Vol. 47, (2007), pp. 412–418.
- [Daus04] Daus, N.A.: *Ultraschallunterstütztes Quer-Seiten- Schleifen*, Dissertation, TU Berlin, (2004).
- [Deag05] De Aguiar, P.R.; Dotto, F.R.L.; Bianchi, E.C.: Study of Thresholds to Burning in Surface Grinding Process, *ABCM*, Vol. XXVII(2), (2005), pp. 150-156.
- [Deme00] Demetriou, M.D.; Lavine, A.S.: Thermal aspects of grinding: the case of upgrinding, and fluid, *Journal of Manufacturing Science and Engineering*, Vol. 122, (2000), pp. 605–611.
- [Demu01] Demuth, H.B.: *Neural network toolbox for use with MATLAB: User's guide*, MathWorks; Release 12, (2001).
- [Denk03] Denkena, B.; Jung, M.; Müller, C.; Walden, L.: Charakterisierung weißer Schichten nach mechanischer und thermischer Einwirkung durch Fertigungsverfahren, *Härtereitechnische-Mitteilungen*, 58, (2003), pp. 211-217
- [Desr70] Des Ruisseaux, N.R.; Zerkle, R.D.: Thermal analysis of the grinding process, *Journal of Engineering for Industry*, Vol. 92, (1970), pp. 428–434.
- [Deva81] De Vathaire, M.; Delamare, F.; Felder, E.: An upper bound model of ploughing by a pyramidal indenter, *Wear*, Vol. 66 (1), (1981), pp. 55-64.
- [Dorn84] Dornfeld, D.; Cai, H. G.: An Investigation of Grinding and Wheel Loading Using Acoustic Emission, *Trans. ASME*, Vol. 106, (1984), pp. 28-33.
- [Enge02] Engelhorn, R.: *Verschleißmerkmale und Schleifeinsatzverhalten zweiphasig verstärkter Sol-Gel-Korunde*, Dissertation, RWTH Aachen, (2002).
- [Fisc00] Fischbacher, M.: *Umweltverträgliches Schleifen im Umfeld der Leistungsmaximierung*. Kolloquium, *Umweltverträgliches Schleifen, Ökologie als Ökonomie der Zukunft*, Shaker Verlag, (2000). pp. 53-72
- [Ghos08] Ghosh, S.; Chattopadhyay, A.B.; Paul, S.: Modeling of specific energy requirement during high-efficiency deep grinding, *International Journal of Machine Tools and Manufacture*, Vol. 48 (11), (2008), pp. 1242-1253.
- [Giew03] Giewerzew, A.: *Spanbildungsmechanismen und tribologisches Prozeßverhalten beim Schleifen mit niedrigen Schnittgeschwindigkeiten*, Dissertation, University of Bremen, (2003).
- [Guo94] Guo, C.; Malkin, S.: Analytical and Experimental Investigation of Burnout in Creep-Feed-Grinding, *Annals of the CIRP*, Vol. 43/1, (1994), pp. 283–286.
- [Guo99] Guo, C.; Wu, Y.; Varghese, V.; Malkin, S.: Temperatures and energy partition for grinding with vitrified CBN wheels, *Annals of the CIRP*, Vol. 48/1, (1999), pp. 247–250.
- [Guo00] Guo, C.; Malkin, S.: Energy partition and cooling during grinding, *Journal of Manufacturing Processes*, Vol. 2 (3), (2000), pp. 151–157.

- [Hahn62] Hahn, R.S.: On the nature of the grinding process, Proceeding of the 3rd International Machine Tool Design and Research Conference, Birmingham, (1962), pp. 129–154.
- [Heck03a] Hecker, R.L.; Ramoneda, M.; Liang, S.Y.: Analysis of wheel topography and grit force for grinding process modelling, *Journal of Manufacturing Processes*, Vol. 5(1), (2003), pp. 13–23.
- [Heck03b] Hecker, R.L.; Liang, S.Y.: Predictive modelling of surface roughness in grinding, *International Journal of Machine Tools and Manufacture*, Vol. 43 (8), (2003), pp. 755–761.
- [Hege00] Hegeman, J.B.J.W.: Fundamentals of Grinding: Surface Conditions of Ground Materials, Dissertation, University of Groningen, (2000).
- [Hein99] Heinzl, C.: Methoden zur Untersuchung und Optimierung der Kühlschmierung beim Schleifen, Dissertation, University of Bremen, (1999).
- [Hein07] Heinzl, C.; Bleil, N.: The Use of the Size Effect in Grinding for Work-hardening, *Annals of the CIRP*, Vol. 56/1, (2007), pp. 327-330.
- [Hoff00] Hoffmeister, H.W.; Langemeyer, A.: Umweltverträgliches Flachprofilschleifen-Technologien zur Kühlschmierstoffsubstitution, Schleiftechnisches, Kolloquium, Umweltverträgliches Schleifen, Ökologie als Ökonomie der Zukunft, Shaker Verlag, (2000), pp.161-175.
- [Hoff02] Hoffmeister, H.W.; Illenseer, S.; Wirtschaftlich vergleich zwischen konventionellem und CD- Schleifen von Inconel 706, *Jahrbuch Schleifen, Honen, Läppen und Polieren*, 60. Ausgabe, (2002), pp. 186-198.
- [Hoff04] Hoffmeister, H.W.; Maiz, K.: Trockenschleifen mit Hilfe der Cryotechnik, 5. Seminar „ 5. Moderne Schleiftechnologie und Feinstbearbeitung“, Stuttgart, Germany, May (2004), pp. 3c.1 - 3c.9,
- [Hoff07] Hoffmeister, H.W.; Maiz, K.: Flachsleifen metallische Werkstoffe unter Verwendung der flüssigem Stickstoff zur Kühlung, *Jahrbuch Schleifen, Honen, Läppen und Polieren*, 63. Ausgabe, (2007), pp. 119-134.
- [Hokk88a] Hokkirigawa, K.; Kato, T.; Li, Z.Z.: The effect of hardness on the transition of the abrasive wear mechanism of steels, *Wear*, Vol.123 (2), (1988), pp. 241-251.
- [Hokk88b] Hokkirigawa, K.; Kato, T.: An experiment and theoretical investigation of ploughing, cutting, and wedge formation during abrasive wear, *Tribology International*, Vol. 21, (1988), pp. 51-57.
- [Hokk98] Hokkirigawa, K.; Kato, T.; Fukuda, T.; Shinooka, M.: Experimental and theoretical analysis of wear mechanism of metals in tilted block on plate type sliding, *Wear*, Vol. 214 (2), (1998), pp.192-201.
- [Hou03a] Hou, Z.B.; Komanduri, R.: On the mechanics of the grinding process-Part I, Stochastic nature of the grinding process, *International Journal of Machine Tools and Manufacture*, Vol. 43 (15), (2003), pp. 1579–1593.

- [Hou03b] Hou, Z.B.; Komanduri, R.: On the mechanics of the grinding process-Part II, Thermal analysis of fine grinding, *International Journal of Machine Tools and Manufacture*, Vol. 44 (2-3), (2004), pp. 247-270.
- [Howe87] Howes, T.D.; Neailey, K.; Harrison, J.: Fluid Film Boiling in Shallow Cut Grinding, *Annals of the CIRP*, Vol. 36/1, (1987), pp. 223-226.
- [Inas96] Inasaki, I.: Grinding process simulation based on the wheel topography measurement, *Annals of the CIRP*, Vol. 45/1, (1996), pp. 347-350.
- [Inou04] Inoue, S.; Aoyama, T.: Application of air cooling technology and minimum quantity lubrication to relief grinding of cutting tools, *Key Engineering Materials*, 257-258, (2004), pp. 345-350.
- [Jack07] Jackson, M.J.; Khangar, A.; Chen, X.; Robinson, G.M.; Venkatesh, V.C.; Dahotre, N.B.: Laser cleaning and dressing of vitrified grinding wheels, *Journal of Materials Processing Technology*, Vol. 185 (1-3), (2007), pp. 17-23.
- [Jaeg42] Jaeger, J.C.: Moving Sources of Heat and the Temperature at Sliding Contacts, *Proceeding Royal Society, New South Wales*, 76 (3), (1942), pp. 203-224.
- [Jin01] Jin, T.; Cai, G.Q.: Analytical thermal models of oblique moving heat source for deep grinding and cutting, *ASME Journal of Manufacturing Science and Engineering*, Vol. 123 (1), (2001) pp. 185-190.
- [Jin02] Jin, T.; Stephenson, D.J.: Investigation of the heat partitioning in high efficiency deep grinding, *International Journal of Machine Tools and Manufacture*, Vol. 43, (2003), pp. 53-59.
- [Kass69] Kassen, G.: Beschreibung der elementaren Kinematik des Schleifvorganges, Dissertation, RWTH Aachen, (1969).
- [Kato00] Kato, T.; Fuji, H.: Temperature Measurement of Workpiece in Conventional Surface Grinding, *Journal of Manufacturing Science and Engineering*, Vol. 122, (2000), pp. 297-303.
- [Kloc95] Klocke, F.; König W.; Lung, D.; Gerschweiler, K.: Trocken erspanen-Eine Herausforderung der Metallbearbeitenden Industrie und Möglichkeiten, *VDI-Z* 135, (1995), pp. 38-42.
- [Kloc96a] Klocke F.; Bückler, C.: Trockenschleifen- Grenzbetrachtung zur Kühlschmierstoffreduzierung, *Industrie Diamanten Rundschau IDR* 1, (1996), pp. 26-35.
- [Kloc96b] Klocke, F.; Gerschweiler, K.: Trockenbearbeitung - Grundlagen, Grenzen, Perspektiven, *VDI-Seminar: Auf dem Weg zur Trockenbearbeitung*, VDI Berichte Nr. 1240, (1996), pp. 1-43
- [Kloc97] Klocke, F.; Eisenblätter, G: Dry cutting, *Annals of the CIRP*, Vol. 46/2, (1997), pp 519-525.
- [Kloc00] Klocke, F.: Umweltverträgliches Schleifen. Kolloquium, Umweltverträgliches Schleifen, Ökologie als Ökonomie der Zukunft, Aachen, Shaker Verlag, (2000), pp 1-14.

- [Kloc03] Klocke, F.: Modeling und simulation in grinding, 1st European Conference on Grinding, Fortschritt-Bericht VDI, No. 643, Aachen, Germany, Nov. (2003), pp 8.1–8.27
- [Kloc05a] Klocke, F.; König, W.: Schleifen, Honen, Läppen; Fertigungsverfahren Band 2, Springer Verlag, (2005).
- [Kloc05b] Klocke, F.; Brinksmeier, E.; Weinert, K.: Capability Profile of Hard Cutting and Grinding Processes, Annals of the CIRP, Vol. 54/ 2, (2005), pp 22-45.
- [Koch00] Koch, K.: Möglichkeiten zur Reduzierung des Kühlschmierstoffvolumenstromes beim Schleifen mit CBN-Schleifscheiben, Schleiftechnisches Kolloquium, Umweltverträgliches Schleifen, Ökologie als Ökonomie der Zukunft, Shaker Verlag, (2000), pp. 39-52
- [Köni94] König, W.; Treffert, C.; Bücker, C.: Hochgeschwindigkeitschleifen mit CBN ohne Kühlschmierstoff, Industrie Diamanten Rundschau IDR 2, (1994), pp. 88-93.
- [Kosh93] Koshy, P.; Jain, V.K.; Lal, G.K.: A model for the topography of diamond grinding wheels, Wear, Vol. 169 (2), (1993), pp. 237–242.
- [Kosh99] Koshy, P.; Ives, L.K.; Jahanmir, S.: Simulation of diamond-ground surface, International Journal of Machine Tools and Manufacture, Vol. 39 (9), (1999) pp. 1451–1470.
- [Kova95] Kovacevic, R.; Mohan, R.: Effect of high speed grinding fluid on surface grinding performance, Technical Papers of the First International Machining and Grinding Conference, Dearborn, Michigan, Sep. (1995), pp. 917–931.
- [Kuma07] Kumar, S.; Choudhury, S.K.: Prediction of wear and surface roughness in electro-discharge diamond grinding, Journal of Materials Processing Technology, Vol. 191 (1-3), (2007), pp. 206-209.
- [Kuri03] Kuriyagawa, T.; Syoji K.; Ohshita, H.: Grinding temperature within contact arc between wheel and workpiece in high-efficiency grinding of ultrahard cutting tool materials, Journal of Materials Processing Technology, Vol.136 (1-3), (2003), pp. 39-47.
- [Kwak01] Kwak, J.S.; Song, J.B.: Trouble diagnosis of the grinding process by using acoustic emission signals, International Journal of Machine Tools and Manufacture, Vol. 41 (6), May, (2001), pp. 899–913.
- [Laue79] Lauer-Schmaltz, H.: Zusetzung von Schleifscheiben, Dissertation, RWTH Aachen, (1979).
- [Laue80] Lauer-Schmaltz, H.; König, W.: Phenomenon of Wheel Loading Mechanisms in Grinding, Annals of the CIRP, Vol. 29/1, (1980), pp. 201-206.
- [Lavi88] Lavine, A.S.: A simple model for convective cooling during the grinding process, Journal of Engineering for Industry, Vol. 110, (1988), pp. 1–6.
- [Lavi90] Lavine, A.S.; Malkin, S.: The Role of Cooling in Creep Feed Grinding, International International Journal of Advanced Manufacturing Technology, Vol. 5, (1990), pp. 97-111.

- [Lavi00] Lavine, A.S.: An exact solution for surface temperature in down grinding, *Journal of Heat and Mass Transfer*, Vol. 43, (2000), pp. 4447–4456.
- [Liao94] Liao, T.W.; Chen, L.J.: A Neural Network Approach for Grinding Processes: Modelling and Optimization, *International Journal of Machine Tools and Manufacture*, Vol. 34 (7), (1994), pp. 919–937.
- [Liao95] Liao, T.W.: Fractal and DDS characterization of diamond wheel profiles, *Journal of Materials Processing Technology*, Vol. 53 (3–4), (1995), pp. 567–581.
- [Liu97] Liu, H.; Chen, T.; Liangsheng, Q.: Predicting grinding burn using artificial neural network, *Journal of Intelligent Manufacture*, Vol.8, (1997), pp.235-237.
- [Lier98] Lierse, T.: Mechanische und thermische Wirkung beim Schleifen keramische Werkstoffe, *Fachricht-Bericht, VDI, Reihe 2, Nr. 471*, Düsseldorf, (1998),
- [Link92] Linke, K.: Kennwerte keramisch gebundener Schleifscheiben aus kubischem Bornitrid, *Produktionstechnik-Berlin*, 101, (1992).
- [Link07] Linke, B.: Wirkmechanismen beim Abrichten keramisch gebundener Schleifscheiben, *Dissertation, RWTH Aachen*, (2007).
- [Lort75] Lortz, W.: Schleifscheibentopographie und Spanbildungsmechanismus beim Schleifen, *Dissertation, RWTH Aachen*, (1975).
- [Maie08] Maier, B.: Beitrag zur thermische Prozessmodellierung des Schleifens, *Dissertation, RWTH Aachen*, (2008).
- [Malk89] Malkin, S.: *Grinding Technology: Theory and Applications of Machining with Abrasives*, Ellis Horwood Limited, Chichester, (1989).
- [Malk06] Malkin, S.; Guo, C.: Model Based Simulation of Grinding Processes, 2nd European Conference on Grinding, Bremen, Germany, Nov. (2006), pp. 3.1-3.28.
- [Malk07] Malkin, S.; Guo, C.: Thermal analysis of grinding, *Annals of the CIRP*, Vol. 56/2, (2007), pp. 760-782.
- [Mari04] Marinescu, I.D.; Rowe, W.B.; Dimitrov, B.; Inasaki, I.: *Tribology of abrasive processes*, William Andrew Publishing, (2004).
- [Mari07] Marinescu, I.D.; Hitchinger, M.; Uhlmann, E.; Rowe, W.B.; Inasaki, I.: *Handbook of machining with grinding wheels*, CRC Press, (2007).
- [Mink03] Mink, E.; Giewerzew A.: CD-Grinding at increased cutting speed, 1st European Conference on Grinding, Fortschritt-Bericht VDI, No. 643, Aachen, Germany, Nov. (2003), pp. 11.1-11.18.
- [Mück99] Mückli, J.H.: Hochgeschwindigkeitsschleifen mit keramisch gebundenen CBN-Schleifscheiben, *Dissertation, RWTH Aachen*, (1999).
- [Naga89] Nagaraj, A. P.; Chattopadhyay, A. K.: On Some Aspect of Wheel Loading, *Wear*, Vol. 135, (1989), pp. 41-52.
- [Niew95] Niewelt, W.: Planschleifen von Nickelbasis-Legierung, *Dissertation, TU Berlin*, (1995).

- [Nguy03] Nguyen T.; Zhang, L.C.: An assessment of the applicability of the cold air and oil mist in surface grinding, *Journal of Material processing technology*, Vol. 140, (2003), pp. 224–230.
- [Nguy05a] Nguyen, T.A.; Butler, D.L.: Simulation of precision grinding process, part 1: generation of the grinding wheel surface, *International Journal of Machine Tools and Manufacture*, Vol. 45 (11), (2005), pp. 1321-1328.
- [Nguy05b] Nguyen, T.A.; Butler, D.L.: Simulation of precision grinding process, part 2: Interaction of abrasive grain with workpiece, *International Journal of Machine Tools and Manufacture*, Vol. 45 (11), September, (2005), pp. 1329-1336.
- [Niew95] Niewelt, W.: *Planschleifen von Nickelbasis-Legierung*, Dissertation, TU Berlin, (1995).
- [Oliv08] Oliveira, J.F.G.; França, T.V.; Wang J.P.: Experimental analysis of wheel/workpiece dynamic interactions in grinding, *Annals of the CIRP*, Vol. 57/1, (2008), pp. 329-332.
- [Oliv10] Oliveira, J.F.G., Bottene, A.C., França, T.V.: A novel dressing technique for texturing of ground surfaces, *Annals of the CIRP*, Vol. 59/1, (2010), pp. 361-364
- [Outw52] Outwater J.O.; Shaw, M.C.: Surface temperature in grinding, *Trans. ASME* 74, (1952), pp. 73–83.
- [Özel05] Özel, T.; Karpat, Y.: Predictive modelling of surface roughness and tool wear in hard turning using regression and neural networks, *International Journal of Machine Tools and Manufacture*, Vol. 45, (2005), pp.467–479.
- [Paul90] Paulmann, R.: *Schleifen, Hönen, Läppen, Grundlagen zu einem Verfahrensvergleich*, Dissertation, TU Braunschweig, (1990).
- [Pint08a] Pinto, F.W.: An experimental and numerical approach to investigate the machining performance of engineering grinding tools, Dissertation, ETH Zurich, (2008).
- [Pint08b] Pinto, F.W.; Vargas, G.E.; Wegener, K.: Simulation for optimizing grain pattern on Engineered Grinding Tools, *Annals of the CIRP*, Vol. 57/1, (2008), pp. 353-356.
- [Qi97] Qi, H. S.; Rowe, W. B.; Mills, B.: Experimental investigation of contact behaviour in grinding, *Tribology International*, Vol. 30 (4), (1997), pp. 283-294.
- [Rame01] Ramesh, K.; Yeo, S.H.; Zhong Z.W.; Sim, K.C.: Coolant shoe development for high efficiency grinding, *Journal of Materials Processing Technology*, Vol. 114, (2001), pp. 240–245.
- [Rowe95] Rowe, W.B.; Black, S.C.E.; Mills, B.; Morgan, M.N.; Qi, H.S.; Experimental investigation of heat transfer in grinding, *Annals of the CIRP*, Vol. 44/1, (1995), pp. 329–332.
- [Rowe96a] Rowe, W.B.; Morgan, M.N.; Black S.C.E.; Mills, B.: A simplified approach to thermal damage in grinding, *Annals of the CIRP*, Vol. 45/1, (1996), pp. 299–302.

- [Rowe96b] Rowe, W.B.; Black, S.C.E.; Mills, B.: Temperature Control in CBN Grinding, *International Journal of Advanced Manufacturing Technology*, Vol. 12 (6), (1996), pp. 387-392.
- [Rowe97] Rowe, W.B.; Chen, X.: Characterisation of the size effect in grinding and the sliced bread analogy, *International Journal of Production Research*, Vol. 35 (3), (1997), pp. 887-899.
- [Rowe98] Rowe, W.B.; Morgan, M.N.; Black, S.C.E.: Validation of thermal properties in grinding, *Annals of the CIRP*, Vol. 47/1, (1998), pp. 275-279.
- [Rowe01a] Rowe, W.B.; Jin, T.: Temperatures in High Efficiency Deep Grinding (HEDG), *Annals of the CIRP*, Vol. 50/1, (2001), pp. 205-208.
- [Rowe01b] Rowe, W.B.: Thermal analysis of high efficiency deep grinding, *International Journal of Machine Tools and Manufacture*, Vol. 41(1), (2001), pp. 1-19.
- [Sade08] Sadeghi, M. H.; Haddad, M. J.; Tawakoli, T.; Emami, M.: Minimal quantity lubrication-MQL in grinding of Ti-6Al-4V titanium alloy, *International Journal of Advanced Manufacturing Technology*, (2008), Available Online DOI 10.1007/s00170-008-1857-y
- [Salm03] Salmon, S.C.: The effects of hard lubricant coatings on the performance of electro-plated superabrasive grinding wheels, *Key Engineering Materials*, Vol. 238-239, (2003), pp. 283-288.
- [Schl82] Schleich, H.: Schärfen von Bornitridschleifen, Dissertation, RWTH Aachen, (1982).
- [Schu96] Schulz, A.: Das Abrichten von keramisch gebundenen CBN Schleifscheiben mit Formrolle, Dissertation, RWTH Aachen, (1996).
- [Shaf75] Shafto, G. R.; Howes, T. D.; Andrew, C.: Thermal Aspects of Creep Feed Grinding, *Proceedings of the Sixteenth International Machine Tool Design and Research Conference*, Manchester, UK, (1975), pp. 31-37
- [Shaj02] Shaji, S.; Radhakrishnan, V.: An Investigation on surface grinding using graphite as lubricant, *International Journal of Machine Tools and Manufacture*, Vol. 42 (6), (2002), pp. 733-740.
- [Shaj03] Shaji S.; Radhakrishnan, V.: Application of solid lubricants in grinding: investigations on graphite sandwiched grinding wheels, *Machining Science and Technology*, Vol. 7(1), (2003), pp. 137-155.
- [Shaw96] Shaw, M.C.: *Principal of abrasive process*, Oxford science publication, (1996).
- [Shi06] Shi, Z.M; Malkin, S.: Wear of electroplated CBN grinding wheels, *Trans. ASME*, Vol. 128, (2006), pp. 110-118.
- [Skur07] Skuratov, D.L.; Ratis, Yu.L.; Selezneva, I.A.; Pérez, J.; Fernández de Córdoba, P.; Urchueguía J.F.: Mathematical modelling and analytical solution for workpiece temperature in grinding, *Applied Mathematical Modelling*, Vol. 31 (6), (2007), pp. 1039-1047.
- [Snoy78] Snoeys, R.; Maris, M.; Peters, J.: Thermally induced damage in grinding, *Annals of the CIRP*, Vol. 27/2, (1978), pp. 571-581.

- [Spie94] Spiegel, P.: Einsatzvorbereitung kunstharzgebundener CBN-Schleifscheiben, Dissertation, University of Kaiserslautern (1994)
- [Steff83] Steffens, K.: Thermomechanik des Schleifens, Dissertation, RWTH Aachen, (1983).
- [Step03] Stephenson, D. J.; Jin, T.: Physical basics in grinding, 1st European Conference on Grinding, Fortschritt-Bericht VDI, No. 643, Aachen, Germany, Nov. (2003), pp.13.1–13.21.
- [Step07] Stepien, P.: Grinding forces in regular surface texture generation, International Journal of Machine Tools and Manufacture, Vol. 47, No. 14, (2007), pp. 2098–2110
- [Taka66] Takazawa, K.: Effects of grinding variables on surface structure of hardened steel, Bulletin of the Japan Society of Grinding Engineers, Vol. 2(1), (1966), pp. 14–21.
- [Tawa93] Tawakoli, T.: High efficiency deep grinding, VDI Verlag and Mechanical Engineering Publications Ltd. (MEP), (1993).
- [Tawa94] Tawakoli, T.: T-Tool neues hochabrasives Werkzeugsystem zum Schleifen und Abrichten, Industrie Diamanten Rundschau, IDR 2, (1994), pp. 78-81.
- [Tawa01] Tawakoli, T.: Innovative Werkzeugsysteme zum Schleifen, Abrichten und Fräsen, Industrie Diamanten Rundschau, IDR 1, (2001), pp. 48-54.
- [Tawa05] Tawakoli, T.; Rabiey, M.; Rasifard, A.: The new developments in CBN grinding technology, 1st International Conference Diamond at work, Proceeding CD, Barcelona, Spain, Oct. (2005).
- [Tawa06] Tawakoli, T.; Rabiey, M.: Innovatives Schleifscheibenkonzept zum Trockenschleifen auf dem Vormarsch, Industrie Diamanten Rundschau , IDR 3, (2006), pp. 30-35.
- [Tawa07a] Tawakoli, T.; Rabiey, M.: Trockenschleifen mit CBN-Schleifscheiben – ein innovatives Konzept, Jahrbuch Schleifen, Honen, Läppen und Polieren, 63. Ausgabe, (2007), pp. 100-118.
- [Tawa07b] Tawakoli, T.; Westkämper, E.; Rabiey, M.: Dry grinding by special conditioning, International Journal of Advanced Manufacturing Technology Vol. 33, (2007), pp. 419-424.
- [Tawa07c] Tawakoli, T.; Westkämper, E.; Rabiey, M.; Rasifard, A.: Influence of the type of coolant lubricant on the grinding with CBN-tools, International Journal of Machine Tools and Manufacture, Vol. 47, (2007), pp. 729-733.
- [Tawa07d] Tawakoli, T.; Rasifard, A.; Rabiey, M.: High Efficiency Internal Cylindrical Grinding with a new Kinematics, International Journal of Machine Tools and Manufacture, Vol. 47, (2007), pp. 734-739.
- [Tawa08a] Tawakoli, T.; Rabiey, M.: An innovative concept and its effects on wheel surface topography in dry grinding by resin and vitrified bond CBN wheel, Journal of Machining science and Technology, Vol. 12 (4), (2008), pp. 514-528.

- [Tawa08b] Tawakoli, T.; Azarhoushang, B.; Rabiey, M.: Ultrasonic assisted dry grinding of 42CrMo4, *International Journal of Advanced Manufacturing Technology*, (2008), Available Online DOI10.1007/500170-008-1646-7
- [Tawa08c] Tawakoli, T.; Azerhoushang, B.; Rabiey, M.: Ultraschalunterstütztes Schleifen von nicht gehärteten Stahl, *Industrie Diamanten Rundschau*, IDR 3, (2008), pp. 42-63.
- [Töns83] Tönshoff, H.K.; Brinksmeier, E.: Eigenspannungen durch Schleifen - wesentliche Einflußgrößen des Prozesses, *Tagungsband Eigenspannungen*, 14.-16. April, Karlsruhe, Deutsche Gesellschaft für Metallkunde e.V., Vol 2, (1983), pp. 251-270.
- [Töns92] Tönshoff, H.K.; Peters, J.; Inasaki, T.; Paul, T.: Modelling and Simulation of Grinding Processes, *Annals of the CIRP*, Vol. 41/2, (1992), pp. 677-688.
- [Töns00] Tönshoff, H.K.; Jung, M.: Einfluss der Kühlschmierbedingungen beim Rundschleifen, *Umweltverträgliches Schleifen. Kolloquium, Umweltverträgliches Schleifen, Ökologie als Ökonomie der Zukunft*, Shaker Verlag, (2000), pp. 99-112.
- [Töns03] Tönshoff, H.K.; Denkena, B.: *Spanen: Grundlagen*, Springer Verlag, Berlin, (2003).
- [Torr78] Torrance, A.A.: The metallography of worn surfaces and some theories of wear, *Wear*, Vol. 50 (1), (1978), pp. 169-182.
- [Torr90] Torrance, A.A.: The correlation of process parameters in grinding, *Wear*, Vol.139 (2), (1990), pp. 383-401.
- [Torr00] Torrance, A.A.; Badger, J.A.: The relation between the traverse dressing of vitrified grinding wheels and their performance, *International Journal of Machine Tools and Manufacture*, Vol. 40 (12), (2000), pp. 1787-1811.
- [Torr05] Torrance, A.A.: Modeling abrasive wear, *Wear*, Vol. 258 (1-4), (2005), pp. 281-293.
- [Trim75] Triemel, J.: *Untersuchung zum Stirnschleifen von Schnellarbeitsstählen mit Bornitridwerkzeugen*, Dissertation, University of Hannover, (1975).
- [Upad07] Upadhyaya, R.P.; Fiecoat, J.H.: Factors Affecting Grinding Performance with Electroplated CBN Wheels, *Annals of the CIRP*, Vol. 56/1, (2007), pp. 339-342.
- [Uhlm94] Uhlmann, E.: *Tiefschleifen hochfester keramischer Werkstoffe*, Dissertation, TU Berlin, (1994).
- [Uhlm98] Uhlmann, E.: Surface Formation in Creep Feed Grinding of Advanced Ceramics with and without Ultrasonic Assistance, *Annals of the CIRP*, Vol. 47/1, (1998), pp. 249-252.
- [Verk76] Verkerk, J.; Pekelharing, A.J.: Kinematical approach to the effect of wheel dressing conditions on the grinding process, *Annals of the CIRP* Vol. 25/1, (1976), pp. 209-214

- [Verk77] Verkerk, J.: Final report concerning CIRP cooperative work on the characterization of grinding wheel topography, *Annals of the CIRP*, Vol. 26/2, (1977), pp. 385–395.
- [Verl94] Verlemann, E.: Prozessgestaltung beim Hochgeschwindigkeitrundschleifen von Ingenieurkeramik, RWTH Aachen, (1994).
- [Voll01] Voll, M.: Modelle zur thermische Optimierung von Trockenschleifprozessen, Dissertation, TU Chemnitz, (2001).
- [Wang01] Wang, Z.; Willett, P.; Aguiar, P.R.; Webster, J.: Neural network detection of grinding burn from acoustic emission, *International Journal of Machine Tools and Manufacture*, Vol. 41, (2001), pp. 283-309.
- [Warn98] Warnecke G.; Zitt, U.: Kinematic Simulation for Analyzing and Predicting High- Performance Grinding Processes, *Annals of the CIRP*, Vol. 47/1, (1998), pp. 265–270.
- [Webe08] Weber, A.: Verschleissverhalten galvanisch belegter Schleifwerkzeuge bei der Bearbeitung von Hochleistungskeramik, Dissertation, RWTH Aachen, (2008).
- [Webs95] Webster, J.A.; Cui, C.; Mindek Jr., R.B.: Grinding fluid application system design, *Annals of the CIRP*, Vol. 44/1, (1995), pp. 333–338.
- [Webs02] Webster, J.A.; Brinksmeier, E.; Heinzel, C.; Wittman, M.; Thoens, K.: Assessment of grinding fluid effectiveness in continuous-dress creep feed grinding, *Annals of the CIRP*, Vol. 48/2, (2002), pp. 581–598.
- [Wein98] Weinert, K.; Buschka, M.; Johlen, G.; Willisch, C.: Schleifen mit Graphit als Schmierstoff, *VDI-Z 140*, 1/2, (1998), pp. 46-49.
- [Wern71] Werner, G.: Kinematik und Mechanik des Schleifprozesses, Dissertation, RWTH Aachen, (1971).
- [Wern86] Werner, G.; Tawakoli, T.: Der Druckeigenspannungszusatz an tiefgeschliffener Stahlbauteile, *Metlbearbeitung 80*, (1986), pp.39-46.
- [West93] Westkämper, E.; Tönshoff, H.K.: CBN or CD Grinding of profile, *Annals of the CIRP*, Vol. 42/1, (1993), pp. 371–374.
- [West95] Westkämper, E.: Grinding assisted by Nd:YAG Laser, *Annals of the CIRP*, Vol. 44/1, (1995), pp. 317–320.
- [Yege86] Yegenoglu, K.: Berechnung von Topographiekenngößen, Dissertation, RWTH Aachen, (1986).
- [Zapp98] Zapp, M.: Ultraschallunterstütztes Schleifen von Hochleistungskeramik - Ein Beitrag zur gezielten Beeinflussung der Eigenschaften von Bauteilen durch eine ganzheitliche Prozesskettenbetrachtung, Dissertation, University of Kaiserslautern, (1998).
- [Zepp05] Zeppenfeld, C.: Schnellhubschleifen von γ -Titanalimniden, Dissertation, RWTH Aachen, (2005).
- [Zhan03] Zhang, P.; Miller, M. H.: Grinding Wheel Loading with and without Vibration Assistance, *Proceeding of the ASPE Annual Meeting*, (2003)

- [Zhou02] Zhou X.; Xi, F.: Modelling and predicting surface roughness of the grinding process, *International Journal of Machine Tools and Manufacture*, Vol. 42, (2002), pp. 969–977.
- [Zitt99] Zitt, U.R.: *Modellierung und Simulation von Hochleistungsschleifprozessen*, Dissertation, University of Kaiserslautern, (1999).
- [Zumg87] Zum Gahr, K.H.: *Microstructure and wear of materials*, Tribology series, 10, Elsevier science publishers, (1987).

